Nonuniqueness of Solutions to 2D Incompressible Euler Equations with Unbounded Vorticity

Hyungjun Choi

25 October 2026

Abstract

We construct two distinct solutions of the two-dimensional incompressible Euler equation with the same initial vorticity in $\bigcap_{1\le p<\infty} L^p(\mathbb{R}^2)$. The vorticities are compactly supported in space and have mean zero, so the corresponding velocities have finite energy. The nonuniqueness mechanism is a cascade of transitions in quadrupole dynamics across infinitely many scales.

Contents

1 Introduction **1**

2 Quadrupole dynamics and cascade mechanism **9**

3 Small patch approximation of point vortices **17**

4 First solution: rotating quadrupoles at all scales **35**

5 Second solution: cascade of separating dipoles **44**

6 Transition in quadrupole configurations **53**

7 Proof of Proposition 5.1 **62**

8 Limit of solution sequences and nonuniqueness **84**

1 Introduction

The incompressible Euler equation on $\mathbb{R}^2$ can be written in terms of velocity u and vorticity $\omega = \partial_1 u_2 - \partial_2 u_1$ as

$$\begin{cases} \partial_t \omega + u \cdot \nabla \omega = 0, \\ u = K * \omega, \quad K(x) = \dfrac{(-x_2, x_1)^t}{2\pi |x|^2} \end{cases}$$

We construct two distinct solutions of the two-dimensional incompressible Euler equation with the same initial vorticity. The initial vorticity is compactly supported, mean zero, and lies in every $L^p(\mathbb{R}^2)$ for $1 \le p < \infty$.

Existence, uniqueness, and the Yudovich conjecture. For smooth, sufficiently decaying initial vorticity, the planar Euler equation has a unique global smooth solution. The classical theory originates with Wolibner [67] and was developed further by Kato [48]. The vorticity is transported by an area-preserving flow, so its L^p norms are conserved. Yudovich [68] extended global existence and uniqueness to bounded integrable vorticity, $\omega_0 \in L^1 \cap L^\infty$. The corresponding velocity is log-Lipschitz, which supplies the modulus of continuity needed for uniqueness. His later work [69] also permits unbounded vorticity under suitable restrictions on the growth of $\|\omega_0\|_{L^p}$ as $p \to \infty$. For a broader account of Euler dynamics and regularity, see [32].

Weak solution existence reaches substantially rougher data. DiPerna and Majda [30] developed compactness and concentration arguments yielding global weak solutions for integrable L^p vorticity, $p > 1$. Delort [29] reached distinguished-sign measure vorticity in H^{-1}_{loc} with locally finite energy. These existence results do not assert uniqueness. Uniqueness for a transport equation with a prescribed Sobolev velocity, as in DiPerna–Lions [31], does not settle Euler uniqueness, because two Euler solutions transport their vorticities by different velocities.

The *Yudovich nonuniqueness conjecture* has the following Lebesgue-space formulation in [2, 55]. For each $2 < p < \infty$, there exist initial velocity and vorticity satisfying

$$u_0 \in L^2(\mathbb{R}^2), \qquad \omega_0 = \operatorname{curl} u_0 \in L^1(\mathbb{R}^2) \cap L^p(\mathbb{R}^2),$$

from which the unforced Euler equation admits distinct weak solutions with

$$u \in C([0,T]; L^2), \qquad \omega \in L^\infty([0,T]; L^1 \cap L^p).$$

Under these regularity conditions, the kinetic energy $\|u(t)\|_{L^2}^2$ and the distribution function of the vorticity $\omega(t)$ is conserved in time t. We discuss several developments relevant to this question before explaining the present construction using point-vortex dynamics.

Self-similar solutions and instability. The use of instability in similarity coordinates has been successful for the similar non-uniqueness problem in three-dimensional Navier–Stokes equations. Jia and Šverák [46, 47] constructed forward self-similar solutions and developed a route from an unstable self-similar profile to nonuniqueness. Guillod and Šverák [39] supplied numerical evidence for the required bifurcation. More recently, Hou, Wang and Yang [41] presented a computer-assisted proof of nonuniqueness of Leray–Hopf weak solutions. Ionescu, Jia and Palasek [44] numerically construct unstable self-similar profiles in the axisymmetric swirl-free class. An unstable trajectory in logarithmic time $\tau = \log t$ can yield a second solution with the same initial trace at $t = 0$, provided the spatial behavior and nonlinear remainder are controlled. Vishik [65] used instability and similarity variables to prove nonuniqueness for the forced two-dimensional Euler equation with L^p vorticity. A detailed account is given in [2]. Albritton, Bruè and Colombo [1] implemented this mechanism for the *forced* three-dimensional Navier–Stokes equations to obtain two Leray–Hopf weak solutions with the same force and initial data.

For the *unforced* two-dimensional Euler equations, there were few constructions of self-similar solutions. Elling [34, 35] constructed algebraic spiral solutions, subsequently developed by Shao, Wei and Zhang [61], and Choi [14] removed the rotational symmetry restriction. Choi and Coiculescu [15] constructed homogeneous steady solutions whose pseudo-velocity field has several stagnation points. Choi [17] and Hou, Qin, Song and Zhang [42] constructed forward self-similar solutions from $-\alpha$-homogeneous initial vorticity for $1 < \alpha < 2$, without smallness or sign assumptions. Bressan and Shen [6] studied self-similar solutions in connection with nonuniqueness and numerically observed competing spiral configurations. However, transferring the Navier–Stokes strategy to the two-dimensional Euler equation presents difficulties [5, 16, 19]. In addition, having two distinct self-similar solutions from the same initial homogeneous data does not guarantee resolution of the problem with integrable vorticity.

Multiscale constructions. While self-similarity provides a concrete route to nonuniqueness, it imposes a fixed continuous relation between spatial scale and time. Multiscale constructions organizing simpler dynamics at separated scales can offer greater flexibility. With infinitely many scales, an infinitesimal difference in the initial data can lead to a distinction between solutions at larger scales. Dyadic models and averaged equations provide examples of singularity formation [49, 63, 57]. See [12] for a survey. Filonov and Khodunov [36] obtained Leray–Hopf nonuniqueness for a forced dyadic model, and Palasek [58] for an unforced model. For the three-dimensional Navier–Stokes equations, Coiculescu and Palasek [20] constructed nonunique solutions from critical BMO^{-1} data on the torus, smooth for positive times. Cheskidov, Dai and Palasek [13] constructed weak solutions that branch from a classical solution through transfer from arbitrarily high to lower frequencies.

Related methods yield Navier–Stokes norm growth [59], loss of Sobolev regularity for two-dimensional Euler [24], and blow-up of classical solutions of the three-dimensional Euler equations [25]. These growth and blow-up results are distinct from nonuniqueness.

Convex integration. The approach of De Lellis and Székelyhidi [28] provides another mechanism for nonuniqueness of weak Euler solutions. Convex integration established the nonconservation direction of Onsager's conjecture [45, 9, 37]. Controlling vorticity in two dimensions is an additional constraint. Bruè and Colombo [7] obtained nonuniqueness with vorticity in the weak-L^1 Lorentz space $L^{1,\infty}$, and Bruè, Colombo and Kumar [8] constructed periodic solutions with vorticity in $C([0,1];L^p)$ for some $p>1$, using concentrated traveling vortices in a convex-integration scheme. However, for structural reasons, it was considered difficult to obtain larger values of p with the convex integration method [7]. Mengual [55] obtained nonunique solutions from initial vorticity in $L^1\cap L^p$ for every finite $p>2$, but the competing solutions are not shown to retain L^p vorticity at positive times.

Point-vortex dynamics as a building block. Point vortices $\omega(t)=\sum_j \Gamma_j\delta(x-x_j(t))$ provide a motion that is described by a Hamiltonian ODE system:

$$\dot{x}_j=\sum_{k\neq j}\Gamma_k K(x_j-x_k).$$

For an extensive list of references on point-vortex dynamics, see, for instance, Aref [3] and the references therein. Grotto and Pappalettera [38] provide a closely related motivation for using point-vortex dynamics to obtain nonuniqueness. They constructed a burst of one point vortex into three and obtained nonuniqueness for atomic vorticity in a symmetrized weak formulation.

Our building block is a quadrupole with dynamics connecting two distinct motions, a rotating rhombus and separating dipoles. The rhombus belongs to the relative equilibria classified by Hampton, Roberts and Santoprete [40]. Its connection with dipole scattering appeared in Eckhardt and Aref [33] and a trajectory connecting the rhombus to separating dipoles appeared in Lydon, Nazarenko and Laurie [51]. Section 2 derives this trajectory and the estimates needed below directly from the four-vortex equations.

We then arrange quadrupoles at decreasing length scales with increasing rotation frequencies. For each finite number of scales, one solution stays near rotating rhombi while a second starts with separating dipoles only at the smallest scale. The separating dipoles activate successively larger scales. The initial discrepancy tends to zero as the number of scales grows, whereas the later discrepancy survives at the largest scale at time 1. The two limits share a common initial datum and differ at time 1. In other words, infinitesimal difference in initial data may result in a visible distinction of Lagrangian trajectories. The following subsections state the theorem and explain the quantitative choices and the limiting argument.

For the actual proof of the main theorem, we replace each point vortex by a small circular patch. See Sections 1.5 and 3 for details in realizing point vortex dynamics by small patches.

Main theorem.

Theorem 1.1. *There exist a compactly supported function ω_0 and two vorticities $\omega^{(1)}, \omega^{(2)}$ such that*

(i) $\omega_0 \in \bigcap_{1 \le p < \infty} L^p(\mathbb{R}^2)$ *and* $\int_{\mathbb{R}^2} \omega_0 \, dx = 0$.

(ii) For every $1 \le p < \infty$ and $j = 1, 2$, each pair $(\omega^{(j)}, u^{(j)})$ is a renormalized solution of the vorticity transport equation with initial data $\omega^{(j)}(0) = \omega_0$ and also a weak solution of the momentum equation. Indeed,

$$\omega^{(j)} \in C([0,\infty); L^p), \quad u^{(j)} = K * \omega^{(j)} \in C([0,\infty); L^2), \quad \|\omega^{(j)}(t)\|_{L^p} = \|\omega_0\|_{L^p}, \qquad t \ge 0.$$

(iii) The two solutions are distinct since these satisfy

$$\|\omega^{(2)}(t=1) - \omega^{(1)}(t=1)\|_{L^1} > 0.$$

Remark. Zero total circulation gives $u_0 = K * \omega_0 \in L^2$. For each fixed $0 < \alpha < 1$, the datum can be chosen with $\|\omega_0\|_{L^p} \asymp p^{4/\alpha}$ for $p \ge 2$, as shown in Section 1.4.

1.1 The quadrupole motion

Identify $\mathbb{R}^2$ with $\mathbb{C}$. Consider circulation $+\Gamma$ at $z_1, -z_1$ and $-\Gamma$ at $z_2, -z_2$, with $\Gamma > 0$. Fix the length $\ell > 0$ by

$$|z_1|^2 - |z_2|^2 = \ell^2, \qquad \Omega = \frac{\Gamma}{2\pi\ell^2}.$$

The four positions

$$\left\{ \pm\ell\sqrt{\frac{\sqrt{2}+1}{2}}\, e^{i(\theta_0 - \Omega t)}, \quad \pm i\ell\sqrt{\frac{\sqrt{2}-1}{2}}\, e^{i(\theta_0 - \Omega t)} \right\}$$

form an exact rotating rhombus. The two vertices on the longer diagonal have circulation $+\Gamma$, and those on the shorter diagonal have circulation $-\Gamma$. This relative equilibrium is part of the classification in Hampton, Roberts and Santoprete [40, Sections 4.2 and 7.4].

There is also a complete, collision-free solution with the following behavior. As $t \to -\infty$, its shape converges to this rhombus. As $t \to +\infty$, each positive vortex pairs with a negative vortex at distance tending to ℓ. The two pair centers move in opposite directions, each with speed tending to $\Omega\ell$. Such a translating positive-negative pair is called a dipole. Lydon, Nazarenko and Laurie [51, Section III.1] describe the limiting incoming motion in which two dipoles approach a rotating rhombus. The symmetry $z_j(t) \mapsto \overline{z_j(-t)}$ converts an incoming motion into a motion of separating dipoles with the same circulations. Eckhardt and Aref [33] studied integrable four-vortex scattering earlier. Section 2 constructs the separating motion using explicit first integrals. It also shows that a small positive unstable shape perturbation grows at rate $2\sqrt{2}\Omega$ near the rhombus, and tends to converge to the separating dipoles solution as $t \to \infty$. The unstable and stable shape variables q and p, defined in Section 2.2, determine the shape of a centrally symmetric quadrupole and describe its unstable and stable deformations from the rhombus.

The transition in quadrupole motion provides a way for a smaller, faster quadrupole to influence a larger, slower one. If θ_∞ is the limiting direction from the negative to the positive member of a dipole, then the second complex moment of the configuration of separating dipoles obeys

$$M_2(t) := 2\Gamma(z_1(t)^2 - z_2(t)^2) = -\frac{2i}{\pi}\Gamma^2 e^{2i\theta_\infty} t + O(1).$$

For a rhombus, by contrast, $|M_2(t)| = 2\sqrt{2}\Gamma\ell^2$. At a distant point z, the spatial derivative of the velocity generated by the quadrupole is proportional, to leading order, to $\overline{M_2}/|z|^4$. The linearly growing moment of a configuration of separating dipoles can deform another rhombus if the two configurations are oriented so that instability amplifies the effect. Section 2 computes the contribution of this influence to the unstable shape variable.

1.2 Scales, construction of two solutions, and cascade

Fix $0 < \alpha < 1$. For each positive integer n, choose

$$d_n = 2^{-n}, \qquad \Omega_n = \Lambda B^n, \qquad \ell_n = e^{-\Omega_n^\alpha}, \qquad \Gamma_n = 2\pi\Omega_n\ell_n^2. \tag{1.1}$$

Here d_n is an initial location on the real axis, ℓ_n is the length scale of the quadrupole, Γ_n is the absolute circulation of each of its four vortices, and Ω_n is its rhombus rotation frequency. As n increases, the quadrupoles become smaller, lie closer to the origin, and rotate faster. The constant $B > 2$ is chosen sufficiently large depending on $0 < \alpha < 1$, and then Λ is chosen sufficiently large.

The quadrupoles remain separated because, for large Λ, the distance traveled by each dipole over an $O(1)$ time interval is small compared with the initial spacing.

$$\sup_{n\geq 1} \frac{\ell_n(1+\Omega_n)}{|d_n - d_{n+1}|} \longrightarrow 0 \quad \text{as } \Lambda \to \infty \text{ with } B \text{ fixed.}$$

Replace each point vortex at scale n by a circular patch of circulation $\pm\Gamma_n$ and vorticity value $\pm A\Omega_n^4$, where A is a fixed sufficiently large constant. The circulation determines the radius a_n through

$$a_n^2 = \frac{2\ell_n^2}{A\Omega_n^3}.$$

The individual patches are consequently much smaller than the distances between the four vortex centers.

For each N, the first solution is denoted by $\omega_N^{(1)}$. It contains four patches at each scale $1 \leq n \leq N$. The initial centroids of patches are chosen so that the shape of the quadrupole stays close to a rotating rhombus throughout $0 \leq t \leq 2$. Simply placing disks at the point-vortex rhombus would not cancel the fields from the other patches. For any prescribed initial phases, the topological argument in Section 4 finds an initial unstable shape variable at each scale, simultaneously, so that all remain small through time 2.

The second solution is denoted by $\omega_N^{(2)}$. At time zero its patches at scales $1, \ldots, N-1$ are identical to those of $\omega_N^{(1)}$. Only the centers of the four patches at scale N are changed. They are placed at a fixed configuration sufficiently far along the separating point-vortex trajectory, with the same radii, vorticity values, and circulations. The intended motion is

	$t = 0$	$0 < t \leq 1$
$\omega_N^{(1)}$	all scales near rhombi	all scales remain near rhombi
$\omega_N^{(2)}$	only scale N already separating	N influences $N-1$, …, 2 influences 1.

These descriptions concern the shape of the quadrupole at each scale.

Here is why the second motion reaches scale 1 in a time bounded independently of N. Once scale $n+1$ activates, the time derivative of its complex second moment has magnitude of order Γ_{n+1}^2. Its resulting strain grows linearly in elapsed time and oscillates in the rotating coordinates of scale n. Formula (2.12) integrates this forcing against $e^{-2\sqrt{2}\Omega_n t}$ and gives a dimensionless coefficient of the exponentially growing response comparable to

$$\frac{\Gamma_{n+1}^2}{\Omega_n^2 |d_n - d_{n+1}|^4}.$$

The two factors of Ω_n^{-1} come from elapsed time in the linearly growing forcing and from integration over the growth time scale. The weighted integral arising from forcing is a sinusoidal function of the orientations. The initial orientations are chosen recursively so that its predicted leading effect is maximized. Exponential growth at rate $2\sqrt{2}\Omega_n$ then reaches a fixed positive size after a time delay of order

$$\frac{1}{2\sqrt{2}\Omega_n}\left[\log\left(\frac{\Omega_n^2|d_n-d_{n+1}|^4}{\Gamma_{n+1}^2}\right)+O(1)\right]=\frac{4\Omega_{n+1}^{\alpha}+O(n+\log B+1)}{2\sqrt{2}\Omega_n}. \tag{1.2}$$

The leading delays are summable given $0<\alpha<1$ since

$$\sum_{n\geq 1}\frac{\Omega_{n+1}^{\alpha}}{\Omega_n}=\frac{\Lambda^{\alpha-1}B^{2\alpha-1}}{1-B^{\alpha-1}}. \tag{1.3}$$

Thus all activation steps occur before time $1/2$ after Λ is chosen large enough. Section 7 establishes these estimates for the fully coupled patch solutions, retaining the responses of slower scales and the effects of every other scale.

Theorem 3.10 compares the point-vortex approximation errors in the centroid equations of the two distinct patch solutions at the same scale. Their difference is bounded by a time integral of centroid and external-field differences from time zero. This integral retains the earlier motion until the predicted transition time. Having this relative bound is essential because an absolute error in the centroid equation that is proportional to some negative power of Ω_n would exceed the exponentially small effect from scale $n+1$ described above.

1.3 Identical limiting initial data and different later solutions

Only the four disks at scale N differ initially. Their amplitudes are $A\Omega_N^4$ and their total absolute circulation is $4\Gamma_N$, so, for every finite $p\geq 1$,

$$\begin{aligned}\|\omega_N^{(2)}(0)-\omega_N^{(1)}(0)\|_{L^p}^p &\leq 2^{p+2}\Gamma_N(A\Omega_N^4)^{p-1}\\ &\leq C_{p,A}\Omega_N^{4p-3}e^{-2\Omega_N^{\alpha}}\longrightarrow 0.\end{aligned} \tag{1.4}$$

To obtain a common initial limit, we also need compactness of either initial solution family. At each fixed scale, the first solution family's disk centers lie in a compact set, while its radii and amplitudes are fixed. A diagonal subsequence makes all these centers converge. Also,

$$\|\omega_N^{(k)}(t=0)\|_{L^p}^p=8\pi A^{p-1}\sum_{n=1}^{N}\Omega_n^{4p-3}e^{-2\Omega_n^{\alpha}}\leq C_{p,A,\alpha,B,\Lambda},\qquad k=1,2. \tag{1.5}$$

The summable tails, together with continuity of translated disks in L^p, give $\omega_N^{(1)}(0)\to\omega_0$ strongly in every finite L^p. Equation (1.4) gives the same limit for the second family. The phases may depend on N, and successive finite constructions need not be compatible.

At time 1, the first solution's four outer patches of scale 1 remain within $C\ell_1$ of d_1, whereas the second solution's outer patches lie at distances comparable to $\Omega_1\ell_1$. A fixed annulus centered at d_1 with radius comparable to $\Omega_1\ell_1$ contains all four outer patches of the second solution and no other patches of either solution. These displacement bounds are uniform in the N-dependent phases. Thus one can choose a fixed smooth function $0\leq\chi\leq 1$, supported in this annulus, such that

$$\int\chi|\omega_N^{(1)}(1)|\,dx=0,\qquad\int\chi|\omega_N^{(2)}(1)|\,dx=4\Gamma_1. \tag{1.6}$$

Passing to a subsequence as $N\to\infty$ gives two solutions $\omega^{(1)},\omega^{(2)}$ with the same initial data $\omega^{(1)}(0)=\omega^{(2)}(0)=\omega_0$, but

$$\|\omega^{(2)}(1)-\omega^{(1)}(1)\|_{L^1}\geq 4\Gamma_1>0.$$

1.4 Patch amplitude and vorticity norms

The vorticity magnitude $A\Omega_n^4$ is chosen to keep each patch close to a disk for a fixed physical time, uniformly over all scales. Its internal rotation has angular speed $A\Omega_n^4/2$, whereas the strain produced by the other three patches in its quadrupole has size $C\Omega_n$. Controlling the deformation of a vortex patch for an $O(1)$ time requires a detailed analysis of the contour equation.

Consider one patch initially equal to a disk, with vorticity magnitude M, whose external strain and time derivative of strain are bounded by L and L^2, respectively, as in Lemma 3.4. After removing the internal rotation and the nonresonant quadratic deformation terms, normal from in Lemma 3.4 bounds the boundary deformation $z(t)$ in physical time by

$$z(t) \le C\frac{L}{M} + C\int_0^t \left(Mz(s)^3 + \frac{L^2}{M} \right) ds.$$

The term Mz^3 is the cubic nonlinear deformation, and L^2/M is the residual external forcing. Balancing these terms controls $z(t)$ under $C(L/M)^{2/3}$ up to time $c\frac{M^{1/3}}{L^{4/3}}$. Lemma 3.6 makes this computation precise, including control of the boundary labels. With $L \asymp \Omega_n$ and a hypothetical amplitude $M = A\Omega_n^\gamma$ with $\gamma > 1$, the guaranteed time is therefore $cA^{1/3}\Omega_n^{(\gamma-4)/3}$. Putting $\gamma = 4$, a sufficiently large fixed A gives the required interval $[0, 2]$ and deformation controlled in $O(\Omega_n^{-2})$.

For the length scales (1.1), the circulation identity gives $a_n^2 = 2\ell_n^2/(A\Omega_n^3)$. Since each quadrupole consists of four disjoint patches, its contribution to the pth power of the norm is its total absolute circulation times the $(p-1)$st power of its amplitude. Consequently,

$$\|\omega_0\|_{L^p}^p = 8\pi A^{p-1} \sum_{n\ge 1} \Omega_n^{4p-3} e^{-2\Omega_n^\alpha}.$$

Estimating the series and taking pth roots gives

$$cp^{4/\alpha} \le \|\omega_0\|_{L^p} \le Cp^{4/\alpha}, \qquad p \ge 2.$$

These constants may depend on α, A, B, Λ, but not on p. Thus these scales yield every norm-growth exponent $4/\alpha > 4$. This range does not establish sharpness of Yudovich's uniqueness condition $\int_2^\infty dp/(p\|\omega_0\|_{L^p}) = \infty$ in [69].

1.5 Realization of point-vortex dynamics by patches.

We replace each point vortex by a small circular patch. Marchioro and Pulvirenti [53, 54] justified the point-vortex approximation on fixed time intervals without point-vortex collisions. As the initial core radii tend to zero, each vorticity component converges weakly to the corresponding moving point mass, and its support remains in a neighborhood of the point-vortex trajectory. See also [64, 10, 56, 27] for further developments in various settings.

Results valid for all time are also available for particular configurations. Zbarsky [70] treats nondegenerate self-similar expanding three-vortex configurations. His proof uses renormalized moments to exploit the internal rotation. Dávila, del Pino, Musso and Parmeshwar [26] construct smooth solutions asymptotic to two vortex pairs traveling in opposite directions as $t \to \infty$. These results concern specific expanding or separating motions and they do not supply the comparison estimates needed below during the unstable transition from a rotating rhombus.

Stability in a vorticity norm and control of a patch boundary require different estimates. Wan–Pulvirenti [66] and Sideris–Vega [62] prove L^1 stability of circular patches. Choi and Jeong [18] prove L^1 stability of small Kelvin waves under localized symmetric perturbations

on any prescribed finite interval, and also construct small L^1 perturbations with arbitrarily large perimeter growth. Chemin [11] and Bertozzi–Constantin [4] prove global persistence of regular patch boundaries. These statements do not give quantitative closeness to a circle in a boundary norm under the coupled external fields considered here.

Contour expansions near a circle were studied by Constantin and Titi [23]. Kida's elliptic-patch solutions [50] describe the competition between internal rotation and imposed linear strain, while Constantin [22] studies approximate far-field interactions of nested contours. A closer precedent for separating vortex locations from shape variables is the conformal formulation of Long, Wang and Zeng [52]. Near concentrated steady patches, their linearized system separates slow location modes from rapidly oscillating shape modes.

In Section 3, we define label-deformation contour coordinates and a normal-form change to control deformation in $C^{1,1/2}$ under the external strain. The bounds are uniform over all scales on a fixed physical time interval. Comparing two evolutions in the same coordinates also gives relative bounds for differences of their moments and centroid errors, without an additive absolute error. Such bounds are needed because the signal transmitted between scales is much smaller than the available absolute error.

Outline of manuscript

The proof proceeds as follows. Section 2 derives the four-vortex motions and outlines the cascade mechanism through their interaction. Section 3 controls patch deformation and derives the centroid and moment equations, including the relative error estimate. Section 4 constructs the first solution by choosing its initial unstable shape variables. Section 5 specifies the second initial configuration and explains how successive departures give a fixed later distinction. Section 6 proves the transition estimates for a single quadrupole with prescribed external strain. Section 7 verifies the hypotheses of these estimates by induction in the coupled system of quadrupoles. Section 8 passes both sequences to limits with the same initial datum and proves that the limits differ at time 1.

History of this work and use of AI/LLM

The author has worked on nonuniqueness for 2D Euler for many years, including a series of works on self-similar solutions [14, 15, 17]. Trial and error in pursuing this problem led the author to consider discrete multiscale construction for the reasons discussed in introduction. Guided by this strategy, the author found the main quadrupole dynamics used in this work and identified a cascade mechanism by which one quadrupole activates the next, as described in Sections 2, 5, and 6.

ChatGPT 5.6 and 6.0 were used under the author's guidance to execute the cascade strategy through a sequence of quadrupole patches. In particular, they helped complete the technical details of replacing point vortices by patches, mainly in Section 3. ChatGPT 6.1 was used for reference searches and language editing. The main ideas of the paper were generated by the author, who takes full responsibility for the correctness of the proof.

Recent works on the Yudovich conjecture

While completing this work, the author learned of an independent preprint by Coiculescu [21] and the Hexagon preprint [60] prepared by Pappalettera and Sorella. The construction in this manuscript differs significantly from those in [21, 60], which used radial vortex supported on concentrated rings. A few days after the posting of this manuscript, Hou–Qin–Song–Zhang [43] posted their independent proof of similar theorem with the quadrupole cascade idea.

Acknowledgments

The author thanks Alexandru Ionescu for his encouragement in pursuing this problem. The author also thanks Peter Constantin, Tarek Elgindi, and Philip Isett for their valuable comments.

2 Quadrupole dynamics and cascade mechanism

We first construct a rotating rhombus quadrupole and an orbit that approaches it in backward time and becomes separating dipoles in forward time. We then calculate the strain produced at another rotating quadrupole. This is the local interaction used in each step of the cascade. The passage from these finite-dimensional point-vortex dynamics to patches is justified in Section 3 and the subsequent construction.

2.1 Equations and the rotating rhombus

The point-vortex system is a Hamiltonian system of ordinary differential equations which describes 2D Euler dynamics with vorticity data being a finite sum of point masses. For point vortices with positions $x_j \in \mathbb{R}^2$ and circulations Γ_j, put Hamiltonian

$$H = -\frac{1}{2\pi}\sum_{i<j}\Gamma_i\Gamma_j \log|x_i - x_j|.$$

Then, the point-vortex system is

$$\Gamma_j \dot{x}_j = -(\nabla_{x_j} H)^\perp = \Gamma_j \sum_{i\neq j}\Gamma_i K(x_j - x_i),$$

and hence the Hamiltonian H is conserved in time.

$$\frac{dH}{dt} = \sum_j \nabla_{x_j} H \cdot \dot{x}_j = -\sum_j \frac{\nabla_{x_j} H \cdot (\nabla_{x_j} H)^\perp}{\Gamma_j} = 0.$$

We will use complex coordinates $z = x_1 + ix_2$, so that $K(z) = i/(2\pi\overline{z})$.

Now, consider a quadrupole with central symmetry. Fix $\Gamma > 0$ and put circulation $+\Gamma$ at $z_1, -z_1$ and $-\Gamma$ at $z_2, -z_2$. In this case,

$$H = -\frac{\Gamma^2}{2\pi}\left[\log(2|z_1|) + \log(2|z_2|) - 2\log|z_1 - z_2| - 2\log|z_1 + z_2|\right] = \frac{\Gamma^2}{2\pi}\log\frac{|z_1^2 - z_2^2|^2}{4|z_1||z_2|}.$$

The central symmetry is preserved by the equations. Summing the three velocities at each independent point gives

$$\dot{z}_1 = \frac{i\Gamma}{2\pi}\left(\frac{1}{2\overline{z}_1} - \frac{1}{\overline{z}_1 - \overline{z}_2} - \frac{1}{\overline{z}_1 + \overline{z}_2}\right), \qquad \dot{z}_2 = \frac{i\Gamma}{2\pi}\left(\frac{1}{\overline{z}_2 - \overline{z}_1} + \frac{1}{\overline{z}_2 + \overline{z}_1} - \frac{1}{2\overline{z}_2}\right).$$

Equivalently,

$$\dot{z}_1 = -\frac{i\Gamma(3\overline{z}_1^2 + \overline{z}_2^2)}{4\pi\overline{z}_1(\overline{z}_1^2 - \overline{z}_2^2)}, \qquad \dot{z}_2 = -\frac{i\Gamma(\overline{z}_1^2 + 3\overline{z}_2^2)}{4\pi\overline{z}_2(\overline{z}_1^2 - \overline{z}_2^2)}. \tag{2.1}$$

The angular impulse $2\Gamma(|z_1|^2 - |z_2|^2)$ is also conserved, since

$$\frac{d}{dt}(|z_1|^2 - |z_2|^2) = 2\,\mathrm{Re}(\overline{z}_1\dot{z}_1 - \overline{z}_2\dot{z}_2) = 2\,\mathrm{Re}\left(-\frac{i\Gamma}{2\pi}\right) = 0.$$

We restrict attention to configurations with $|z_1| > |z_2|$ and fix

$$|z_1|^2 - |z_2|^2 = \ell^2 > 0, \qquad \Omega = \frac{\Gamma}{2\pi\ell^2}.$$

The length scale is ℓ while time scale is $1/\Omega$. Dividing positions by ℓ and measuring time in the variable Ωt changes the coefficient in (2.1) to dimensionless number $\Gamma/(4\pi\ell^2\Omega) = 1/2$.

Proposition 2.1. *A uniformly rotating solution of* (2.1) *is, for* $\theta_0 \in \mathbb{R}$,

$$z_1(t) = \ell\sqrt{\frac{\sqrt{2}+1}{2}}\, e^{i(\theta_0 - \Omega t)}, \qquad z_2(t) = i\ell\sqrt{\frac{\sqrt{2}-1}{2}}\, e^{i(\theta_0 - \Omega t)}. \tag{2.2}$$

Proof. If a quadrupole rotates by a rigid rotation, then

$$\frac{\dot z_1}{z_1} = \frac{\dot z_2}{z_2} \in i\mathbb{R} \iff \frac{3z_1^2 + z_2^2}{|z_1|^2(z_1^2 - z_2^2)} = \frac{z_1^2 + 3z_2^2}{|z_2|^2(z_1^2 - z_2^2)} \in \mathbb{R}.$$

Solving the equation gives $(z_2/z_1)^2 = -3 + 2\sqrt{2}$. Combining with $|z_1|^2 - |z_2|^2 = \ell^2$ gives $|z_1|$ and $|z_2|$ as (2.2) and the frequency $-\Omega = -\Gamma/(2\pi\ell^2)$. □

2.2 The shape variables

To distinguish the shape of a quadrupole from rigid rotation, define

$$Re^{i\phi} = \left(\frac{z_2}{z_1}\right)^2, \qquad \theta = \arg z_1.$$

Here $0 < R < 1$ and angles are chosen continuously along the trajectory. The pair (R, ϕ) is unchanged by a rigid rotation and determines the shape, while θ records that rotation. Since the angular impulse is fixed, the original positions are recovered by

$$z_1 = \frac{\ell e^{i\theta}}{\sqrt{1-R}}, \qquad z_2 = \frac{\ell\sqrt{R}\, e^{i(\theta+\phi/2)}}{\sqrt{1-R}}.$$

After fixing the angular impulse and quotienting by rotations, the planar shape system has one remaining independent first integral H. Its level curves give the trajectories.

The logarithmic derivatives from (2.1) are

$$\frac{\dot z_1}{z_1} = -\frac{i\Omega(1-R)}{2}\frac{3 + Re^{-i\phi}}{1 - Re^{-i\phi}}, \qquad \frac{\dot z_2}{z_2} = -\frac{i\Omega(1-R)}{2R}\frac{1 + 3Re^{-i\phi}}{1 - Re^{-i\phi}}.$$

Using $\dot R/R = 2\,\mathrm{Re}(\dot z_2/z_2 - \dot z_1/z_1)$ and $\dot\phi = 2\,\mathrm{Im}(\dot z_2/z_2 - \dot z_1/z_1)$, we get

$$\begin{aligned}
\dot R &= -\frac{4\Omega R(1-R)^2 \sin\phi}{1 + R^2 - 2R\cos\phi},\\
\dot\phi &= -\frac{\Omega(1-R^2)(1 - 4R + R^2 + 2R\cos\phi)}{R(1 + R^2 - 2R\cos\phi)},\\
\dot\theta &= -\frac{\Omega(1-R)(3 - 2R\cos\phi - R^2)}{2(1 + R^2 - 2R\cos\phi)}.
\end{aligned} \tag{2.3}$$

The rhombus in Proposition 2.1 corresponds to the fixed shape

$$R_* = 3 - 2\sqrt{2}, \qquad \phi = \pi.$$

The third equation then gives $\dot{\theta} = -\Omega$, in agreement with (2.2). In a neighborhood of this fixed shape, introduce the dimensionless deviations $x = \frac{R-R_*}{R_*}$ and $y = \frac{\phi-\pi}{\sqrt{2}}$. Differentiating the first two equations in (2.3) at (R_*, π) gives

$$\partial_\phi \dot{R}\Big|_{(R_*,\pi)} = 2\Omega R_*, \qquad \partial_R \dot{\phi}\Big|_{(R_*,\pi)} = \frac{4\Omega}{R_*}, \qquad \partial_R \dot{R}\Big|_{(R_*,\pi)} = \partial_\phi \dot{\phi}\Big|_{(R_*,\pi)} = 0.$$

Consequently,

$$\begin{pmatrix} \dot{x} \\ \dot{y} \end{pmatrix} = 2\sqrt{2}\Omega \begin{pmatrix} 0 & 1 \\ 1 & 0 \end{pmatrix} \begin{pmatrix} x \\ y \end{pmatrix} + O\Big(\Omega(x^2+y^2)\Big). \tag{2.4}$$

The linearized flow expands on $x = y$ and contracts on $x = -y$. Define the unstable shape variable q and the stable shape variable p by

$$q = \frac{x+y}{2}, \quad p = \frac{x-y}{2}.$$

The next subsection constructs the exact nonlinear trajectory where q increases from 0.

The phase equation has a linear correction that will be useful when comparing orientations between these quadrupoles. Expansion of the third equation in (2.3) gives

$$\dot{\theta} = -\Omega + \Omega(\sqrt{2}-1)x + O\Big(\Omega(x^2+y^2)\Big), \qquad \dot{\phi} = 4\Omega x + O\Big(\Omega(x^2+y^2)\Big).$$

Therefore the adjusted phase

$$\Theta = \theta - \frac{\sqrt{2}-1}{4}(\phi - \pi) \tag{2.5}$$

satisfies $\dot{\Theta} = -\Omega + O(\Omega(x^2+y^2))$. This subtraction removes the linear change of orientation caused by the shape deformation.

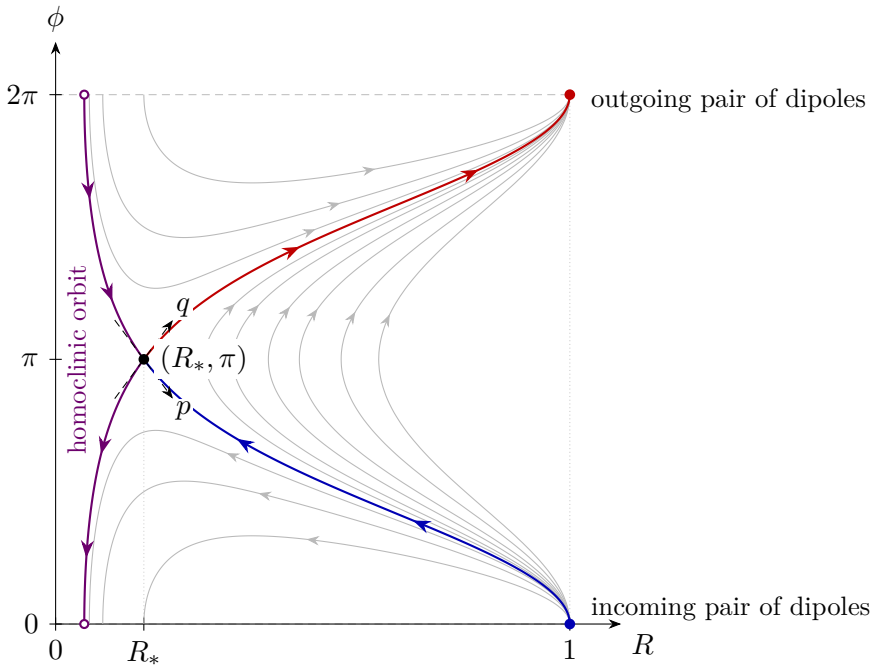


Figure 1: Phase portrait of the (R, ϕ) subsystem of (2.3). Blue and red indicate the stable and unstable branches while purple indicates the homoclinic orbit. The limiting points $(1, 0)$ and $(1, 2\pi)$ represent incoming and outgoing pairs of dipoles, respectively. The small p, q axes are tangent to the stable and unstable directions at (R_*, π). Prepared by ChatGPT 6.1.

2.3 The complete separating trajectory

Proposition 2.2. *There is a solution of* (2.1)*, defined for all* $t \in \mathbb{R}$*, whose shape tends to* (R_*, π) *with* $q > 0$ *and* $p/q \to 0$ *as* $t \to -\infty$*, and for which* $(R, \phi) \to (1, 2\pi)$ *as* $t \to +\infty$*. Every distance between two vortices is bounded below by a positive constant times* ℓ*. There are constants* $\theta_\infty \in \mathbb{R}$ *and* $Z_\infty \in \mathbb{C}$ *such that*

$$\begin{aligned} &z_1(t) - z_2(t) = \ell e^{i\theta_\infty} + O(t^{-2}), \\ &\frac{z_1(t) + z_2(t)}{2} = -i\Omega\ell e^{i\theta_\infty} t + Z_\infty + O(t^{-1}) \qquad (t \to +\infty). \end{aligned} \tag{2.6}$$

After fixing θ_∞*, the constant* Z_∞ *is determined modulo time shift by the conservation of the impulse. The two dipoles have limiting internal distance* ℓ *and limiting velocities* $\pm i\Omega\ell e^{i\theta_\infty}$*.*

Proof. The polar coordinates R, ϕ and the fixed impulse $\ell^2 = |z_1|^2 - |z_2|^2$ give

$$|z_1^2 - z_2^2|^2 = |z_1|^4(1 + R^2 - 2R\cos\phi), \qquad |z_1||z_2| = |z_1|^2\sqrt{R}, \qquad |z_1|^2 = \frac{\ell^2}{1-R}.$$

Substitution yields

$$H = \frac{\Gamma^2}{2\pi}\log\left[\frac{\ell^2}{4}\frac{1 + R^2 - 2R\cos\phi}{\sqrt{R}(1-R)}\right], \qquad \frac{1 + R^2 - 2R\cos\phi}{\sqrt{R}(1-R)} = \frac{4}{\ell^2}e^{2\pi H/\Gamma^2}.$$

Since both H and ℓ are constant, the last expression is conserved and its value at (R_*, π) is 4. Every trajectory approaching this uniformly rotating rhombus lies on this energy level. We select the branch with $R_* < R < 1$ and $\pi < \phi < 2\pi$. The scalar equation below establishes its time direction and its two limits.

Put $s = \sqrt{R}$. The invariant and the choice $\sin\phi < 0$ give

$$\cos\phi = \frac{s^4 + 4s^3 - 4s + 1}{2s^2}, \qquad \sin\phi = -\frac{s^2 + 2s - 1}{2s^2}\sqrt{(1-s^2)(s^2 + 4s - 1)}.$$

These formulas specify a unique continuous function $\phi(s) \in (\pi, 2\pi)$ for $\sqrt{2} - 1 < s < 1$. Substituting the sine into the first equation of (2.3) yields

$$\dot{s} = \frac{\Omega}{4}\frac{(1-s^2)^{3/2}}{s^2}(s^2 + 2s - 1)\sqrt{s^2 + 4s - 1}. \tag{2.7}$$

The solution is specified by the explicit quadrature

$$t = \frac{4}{\Omega}\int_{s(0)}^{s(t)} \frac{\sigma^2\, d\sigma}{(1-\sigma^2)^{3/2}(\sigma^2 + 2\sigma - 1)\sqrt{\sigma^2 + 4\sigma - 1}}.$$

The integrand is positive, is comparable to $(\sigma - (\sqrt{2}-1))^{-1}$ at $\sqrt{2}-1$ and to $(1-\sigma)^{-3/2}$ near 1. Thus the integral tends to $-\infty$ and $+\infty$ at the respective endpoints. It gives a unique increasing $s(t)$ modulo time translation, and the function $\phi(t)$ is given by the preceding trigonometric formulas. The derivative of the invariant with respect to ϕ is nonzero on $\pi < \phi < 2\pi$, so differentiating its constant value together with the equation for $R = s^2$ recovers the second equation in (2.3).

Differentiating the right side of (2.7) at $s = \sqrt{2} - 1$ gives $2\sqrt{2}\Omega$. Hence $s - (\sqrt{2} - 1)$ is a positive constant times $e^{2\sqrt{2}\Omega t}(1 + o(1))$ as $t \to -\infty$. The sine formula gives $y/x \to 1$. The phase equation shows that $\dot{\theta} + \Omega$ is integrable on $(-\infty, 0]$, so $\theta(t) + \Omega t$ has a limit there. This proves convergence to a rotating rhombus.

To verify all distance claims, the two squared opposite-sign distances have sum and product

$$|z_1 - z_2|^2 + |z_1 + z_2|^2 = \frac{2\ell^2(1+s^2)}{1-s^2}, \qquad |z_1 - z_2|^2|z_1 + z_2|^2 = \frac{4\ell^4 s}{1-s^2}.$$

Solving this quadratic gives

$$\min\{|z_1 - z_2|^2, |z_1 + z_2|^2\} = \frac{2\ell^2}{1+s}, \qquad \max\{|z_1 - z_2|^2, |z_1 + z_2|^2\} = \frac{2\ell^2 s}{1-s}. \tag{2.8}$$

As $s \to 1$, the shorter distance tends to ℓ, and the longer one diverges.

The large-time rate also follows directly from (2.7). Expanding at $R = 1$ gives

$$\frac{d}{dt}(1-R) = -2\Omega(1-R)^{3/2}(1+O(1-R)) \implies \frac{d}{dt}(1-R)^{-1/2} = \Omega(1+O(1-R)).$$

First this proves $1 - R \asymp t^{-2}$. The error in the second identity is consequently integrable, so for a constant t_*,

$$(1-R)^{-1/2} = \Omega(t - t_*) + O(t^{-1}) \implies 1 - R = \frac{1}{\Omega^2(t-t_*)^2} + O(t^{-4}).$$

Here O bounds the absolute error by a constant times the displayed quantity, and $\asymp$ bounds the ratio above and below by positive constants.

Relabel the two negative vortices so that $z_1 - z_2$ has smaller magnitude than $z_1 + z_2$. Write $Z = (z_1 + z_2)/2$ for the center of this dipole. The other dipole has center $-Z$. Formula (2.8) and the preceding rate give $|Z| \asymp t$ and $|z_1 - z_2| \asymp \ell$. A dipole with bounded internal distance, viewed at distance comparable to t, has velocity $O(t^{-2})$ and velocity gradient $O(t^{-3})$. These bounds follow by subtracting its two kernels and applying the mean value theorem to $1/\overline{z}$ and its derivative. In addition, the self-induced velocities of the dipole z_1, z_2 are equal to $-i\Gamma/(2\pi\overline{z_1 - z_2})$. Therefore,

$$\frac{d}{dt}(z_1 - z_2) = O(t^{-3}), \qquad \dot{Z} = -\frac{i\Gamma}{2\pi\overline{z_1 - z_2}} + O(t^{-2}).$$

Integrating the first estimate and using the limiting distance proves $z_1 - z_2 = \ell e^{i\theta_\infty} + O(t^{-2})$. Substitution in the second proves $\dot{Z} = -i\Omega\ell e^{i\theta_\infty} + O(t^{-2})$. One more integration gives (2.6).

It remains to identify Z_∞. The exact impulse identity and the two asymptotic expansions just proved give

$$\ell^2 = |z_1|^2 - |z_2|^2 = 2\,\mathrm{Re}(Z\overline{z_1 - z_2}) = 2\ell\,\mathrm{Re}(e^{-i\theta_\infty} Z_\infty) + O(t^{-1}).$$

Indeed, the term of order t in this real part vanishes because $-i\Omega\ell^2 t$ is purely imaginary, and multiplying the $O(t^{-2})$ separation error by $Z = O(t)$ gives $O(t^{-1})$. Letting $t \to +\infty$ proves $\mathrm{Re}(e^{-i\theta_\infty} Z_\infty) = \ell/2$. We may therefore choose the time origin so that $Z_\infty = \frac{1}{2}\ell e^{i\theta_\infty}$, since a time translation by τ adds $i\Omega\tau\ell e^{i\theta_\infty}$ to Z_∞. □

Remark. Time translation and rotation preserve the equations. Thus, if $z_j(t)$ is the trajectory just constructed, then $e^{i(\varphi - \Omega T)} z_j(t - T)$ is also a solution for any $T, \varphi \in \mathbb{R}$.

2.4 How separating dipoles force a rotating quadrupole

2.4.1. The far field of a quadrupole. The second complex moment of the four points is

$$M_2 = \Gamma z_1^2 + \Gamma(-z_1)^2 - \Gamma z_2^2 - \Gamma(-z_2)^2 = 2\Gamma(z_1^2 - z_2^2).$$

For the uniformly rotating rhombus solution (2.2), this gives

$$M_2 = 2\sqrt{2}\Gamma\ell^2 e^{2i(\theta_0-\Omega t)}.$$

Along the separating trajectory, the identity $M_2 = 4\Gamma Z(z_1 - z_2)$ and the estimates just proved give a constant $M_{2,\infty} \in \mathbb{C}$ such that

$$M_2(t) = -\frac{2i}{\pi}\Gamma^2 e^{2i\theta_\infty} t + M_{2,\infty} + O(t^{-1}), \qquad \dot{M}_2(t) = -\frac{2i}{\pi}\Gamma^2 e^{2i\theta_\infty} + O(t^{-2}). \tag{2.9}$$

For $|z| > \max\{|z_1|, |z_2|\}$, the velocity from the quadrupole is

$$\begin{aligned} u(z) &= \frac{i\Gamma}{2\pi}\left(\frac{1}{\overline{z}-\overline{z}_1} + \frac{1}{\overline{z}+\overline{z}_1} - \frac{1}{\overline{z}-\overline{z}_2} - \frac{1}{\overline{z}+\overline{z}_2}\right) \\ &= \frac{i\overline{M_2}}{2\pi\overline{z}^3}\frac{1}{(1-\overline{z}_1^2/\overline{z}^2)(1-\overline{z}_2^2/\overline{z}^2)}. \end{aligned}$$

The zero total circulation and the central symmetry have canceled the first two orders. If $|z| \gg |z_1|, |z_2|$,

$$\partial_{\overline{z}} u(z) = -\frac{3i\overline{M_2}}{2\pi\overline{z}^4} + O\left(\frac{|M_2|\max(|z_1|^2, |z_2|^2)}{|z|^6}\right). \tag{2.10}$$

Here $\partial_{\overline{z}} = (\partial_{x_1} + i\partial_{x_2})/2$. Since this velocity depends analytically on $\overline{z}$, its linear relative velocity near a point z is $S\overline{\zeta}$, where $S = \partial_{\overline{z}} u(z)$ and ζ is the displacement from z. For a quadrupole centered at d_s and a second one centered at d_r, the leading strain at the latter is obtained by substituting $z = d_r - d_s$ in (2.10).

2.4.2. Deformation of the rhombus by external strain. Compute how a prescribed external strain acts on the rhombus. Add the velocity $S(t)\overline{z}$ to each point equation. At the rhombus, z_1 has argument θ and z_2 has argument $\theta + \pi/2$. The external contributions to their logarithmic velocities are therefore $Se^{-2i\theta}$ and $-Se^{-2i\theta}$. The definitions of R, ϕ give

$$\dot{R}\Big|_{\text{ext}} = -4R_* \operatorname{Re}(Se^{-2i\theta}), \qquad \dot{\phi}\Big|_{\text{ext}} = -4\operatorname{Im}(Se^{-2i\theta}).$$

The linearized equation for the unstable shape variable q is

$$\dot{q} = 2\sqrt{2}\Omega q - 2\operatorname{Re}(Se^{-2i\theta}) - \sqrt{2}\operatorname{Im}(Se^{-2i\theta}). \tag{2.11}$$

2.4.3. Cascade of quadrupole separation. Now distinguish the source and receiving configurations by subscripts s and r. The separating source has circulation magnitude Γ_s, length ℓ_s, and frequency $\Omega_s = \Gamma_s/(2\pi\ell_s^2)$. The receiving rhombus has frequency Ω_r and phase $\theta_r - \Omega_r t$. We first make an ideal linear calculation with fixed centers d_s, d_r. Put $\vartheta = \arg(d_r - d_s)$ and retain the term linear in time from (2.9). Its leading strain at the rhombus is

$$S(t) = \frac{3\Gamma_s^2}{\pi^2|d_r - d_s|^4}\, t\, e^{i(4\vartheta - 2\theta_\infty)}.$$

Let $f(t)$ denote the last two terms in (2.11), with this prescribed $S(t)$ and $\theta = \theta_r - \Omega_r t$. The solution of this linear equation is

$$q(t) = e^{2\sqrt{2}\Omega_r t}\left(q(0) + \int_0^t e^{-2\sqrt{2}\Omega_r s} f(s)\, ds\right).$$

The weighted forcing integral contributes to the coefficient of the growing exponential. Using $\int_0^\infty te^{-at}\,dt = a^{-2}$ for $\operatorname{Re} a > 0$ gives

$$\int_0^\infty e^{-2\sqrt{2}\Omega_r t} f(t)\,dt = \frac{\sqrt{3}\,\Gamma_s^2}{2\sqrt{2}\pi^2\Omega_r^2|d_r - d_s|^4} \cos\!\left(4\vartheta - 2\theta_r - 2\theta_\infty + \arctan\frac{1}{\sqrt{2}} - \pi\right). \quad (2.12)$$

Its positive maximum is attained at

$$4\vartheta - 2\theta_r - 2\theta_\infty = \pi - \arctan\frac{1}{\sqrt{2}} \pmod{2\pi}.$$

At this orientation, an error of size δ in the displayed phase combination changes the cosine only by $O(\delta^2)$. Denote the positive maximum by $\kappa = \sqrt{3}\,\Gamma_s^2/(2\sqrt{2}\pi^2\Omega_r^2|d_r - d_s|^4)$. The same integration, now over $[0, t]$, gives

$$q(t) = (q(0) + \kappa)e^{2\sqrt{2}\Omega_r t} - \kappa\big[(1 + 2\sqrt{2}\Omega_r t)\cos(2\Omega_r t) + 2\Omega_r t \sin(2\Omega_r t)\big].$$

In particular, $|q(t) - (q(0)+\kappa)e^{2\sqrt{2}\Omega_r t}| \le \kappa(1+2\sqrt{3}\Omega_r t)$ for $t \ge 0$. Thus an initially unperturbed rhombus, $q(0) = 0$, has a positive growing response. Fix a small threshold $q_* > 0$. When $\kappa/q_* \ll 1$, its first crossing time satisfies

$$T = \frac{1}{2\sqrt{2}\Omega_r} \log\frac{q_*}{\kappa} + O(\Omega_r^{-1}).$$

Normalize the orbit of Proposition 2.2 with $\ell = \Omega = 1$ by $e^{-2\sqrt{2}s}q(s) \to 1$ and $\theta(s) + s \to 0$ as $s \to -\infty$. Fix a large K, let r_{out} be distance between dipole centers at time $s = K$, and let $\beta = K + \theta_\infty$.

Proposition 2.3. *Suppose the receiver quadrupole starts at the rotating rhombus configuration* (2.2) *with* $(\ell, \Omega, \theta_0) = (\ell_r, \Omega_r, \theta_r)$ *and is subject to a continuous prescribed velocity* $S(t)\overline{z}$. *Let* θ_s *be the source dipole angle, and suppose*

$$\left|S(t) - \frac{3\Gamma_s^2 t}{\pi^2|d_r - d_s|^4} e^{i(4\vartheta - 2\theta_s)}\right| \le \frac{\varepsilon\Gamma_s^2}{|d_r - d_s|^4}(t + \Omega_r^{-1}) \quad (2.13)$$

for $t \ge 0$. *Assume*

$$4\vartheta - 2\theta_r - 2\theta_s = \pi - \arctan(1/\sqrt{2}) + \delta \pmod{2\pi}, \qquad |\delta| \le \tfrac{1}{4},$$

and $0 < \kappa < 1$ *with* $\kappa(1 + \log(1/\kappa))^3 \le \varepsilon \ll 1$. *Then the receiver quadrupole changes its configuration to the separating dipoles, and dipole centers first reach distance* $r_{\text{out}}\ell_r$, *at a time* T. *Define* $\theta_d = \arg z_1(T) - \theta(K) + \theta_\infty \pmod{\pi}$. *Then*

$$\Omega_r T = \frac{1}{2\sqrt{2}} \log\frac{1}{\kappa\cos\delta} + K + O(\varepsilon), \qquad \theta_d = \theta_r - \Omega_r T + \beta + O(\varepsilon). \quad (2.14)$$

Here $\theta(K)$ *and* $\theta_\infty = \beta - K$ *belong to the normalized orbit fixed above. The actual dipole angle differs from* θ_d *by* $O(\varepsilon + r_{\text{out}}^{-2})$ *modulo* π. *Constants depend only on* K.

Proof. Set $s = \Omega_r t$ and $D = |z_1|^2 - |z_2|^2$. Central symmetry persists. The unforced separating orbit is an analytic graph $p = h(q)$ near zero, with $h(0) = h'(0) = 0$. On this graph write $q_s = f(q) = 2\sqrt{2}q + O(q^2)$ and set

$$\widehat{q} = q\exp\left(\int_0^q \left[\frac{2\sqrt{2}}{f(r)} - \frac{1}{r}\right] dr\right), \qquad \widehat{p} = p - h(q). \quad (2.15)$$

For $D = \ell_r^2$, write the unforced adjusted phase equation as $\Theta_s = -1 + \psi(\widehat{q}, \widehat{p})$, where (2.5) gives $\psi = O((|\widehat{q}| + |\widehat{p}|)^2)$, and put

$$\widehat{\Theta} = \Theta - \int_0^{\widehat{q}} \frac{\psi(r,0)}{2\sqrt{2}r}\, dr. \tag{2.16}$$

Both integrands are analytic at zero. Differentiation and invariance of $p = h(q)$ give the unforced equations

$$(\widehat{q}, \widehat{p}, \widehat{\Theta})_s = \frac{\ell_r^2}{D}(2\sqrt{2}\widehat{q}, -2\sqrt{2}\widehat{p}, -1) + O(|\widehat{p}|(|\widehat{q}| + |\widehat{p}|))\,.$$

On the unforced separating orbit with $D = \ell_r^2$, $\widehat{p} = 0$, so the remainder vanishes. The normalization gives $\widehat{q} = e^{2\sqrt{2}s}$ and $\widehat{\Theta} = -s$.

The input bound gives $|S(s/\Omega_r)|/\Omega_r \le C\kappa(1+s)$. Fix $q_* > 0$ sufficiently small and consider the fixed interval $0 \le s \le (2\sqrt{2})^{-1}\log(2q_*/\kappa)$. The $\hat{p}$ equation, the exact identity

$$D_s = \frac{2}{\Omega_r}\operatorname{Re}\Big(S\,\overline{z_1^2 - z_2^2}\Big)\,,$$

and the phase $\hat{\Theta}$ equation give

$$|\widehat{p}| \le C\kappa(1+s), \qquad |D/\ell_r^2 - 1| \le C\kappa(1+s)^2, \qquad |\widehat{\Theta} - \theta_r + s| \le C\kappa(1+s)^3. \tag{2.17}$$

Write $\widehat{q}_s = 2\sqrt{2}\widehat{q} + \kappa f_q + r_q$, where κf_q is the forcing obtained by substituting the leading strain term into (2.11) along the rotating rhombus. Since $\kappa(1+s)^3 \le C\varepsilon$, the input error and (2.17) give

$$|r_q(s)| \le C\kappa(1+s)^2|\widehat{q}(s)| + C\varepsilon\kappa(1+s).$$

Since $\widehat{q}(0) = 0$ and $|f_q(r)| \le C(1+r)$, Duhamel's formula and the preceding remainder bound give

$$e^{-2\sqrt{2}s}|\widehat{q}(s)| \le C\kappa + C\kappa\int_0^s (1+r)^2 e^{-2\sqrt{2}r}|\widehat{q}(r)|\, dr.$$

Gronwall's inequality gives $e^{-2\sqrt{2}s}|\widehat{q}(s)| \le C\kappa e^{C\kappa(1+s)^3} \le C\kappa$, since $\kappa(1+s)^3 \le C\varepsilon$. On the chosen interval this implies $|\widehat{q}(s)| \le 2Cq_*$. Together with (2.17), this keeps the shape and impulse strictly inside the coordinate neighborhood for small q_*, ε. ODE continuation therefore gives these estimates on the whole interval. Substituting the growth bound into the remainder estimate now gives

$$\int_0^s e^{-2\sqrt{2}r}|r_q(r)|\, dr \le C\kappa^2(1+s)^3 + C\varepsilon\kappa \le C\varepsilon\kappa.$$

Formula (2.12) gives $\int_0^\infty e^{-2\sqrt{2}s} f_q(s)\, ds = \cos\delta$. Duhamel's formula and $\int_s^\infty e^{-2\sqrt{2}r}|f_q(r)|\, dr \le C(1+s)e^{-2\sqrt{2}s}$ give

$$\frac{\widehat{q}(s)}{\kappa e^{2\sqrt{2}s}} = \cos\delta + O(\varepsilon) + O\Big((1+s)e^{-2\sqrt{2}s}\Big)\,.$$

At the right endpoint, $\widehat{q} = 2q_*(\cos\delta + O(\varepsilon)) > q_*$. Hence there is a first crossing $\widehat{q} = q_*$. At that crossing the growth bound makes the forcing tail $O(\kappa(1 + \log(1/\kappa))) = O(\varepsilon)$, so

$$s = \frac{1}{2\sqrt{2}}\log\frac{q_*}{\kappa\cos\delta} + O(\varepsilon).$$

At this crossing, (2.17) gives $O(\varepsilon)$ agreement with the orbit at time $\log q_*/(2\sqrt{2})$ after rotation by $\theta_r - s + \log q_*/(2\sqrt{2})$.

The remaining orbit segment to K is fixed and collision-free. Gronwall's inequality preserves this error, since the normalized strain there is $O(\kappa(1+\log(1/\kappa)))$. The pair-center distance on the orbit increases strictly and has derivative $2+O(r_{\mathrm{out}}^{-2}) \geq 1$ at K, by (2.8) and (2.6). Hence the first crossing time changes by $O(\varepsilon)$; the initial neighborhood has smaller pair-center distance. Adding the durations and matching phases proves (2.14). The actual dipole angle follows from (2.6) and the same comparison. □

3 Small patch approximation of point vortices

We replace point vortices by small patches. First, the fast rotation of each patch limits its deformation by the external velocity. Second, the patch centroids and moments satisfy the point-vortex equations up to controlled errors. Third, we compare the boundary deformations, centroids, and moments of two patch solutions. The absolute and relative centroid errors are estimated in (3.6) and (3.8), respectively, in Theorem 3.10. Their geometric hypotheses are verified in the later bootstrap arguments in Sections 4–7.

3.1 Contour coordinates near a disk

A uniform patch of circulation Γ and area πa^2 has vorticity $\Gamma/(\pi a^2)$. For vorticity $\sigma\Omega_{\mathrm{patch}}$, $\sigma = \pm 1$, let $w(t)$ be its centroid and let $X(t,\theta)$ follow its boundary particles. Remove translation and the disk's internal rotation by

$$F(t,\theta) = e^{-i\sigma\Omega_{\mathrm{patch}}t/2}\frac{X(t,\theta)-w(t)}{a}, \qquad \theta \in \mathbb{T} = \mathbb{R}/(2\pi\mathbb{Z}).$$

The normalized domain has area π and centroid zero. An initial disk with standard labels has $F(0,\theta) = e^{i\theta}$. Unless specified otherwise, we use the contour norm

$$\|f\|_{C^{1,1/2}} = \|f\|_{L^\infty} + \|f'\|_{L^\infty} + \sup_{\theta\neq\beta}\frac{|f'(\theta)-f'(\beta)|}{\mathrm{dist}_{\mathbb{T}}(\theta,\beta)^{1/2}}, \qquad \mathrm{dist}_{\mathbb{T}}(\theta,\beta) = \min_{k\in\mathbb{Z}}|\theta-\beta+2\pi k|.$$

We use $K(z) = i/(2\pi\bar{z})$. The external velocity of a patch is the sum of the velocities induced by all other patches, including those in the same quadrupole. We estimate its Taylor coefficients with weights 2^k, corresponding to the disk $B(w,2a)$ after scaling lengths by a. Constants may depend on the fixed contour neighborhood, but not on the number of patches or their vorticity magnitudes.

Write D_F for the bounded interior of F. By a normalized contour we mean a positively oriented $C^{1,1/2}$ embedding near $F_0(\theta) = e^{i\theta}$ satisfying

$$|D_F| = \pi, \qquad \int_{D_F} w\, dA(w) = 0, \qquad |F(\theta)-F(\beta)| \geq c\,\mathrm{dist}_{\mathbb{T}}(\theta,\beta).$$

The last inequality prevents distinct boundary labels from approaching the same point too closely. Among these contours,

$$E(\eta)(\theta) = e^{i(\theta+\eta(\theta))}, \qquad \eta \text{ real}, \quad \|\eta\|_{C^{1,1/2}} \text{ small},$$

all describe the unit circle with different labels. Since $1+\eta' > 0$, the labels preserve orientation. We use η for the change of labels and a second coordinate for deformation of the circle.

Lemma 3.1 (Contour equation)**.** *Let $X = C^{1,1/2}(\mathbb{T};\mathbb{C})$, regarded as a real Banach space, and let $F_0(\theta) = e^{i\theta}$. In a neighborhood of F_0 consisting of positively oriented embeddings satisfying the separation bound above, the unit-vorticity boundary velocity*

$$V(F)(\theta) = -\frac{1}{2\pi}\int_0^{2\pi}\log|F(\theta)-F(\beta)|F'(\beta)\,d\beta$$

is a real-analytic map from X to X. On a fixed smaller neighborhood its derivatives satisfy $\|D^m V\| \le C m! r^{-m}$ for some $r > 0$. Area and the two real components of the area centroid are analytic contour functionals. The normalized contours near F_0 admit local analytic coordinates with an analytic inverse.

Proof. To prove real analyticity, we temporarily regard F and its conjugate as independent complex functions F_+, F_- near $e^{i\theta}, e^{-i\theta}$. The original contour equation is recovered by setting $F_- = \overline{F_+}$. On a sufficiently small C^1 neighborhood,

$$\sup_{\theta \neq \beta} \left| \frac{F_\pm(\theta) - F_\pm(\beta)}{e^{\pm i\theta} - e^{\pm i\beta}} - 1 \right| < \frac{1}{2}.$$

Hence

$$\log \frac{F_\pm(\theta) - F_\pm(\beta)}{e^{\pm i\theta} - e^{\pm i\beta}} = \sum_{m \ge 1} \frac{(-1)^{m+1}}{m} \left(\frac{F_\pm(\theta) - F_\pm(\beta)}{e^{\pm i\theta} - e^{\pm i\beta}} - 1 \right)^m.$$

The uniformly convergent series define the complexified logarithm and make the velocity holomorphic on each complex line. The original logarithm is the circle logarithm plus half their sum. Since the circle logarithm is integrable, V is locally bounded in L^∞. Differentiating once gives

$$\partial_\theta V = -\frac{1}{4\pi} \left(F_+'(\theta) \operatorname{pv} \int \frac{F_+'(\beta)}{F_+(\theta) - F_+(\beta)} \, d\beta + F_-'(\theta) \operatorname{pv} \int \frac{F_+'(\beta)}{F_-(\theta) - F_-(\beta)} \, d\beta \right).$$

The first integral is constant. In the second, write $F_+' = (F_+'/F_-')F_-'$. Since F_-' is bounded away from zero, the quotient is uniformly bounded in $C^{1/2}$.

For a nearby curve F, the Cauchy kernel $F'(\beta)/(F(\theta) - F(\beta))$ is bounded by $C|\theta - \beta|^{-1}$. Replacing θ by $\theta + h$ changes it by at most $C|h||\theta - \beta|^{-2}$ when $|\theta - \beta| > 2|h|$. Its principal-value integral on constants is constant. Its truncated integrals are uniformly bounded because subtracting $-(\beta - \theta)^{-1}$ leaves a local remainder $O(|\theta - \beta|^{-1/2})$. For a density $f \in C^{1/2}$, subtract $f(\theta)$. The near and far parts of the Hölder difference are bounded by $C\|f\|_{C^{1/2}}|h|^{1/2}$. The difference of the subtracted constants is multiplied by a bounded truncated integral. Thus the Cauchy integral is uniformly bounded on $C^{1/2}$. Both complexified curves satisfy these estimates, so V is locally bounded in $C^{1,1/2}$.

Apply the one-variable Cauchy formula along each complex line to the velocity and its first derivative. The uniform Hölder bound gives an X bound Cr^{-m} for the Taylor coefficient of order m. The resulting series converges in X and agrees with the velocity in C^0. Polarization, with a smaller r, gives $\|D^m V\| \le C m! r^{-m}$.

Green's formula expresses area and first moments as polynomial contour functionals,

$$\int_{D_F} z^k \, dA = \frac{1}{2i} \int_0^{2\pi} F^k \bar{F} F' \, d\theta.$$

The area is nonzero near F_0, so dividing the first moment by area proves analyticity of the centroid. Write $F = e^{i\theta}(1 + h + ik)$, with h, k real. At the circle, the differentials of area and the first complex moment are $\int h \, d\theta$ and $\int e^{i\theta} h \, d\theta$. Their restriction to $h = 1, \cos\theta, \sin\theta$ is invertible. The analytic implicit-function theorem solves for these three radial coefficients in terms of the others. The coordinate map χ retains the remaining radial modes and all tangential modes. Its inverse inserts the three solved coefficients. Both maps have bounded derivatives on a smaller neighborhood. Since the removed radial directions are invariant under angular translation, uniqueness gives $\chi(e^{-i\varphi} F(\cdot + \varphi)) = \chi(F)(\cdot + \varphi)$. □

The bounded first derivative gives local existence and uniqueness for the contour equation with continuous time-dependent analytic external coefficients. For finitely many separated

patches, each interaction is a nonsingular boundary integral, analytic in the two contours and their centers. The coupled field is locally Lipschitz, so solutions depend continuously on their initial contours and continue while they remain in the chart and stay separated. Reynolds' formula and the divergence-free boundary velocity give the weak transport equation for each patch indicator. Patch areas and vorticity values are preserved.

The periodic Hilbert transform is defined by $He^{im\theta} = -i\,\mathrm{sgn}(m)e^{im\theta}$. On the modes $|m| \geq 1$, it satisfies $H^2 = -I$.

Lemma 3.2. *For a unit-vorticity patch, let τ denote time in the spatial frame rotating at angular velocity $1/2$. The unforced equation for normalized contours is $F_\tau = G(F)$, where $G(F) = V(F) - iF/2$. There are local analytic coordinates (η, z), with η, z real in $C^{1,1/2}$ and $\widehat{z}(0) = \widehat{z}(1) = \widehat{z}(-1) = 0$, such that $z = 0$ corresponds exactly to $F = E(\eta)$, which is a relabelling of the circle. Thus η records the labels on a circle and z measures deformation from it. In these coordinates,*

$$\eta_\tau = O(\|z\|^2), \qquad z_\tau = -\tfrac{1}{2}Hz + Q(\eta)[z, z] + O(\|z\|^3).$$

The coordinate map $F = \mathcal{C}(\eta, z)$ is invariant under phase translation in the sense that $\mathcal{C}(S_\varphi\eta, S_\varphi z) = \mathcal{T}_\varphi\mathcal{C}(\eta, z)$ where $S_\varphi f = f(\cdot + \varphi)$ and $\mathcal{T}_\varphi F = e^{-i\varphi}F(\cdot + \varphi)$.

Proof. The disk velocity is $i\zeta/2$ at the boundary point ζ, so $G(E(\eta)) = 0$. At F_0, write a perturbation as $e^{i\theta}(h+ik)$, with h, k real. For the Fourier coefficients $\widehat{h}(m) = (2\pi)^{-1}\int_0^{2\pi} h(\theta)e^{-im\theta}\,d\theta$, the linearized area and centroid constraints are $\widehat{h}(0) = \widehat{h}(1) = \widehat{h}(-1) = 0$. For $|\zeta| < 1$, the domain variation under a radial displacement h is

$$\frac{i}{2\pi}\int_0^{2\pi} \frac{h(\beta)}{\bar{\zeta} - e^{-i\beta}}\,d\beta = -i\sum_{m\geq 1} \widehat{h}(-m)\bar{\zeta}^{m-1}.$$

Take the interior trace of this formula and combine it with the interior evaluation-point derivative $ie^{i\theta}(h + ik)/2$, which cancels the rotating-frame term in DG. Equivalently, differentiating the contour formula and its circle Fourier series gives

$$DG(F_0)[e^{i\theta}(h + ik)] = -ie^{i\theta}\sum_{m\leq -2} \widehat{h}(m)e^{im\theta} = e^{i\theta}\left(-\tfrac{1}{2}Hh - \tfrac{i}{2}h\right).$$

The resulting linear equations are

$$h_\tau = -\tfrac{1}{2}Hh, \qquad k_\tau = -\tfrac{1}{2}h.$$

Thus $\eta = k + Hh$ is stationary, and the positive and negative modes of h have eigenvalues $i/2$ and $-i/2$, respectively. The Hilbert transform is bounded by the cancellation estimate in Lemma 3.1 and commutes with differentiation. Hence $(h, k) \mapsto (h, k + Hh)$ is a bounded change of coordinates.

In the original (h, k) coordinates, the projections onto these three spaces are

$$P_0(h, k) = (0, k + Hh), \qquad P_\pm(h, k) = (\Pi_\pm h, -H\Pi_\pm h), \qquad \Pi_\pm = \frac{1}{2}(I \pm iH).$$

These formulas allow complex-valued (h, k) satisfying the linearized constraints. For real inputs, P_0 is real and P_- is the conjugate of P_+. The oscillating deformation has both components $(h, -Hh)$ and evolves by $-H/2$.

Fix $\psi(\theta) = \theta + \eta(\theta)$, so that $F_0 \circ \psi = E(\eta)$. A change of variable gives $G(F \circ \psi) = G(F) \circ \psi$. Composition with ψ is bounded on $C^{1,1/2}$, since

$$[(f \circ \psi)']_{1/2} \leq [f']_{1/2}\|\psi'\|_{L^\infty}^{3/2} + \|f'\|_{L^\infty}[\psi']_{1/2}.$$

The same estimate holds for ψ^{-1} in the fixed small neighborhood. Thus a fixed change of labels conjugates $DG(F_0)$ to the differential at any nearby parameterized disk.

We choose coordinates so that $DG(\eta, 0) = \operatorname{diag}(0, -H/2)$ for every small η. Use the constraint chart χ from Lemma 3.1. Write $e(\eta) = \chi(E(\eta))$ and let $A(\eta)$ be the differential of the field in this chart at $e(\eta)$. Fixed relabeling conjugates it to the circle differential, so $A(\eta)(A(\eta)^2 + I/4) = 0$. Consequently the projections onto its three eigenspaces are

$$P_0(\eta) = I + 4A(\eta)^2, \qquad P_\pm(\eta) = -2A(\eta)^2 \mp iA(\eta).$$

They sum to I, have pairwise zero products, and satisfy $AP_0 = 0$ and $AP_\pm = \pm(i/2)P_\pm$. They are analytic and uniformly bounded. Define

$$T(\eta)z = \sum_{\pm} P_\pm(\eta)(\Pi_\pm z, -H\Pi_\pm z), \qquad A(\eta)T(\eta) = -\tfrac{1}{2}T(\eta)H.$$

Since $T(\eta)$ and $P_\pm(\eta)$ differ by $O(\|\eta\|)$ from their values at zero, $T(\eta)$ maps the z variables invertibly onto the range of $P_+(\eta) + P_-(\eta)$, with uniformly bounded inverse. The map $\mathcal{C}(\eta, z) = \chi^{-1}(e(\eta) + T(\eta)z)$ has invertible differential at $(0, 0)$ because its η derivative gives the stationary label changes and its z derivative gives the two oscillating parts. Thus $\mathcal{C}$ gives local analytic coordinates for normalized contours. The field in this chart, again denoted by G, satisfies

$$G(\eta, 0) = 0, \qquad DG(\eta, 0) = \begin{pmatrix} 0 & 0 \\ 0 & -H/2 \end{pmatrix}.$$

$$G(\eta, z) = (O(\|z\|^2), -\tfrac{1}{2}Hz + Q(\eta)[z, z] + O(\|z\|^3)).$$

Coordinate changes in this chart preserve area and centroid after applying $\mathcal{C}$.

The identities $\chi(\mathcal{T}_\varphi F) = S_\varphi \chi(F)$ and $G(\mathcal{T}_\varphi F) = \mathcal{T}_\varphi G(F)$, together with the commutation of H with S_φ, give $\mathcal{C}(S_\varphi \eta, S_\varphi z) = \mathcal{T}_\varphi \mathcal{C}(\eta, z)$ directly from the construction. □

Remark. All coordinate maps and remainder coefficients above are analytic and uniformly bounded on a fixed smaller neighborhood.

Since $e^{-\tau H/2} = \cos(\tau/2)I - \sin(\tau/2)H$ on the deformation space, the norm

$$\|z\|_* := \sup_{\tau \in \mathbb{R}} \|e^{-\tau H/2} z\|_{C^{1,1/2}}$$

is equivalent to the $C^{1,1/2}$ norm and satisfies $\|e^{-\tau H/2} z\|_* = \|z\|_*$.

Fix $\delta_0 < 1/8$ sufficiently small that the preceding coordinates are defined whenever

$$\|\eta\|_{C^{1,1/2}} < \delta_0, \qquad \|F - e^{i(\cdot + \eta)}\|_{C^{1,1/2}} < \delta_0. \tag{3.1}$$

The first inequality gives $1 - \delta_0 < 1 + \eta' < 1 + \delta_0$, so the labels preserve orientation. The two inequalities give a uniform chord-arc bound and place the patch in $B(w, 2a)$. We retain these material labels when the quadrupole changes configuration.

3.2 Normal form with external field

We first remove $Q(\eta)[z, z]$ by a quadratic change $z = w + O(w^2)$. We then remove the terms linear in the external forcing from its value and first derivative at $w = 0$. The final coordinates will again be denoted by (η, z).

Lemma 3.3. *In the coordinates of Lemma 3.2, there is an analytic quadratic change* $z = w + H_2(\eta)[w,w]$ *such that the unforced equation becomes*

$$\eta_\tau = O(\|w\|^2), \qquad w_\tau = -\tfrac{1}{2}Hw + O(\|w\|^3).$$

The change fixes $w = 0$ *and has an analytic inverse. Its coefficients and the remainder coefficients have uniform analytic bounds on a fixed neighborhood. The resulting contour map* $F = \mathcal{C}_{\mathrm{u}}(\eta, w)$ *satisfies*

$$\mathcal{C}_{\mathrm{u}}(\eta, 0) = E(\eta), \qquad \mathcal{C}_{\mathrm{u}}(S_\varphi\eta, S_\varphi w) = \mathcal{T}_\varphi \mathcal{C}_{\mathrm{u}}(\eta, w).$$

This map $\mathcal{C}_{\mathrm{u}}$ *and its inverse have uniformly bounded first two derivatives.*

Proof. Put $\lambda_\pm = \pm i/2$ and $\Pi_\pm = (I \pm iH)/2$, and define

$$H_2(\eta)[v,w] = \sum_{j,a,b\in\{+,-\}} \frac{\Pi_j Q(\eta)[\Pi_a v, \Pi_b w]}{\lambda_a + \lambda_b - \lambda_j}.$$

Every denominator belongs to $\{\pm i/2, \pm 3i/2\}$. Conjugation interchanges the two signs, so $H_2(\eta)[w,w]$ is real for real η, w. Under $z = w + H_2(\eta)[w,w]$, the quadratic terms in the w equation cancel by

$$\Pi_j Q(\eta)[\Pi_a w, \Pi_b w] - (\lambda_a + \lambda_b - \lambda_j)\Pi_j H_2(\eta)[\Pi_a w, \Pi_b w] = 0.$$

Also $D_\eta H_2[\eta_\tau][w,w] = O(\|w\|^4)$, since $\eta_\tau = O(\|w\|^2)$. The derivative of the change is $I + O(\|w\|)$, so it has an analytic inverse on a smaller neighborhood. The analytic bounds in Lemmas 3.1 and 3.2 give the stated coefficient and derivative bounds.

The phase-translation identity in Lemma 3.2 and $\Pi_\pm S_\varphi = S_\varphi \Pi_\pm$ give

$$H_2(S_\varphi\eta)[S_\varphi v, S_\varphi w] = S_\varphi H_2(\eta)[v,w].$$

The identities for $\mathcal{C}_{\mathrm{u}}(\eta, w) := \mathcal{C}(\eta, w + H_2(\eta)[w,w])$ follow. □

Lemma 3.4. *Let* $L > 0$ *and let a positive-vorticity patch of area* πa^2 *have centroid* $d(t)$*. Assume its external velocity* $u_{\mathrm{ext}}(t,\cdot)$ *is curl-free and divergence-free on* $B(d(t), 2a)$*, and write*

$$\frac{u_{\mathrm{ext}}(t, d(t) + a\zeta) - u_{\mathrm{ext}}(t, d(t))}{a} = \sum_{k\geq 1} a_k(t)\bar{\zeta}^k.$$

Assume the coefficients satisfy

$$\sum_{k\geq 1} 2^k |a_k(t)| \leq L, \qquad \sum_{k\geq 1} 2^k |\dot{a}_k(t)| \leq L^2.$$

Let $\Omega_{\mathrm{patch}} > 0$ *be the patch vorticity and put* $\varepsilon = L/\Omega_{\mathrm{patch}}$*. Starting from the coordinates of Lemma 3.3, for sufficiently small* ε *there is an analytic forcing-dependent change which, in time* $\tau = \Omega_{\mathrm{patch}} t$ *and the spatial frame rotating at speed* $\Omega_{\mathrm{patch}}/2$*, gives*

$$\begin{aligned} &\eta_\tau = R_\eta(\eta, z, \tau), \qquad z_\tau = -\tfrac{1}{2}Hz + R_0(\eta, z, \tau), \\ &R_\eta = O(\|z\|^2 + \varepsilon^2), \quad R_0 = O(\|z\|^3 + \varepsilon^2). \end{aligned} \tag{3.2}$$

The forcing-dependent change differs from the identity by $O(\varepsilon)$*, including its first two coordinate derivatives, uniformly in time on a fixed coordinate neighborhood. The remainders are analytic in* (η, z) *on a fixed neighborhood and satisfy*

$$\|D_\eta R_\eta\| \leq C(\|z\|^2 + \varepsilon^2), \qquad \|D_z R_\eta\| \leq C(\|z\| + \varepsilon^2),$$

$$\|D_\eta R_0\| \le C(\|z\|^3 + \varepsilon^2), \qquad \|D_z R_0\| \le C(\|z\|^2 + \varepsilon^2).$$

The resulting map and its inverse between contours F and final coordinates (z, η) have uniformly bounded first two derivatives. At each time t, the forcing-dependent change depends on the external field only through $\{a_k(t)\}_{k\ge1}$. From the next subsection onward, (η, z) denotes these final coordinates unless the original contour coordinates are explicitly specified. When $a_k \equiv 0$, this change is the identity and $z = 0$ describes $E(\eta)$. With an external field, a circle has deformation coordinate $z = O(\varepsilon)$.

Proof. In this proof, write (η, z) for the coordinates (η, w) of Lemma 3.3. Let G be the unforced field in these coordinates. We construct a change for which the external forcing and its first derivative vanish at $z = 0$, up to terms of order ε^2.

The external field in contour coordinates.

By antisymmetry of the Biot–Savart kernel, the self-induced velocity has zero patch average. The centroid therefore follows the patch average of the external velocity. The centered kth external field is

$$\overline{F}^k - \frac{1}{\pi}\int_{D_F} \overline{w}^k \, dA(w).$$

For independent complex variables $\mathbf{F} = (F_+, F_-)$, define

$$m_{k,-}(\mathbf{F}) = \frac{1}{2\pi i(k+1)}\int_0^{2\pi} F_-^{k+1} F_+' \, d\theta,$$
$$m_{k,+}(\mathbf{F}) = -\frac{1}{2\pi i(k+1)}\int_0^{2\pi} F_+^{k+1} F_-' \, d\theta.$$

When $F_+ = F$ and $F_- = \overline{F}$, these are the normalized area averages of $\overline{w}^k$ and w^k. Define the complex vector fields and the forcing in the rotating frame by

$$X_{k,+}(\mathbf{F}) = \big(F_-^k - m_{k,-}(\mathbf{F}), 0\big), \qquad X_{k,-}(\mathbf{F}) = \big(0, F_+^k - m_{k,+}(\mathbf{F})\big),$$

$$f_a(\tau, \mathbf{F}) = \frac{1}{\Omega_{\text{patch}}}\sum_{k\ge1}\big(a_k(t)e^{-i(k+1)\tau/2}X_{k,+}(\mathbf{F}) + \overline{a_k(t)}e^{i(k+1)\tau/2}X_{k,-}(\mathbf{F})\big), \quad t = \frac{\tau}{\Omega_{\text{patch}}}.$$

Each field preserves the complexified area and centroid constraints. The area derivative integrates a derivative of F_-^{k+1} or F_+^{k+1}, and the potentially nonzero first-moment derivative is $\pi m_{k,\pm} - \pi m_{k,\pm} = 0$. When $F_- = \overline{F}_+$, the components of f_a are conjugate, so they represent the physical velocity. Using $\mathcal{C}_{\text{u}}$ also for its complexification, set

$$X_{k,\pm}^{\mathcal{C}_{\text{u}}}(\eta, z) = \big(D\mathcal{C}_{\text{u}}(\eta, z)\big)^{-1} X_{k,\pm}(\mathcal{C}_{\text{u}}(\eta, z)).$$

Consider one term $\xi e^{i\nu\tau}X$, where ξ is constant, $X = X_{k,\pm}^{\mathcal{C}_{\text{u}}}$, and $\nu = \mp(k+1)/2$. Put $A = \operatorname{diag}(0, -H/2)$ and let P_0, P_+, P_- be its projections; Lemma 3.3 gives $G(\eta, 0) = 0$ and $DG(\eta, 0) = A$. Here x, y are pairs of contour coordinates (η, z). Under the substitution $x = y + \xi e^{i\nu\tau}Y(y)$, the coefficient of $\xi e^{i\nu\tau}$ in the transformed forcing is

$$X + DG\,Y - DY\,G - i\nu Y.$$

Put $Y_0(\eta) = Y(\eta, 0)$ and $Y_1(\eta) = DY(\eta, 0)$, and define

$$B(\eta) = DX(\eta, 0) + D^2G(\eta, 0)[\,\cdot\,, Y_0(\eta)].$$

The residual and its first derivative vanish at $z = 0$ if

$$(i\nu - A)Y_0 = X(\eta, 0), \qquad i\nu Y_1 + Y_1 A - AY_1 = B(\eta).$$

Projecting onto the eigenspaces gives

$$Y_0 = \sum_j \frac{P_j X(\eta,0)}{i\nu - \lambda_j}, \qquad P_j Y_1 P_l = \frac{P_j B(\eta) P_l}{i\nu + \lambda_l - \lambda_j}, \qquad \lambda_0 = 0, \quad \lambda_\pm = \pm i/2.$$

The denominators in Y_0 have modulus at least $1/2$. We use the formula for $P_j Y_1 P_l$ when its denominator is nonzero and verify below that its numerator vanishes otherwise. Since A is constant, differentiating the equation for Y_0 gives $(i\nu - A)D_\eta Y_0 = D_\eta X(\eta,0)$. Since $D_\eta DG(\eta,0) = 0$, this agrees with the equation for Y_1 on inputs of the form $(h,0)$. We set $P_j Y_1 P_l = 0$ whenever its denominator vanishes.

Vanishing numerators when the denominator is zero.

Only a forcing term between the two deformation eigenspaces can have zero denominator. We rule it out by computing its angular modes. The circle-fixing action extends to the independent variables by

$$\mathcal{T}_\varphi(F_+, F_-) = (e^{-i\varphi} S_\varphi F_+, e^{i\varphi} S_\varphi F_-).$$

Substitution in the contour moments gives

$$\mathcal{T}_\varphi X_{k,+}(\mathcal{T}_\varphi^{-1}\mathbf{F}) = e^{-i(k+1)\varphi} X_{k,+}(\mathbf{F}).$$

For $X = X^{\mathcal{C}_\mathrm{u}}_{k,+}$, Lemma 3.3 gives

$$S_\varphi G(S_\varphi^{-1} x) = G(x), \qquad S_\varphi X(S_\varphi^{-1} x) = e^{-i(k+1)\varphi} X(x).$$

The $X_{k,-}$ formulas are their conjugates. At the standard circle the projections commute with S_φ, so

$$S_\varphi Y_0 = e^{-i(k+1)\varphi} Y_0, \qquad S_\varphi B S_\varphi^{-1} = e^{-i(k+1)\varphi} B.$$

The second identity includes $D^2 G[\cdot, Y_0]$ by equivariance of $D^2 G$ and the first identity.

Let B_{nm} map the coefficients of angular mode m to those of mode n. Then

$$e^{i(n-m)\varphi} B_{nm} = e^{-i(k+1)\varphi} B_{nm} \quad \text{for every } \varphi, \qquad B_{nm} = 0 \text{ unless } n = m - (k+1).$$

For $X_{k,+}$, the denominator can vanish only when $k = 1$, $\lambda_l = i/2$, and $\lambda_j = -i/2$. The corresponding numerator would require $m \geq 2$ and $n = m - 2 \leq -2$, which is impossible. For $X_{k,-}$ the inequalities are reversed, with the same conclusion. Every nonzero denominator has modulus at least $1/2$.

The calculation first applies to trigonometric polynomials. Fix $0 < \beta < 1/2$. The Cauchy integrals, chart derivatives, and projections are also bounded on $C^{1,\beta}$. Fourier smoothing converges in that norm and commutes with $\Pi_\pm$, so the numerator vanishes on every $C^{1,1/2}$ input.

To transfer this cancellation from the standard circle to $E(\eta)$, fix $\psi(\theta) = \theta + \eta(\theta)$ and $\Psi(x) = \mathcal{C}_\mathrm{u}^{-1}(\mathcal{C}_\mathrm{u}(x) \circ \psi)$, so $\Psi(0) = (\eta, 0)$. Relabeling preserves the contour moments, giving $G \circ \Psi = D\Psi\, G$ and $X \circ \Psi = D\Psi\, X$. Choose an affine Y realizing $Y_0(0), Y_1(0)$ and put $\widetilde{Y} \circ \Psi = D\Psi\, Y$. Since $D^2\Psi[Y, G] = D^2\Psi[G, Y]$,

$$(X + DG\,\widetilde{Y} - D\widetilde{Y}\,G - i\nu\widetilde{Y}) \circ \Psi = D\Psi(X + DG\,Y - DY\,G - i\nu Y).$$

Thus the residual and its first derivative vanish at $(\eta, 0)$. Uniqueness in the value equation gives $\widetilde{Y}(\eta, 0) = Y_0(\eta)$. The derivative equation therefore gives $P_j B(\eta) P_l = 0$ whenever $i\nu + \lambda_l - \lambda_j = 0$.

The displayed formulas define analytic $Y_0(\eta), Y_1(\eta)$ at $z = 0$. Since $Y_1(\eta)(h, 0) = D_\eta Y_0(\eta) h$, the extension $Y(\eta, z) = Y_0(\eta) + Y_1(\eta)(0, z)$ has the prescribed value and first derivative at $z = 0$.

Summation and remainder estimates.

Shrink the contour neighborhood so that $|F_\pm| \le 3/2$, and denote the solutions just constructed by $Y_{k,\pm}$. Conjugation in the complexified chart allows the choice $Y_{k,-}(x) = \overline{Y_{k,+}(\overline{x})}$. For each fixed derivative order, the derivatives of the powers and contour moments are bounded by a polynomial in k times $(3/2)^k$. The projection, denominator, and chart bounds therefore give fixed p, C such that

$$\|Y_{k,+}\|_{C^3} + \|Y_{k,-}\|_{C^3} \le C(1+k)^p (3/2)^k.$$

Here C^m denotes the supremum of the function and its first m Fréchet derivatives on a fixed smaller chart neighborhood. Summing over $k \ge 1$ and $\sigma \in \{+,-\}$ gives

$$\sum_{k,\sigma} \frac{|a_k|}{\Omega_{\text{patch}}} \|Y_{k,\sigma}\|_{C^3} \le C\varepsilon, \qquad \sum_{k,\sigma} \frac{|\dot a_k|}{\Omega_{\text{patch}}^2} \|Y_{k,\sigma}\|_{C^2} \le C\varepsilon^2.$$

Here we used $\sup_{k\ge 1}(1+k)^p(3/4)^k < \infty$. Set

$$\mathcal{S}(\tau, x) = \frac{1}{\Omega_{\text{patch}}} \sum_{k\ge 1} \big(a_k(t) e^{-i(k+1)\tau/2} Y_{k,+}(x) + \overline{a_k(t)} e^{i(k+1)\tau/2} Y_{k,-}(x)\big), \qquad t = \frac{\tau}{\Omega_{\text{patch}}}.$$

Then $\mathcal{S}$ is real on the real chart. Differentiating an exponential adds a factor bounded by $k+1$, which is absorbed by increasing p. Hence $\|\mathcal{S}\|_{C^3} + \|\partial_\tau \mathcal{S}\|_{C^2} \le C\varepsilon$. The part containing $\dot a_k$ is $O(\varepsilon^2)$ in C^2, while $\mathcal{S}$ uses only a_k. For small ε, $\|D\mathcal{S}\| \le 1/2$, so $x = y + \mathcal{S}(\tau, y)$ has an inverse on a smaller fixed neighborhood with uniformly bounded first two derivatives. Products of two corrections, including their required derivatives, are $O(\varepsilon^2)$. The first-order residual and its first z derivative vanish at $z = 0$, so the residual is bounded by $C\varepsilon\|z\|^2$.

Let $R_\eta^{\mathrm{u}} = O(\|z\|^2)$ and $R_0^{\mathrm{u}} = O(\|z\|^3)$ denote the unforced remainders from Lemma 3.3. Then

$$R_\eta = R_\eta^{\mathrm{u}} + O(\varepsilon\|z\|^2 + \varepsilon^2),$$
$$R_0 = R_0^{\mathrm{u}} + O(\varepsilon\|z\|^2 + \varepsilon^2).$$

All remainder coefficients are analytic and uniformly bounded on a fixed larger complex neighborhood. If $\mathcal{R}(\eta, 0) = D_z\mathcal{R}(\eta, 0) = 0$, then

$$\mathcal{R}(\eta, z) = \int_0^1 (1-s) D_z^2 \mathcal{R}(\eta, sz)[z, z]\, ds.$$

This identity, its third-order analogue, and the uniform analytic derivative bounds give the asserted estimates, including the $C\varepsilon^2$ bound for the η derivative of the forcing residual. The mixed terms are absorbed by

$$\varepsilon\|z\|^2 \le C(\|z\|^3 + \varepsilon^3), \qquad \varepsilon\|z\| \le C(\|z\|^2 + \varepsilon^2), \qquad \varepsilon \le 1.$$

This proves (3.2) and its derivative bounds. □

We next verify the coefficient bounds of Lemma 3.4 from the distances and circulations of the other patches.

Lemma 3.5 (External velocity estimates)**.** *Consider a finite collection of transported bounded uniform patches with separated $C^{1,1/2}$ boundaries. Let a distinguished one-sign patch of circulation Γ and centroid $d(t)$ be contained in $B(d(t), 2a)$. Suppose the remaining vorticity ω_S is at distance at least $\rho \ge 8a$ from $d(t)$, and set*

$$u_S = K * \omega_S, \qquad L_1(x) = \int \frac{|\omega_S(y)|}{|x-y|^2}\, dA(y), \qquad L_0 = L_1(d) + |\Gamma|/\rho^2,$$

where x is outside the source supports. For the coupled Euler evolution,

$$|D^k u_S(d)| \le C^{k+1} k! L_1(d) \rho^{-(k-1)}, \qquad \left|\frac{d}{dt} D^k u_S(t, d(t))\right| \le C^{k+1}(k+1)! L_0^2 \rho^{-(k-1)}, \qquad k \ge 1.$$

Hence, for a/ρ sufficiently small, the normalized external coefficients a_k of Lemma 3.4, with $u_{\text{ext}} = u_S$, satisfy

$$\sum_{k\ge 1} 2^k |a_k| \le C L_0, \qquad \sum_{k\ge 1} 2^k |\dot a_k| \le C L_0^2.$$

The constants are independent of the internal vorticity magnitudes and the number of patches. On a time interval where L_0 is uniformly bounded, these are the coefficient bounds of Lemma 3.4 with $L = C \sup_t L_0(t)$.

Proof. Differentiating K outside the supports gives the spatial derivative bound. If the sources are transported by u_S alone, transport and integration by parts give

$$(\partial_t + u_S(x)\cdot\nabla_x) D^k u_S(x) = \int D^{k+1} K(x-y)[u_S(x) - u_S(y)]\omega_S(y)\, dA(y).$$

Substituting $u_S = K * \omega_S$ and interchanging y, z gives the double-integral kernel

$$\begin{aligned} B_k(x,y,z) = \tfrac{1}{2}\big(&D^{k+1}K(x-y)[K(x-z) - K(y-z)] \\ &+ D^{k+1}K(x-z)[K(x-y) - K(z-y)]\big). \end{aligned}$$

Here the last derivative index is contracted with the velocity. For simplicity, translate x to zero. For $|y| \le |z|/2$, the first velocity difference is at most $C|y|/|z|^2$ by the mean value theorem, and the second is at most $C/|y|$. The two terms are therefore bounded, respectively, by

$$C^{k+1}(k+1)!\, |y|^{-k-1}|z|^{-2} \qquad \text{and} \qquad C^{k+1}(k+1)!\, |y|^{-1}|z|^{-k-2}.$$

The case $|z| \le |y|/2$ is symmetric. When $|y|$ and $|z|$ are comparable and $|y - z| \ge c|y|$, each term is at most $C^{k+1}(k+1)!|y|^{-k-3}$. In the remaining case the singular part is

$$\begin{aligned} &-\tfrac{1}{2}[D^{k+1}K(-y) - D^{k+1}K(-z)]K(y-z), \\ &|D^{k+1}K(-y) - D^{k+1}K(-z)| \le C^{k+1}(k+1)!|y-z||y|^{-k-3}. \end{aligned}$$

The factor $|y - z|$ cancels the singularity of $K(y - z)$, and the nonsingular terms have the same bound. We used $|D^m K(x)| \le C^{m+1} m! |x|^{-m-1}$, absorbing the additional factor $k + 2$ into C^{k+1}. Thus

$$|B_k(x,y,z)| \le C^{k+1}(k+1)!\left(|x-y|^{-k-1}|x-z|^{-2} + |x-y|^{-2}|x-z|^{-k-1}\right).$$

At $x = d$, integration gives $C^{k+1}(k+1)!\rho^{-(k-1)}L_1(d)^2$. The identities follow for bounded patch vorticity by first excluding $|y - z| < \epsilon$ and then using this integrable bound to pass to the limit.

The distinguished patch induces velocity at most $C|\Gamma|/|d - y|$ on the source supports. Its additional transport contribution is bounded by

$$C^{k+1}(k+1)!|\Gamma| \int \frac{|\omega_S(y)|}{|d-y|^{k+3}}\, dA(y) \le C^{k+1}(k+1)!\rho^{-(k-1)}\frac{|\Gamma|}{\rho^2} L_1(d).$$

The centroid equation and the one-sign assumption give

$$\dot d = \Gamma^{-1}\int \omega_{\text{patch}}(z) u_S(z)\, dA(z), \qquad |\dot d - u_S(d)| \le C a L_1(d).$$

Multiplication by the spatial bound for $D^{k+1}u_S$ shows that changing to the path $d(t)$ adds at most

$$C^{k+1}(k+1)!\rho^{-(k-1)}\frac{a}{\rho}L_1(d)^2.$$

Since $a/\rho \le 1/8$, the sum is bounded by $C^{k+1}(k+1)!\rho^{-(k-1)}L_0^2$.

The external velocity is anti-holomorphic, so $a_k = a^{k-1}\partial_{\bar z}^k u_S(d)/k!$. The derivative estimates yield geometric series with ratio $2Ca/\rho$, and the time-derivative series has an additional factor $k+1$. Both sums have the asserted bounds when $2Ca/\rho < 1/2$. □

3.3 Uniform boundary control

Decrease the fixed δ_0 in (3.1), if necessary, so that the coordinate changes of Lemma 3.4 and their inverses are defined throughout that neighborhood. We keep this choice of δ_0 below.

Lemma 3.6. *Let a vortex patch have uniform vorticity magnitude Ω_{patch}, area πa^2, and centroid $d(t)$. Assume that an external velocity field satisfies the bounds of Lemma 3.4, with constant L. Suppose the initial normalized contour satisfies, for some real η_0,*

$$\|\eta_0\|_{C^{1,1/2}} \le \delta_0/2, \qquad \|F(0) - E(\eta_0)\|_{C^{1,1/2}} \le C_0\varepsilon, \qquad \varepsilon = \frac{L}{\Omega_{\text{patch}}}.$$

There are $c, C, \varepsilon_0 > 0$, depending on the fixed coordinate maps, C_0, and δ_0, such that for $\varepsilon \le \varepsilon_0$, the normalized contour stays within $C\varepsilon^{2/3}$ of a parameterized unit circle for

$$0 \le t \le c\frac{\Omega_{\text{patch}}^{1/3}}{L^{4/3}}.$$

The original label coordinate satisfies $\|\eta(t) - \eta_0\|_{C^{1,1/2}} \le \delta_0/4$. The patch is therefore contained in $B(d(t), a(1 + C\varepsilon^{2/3}))$. The condition $\Omega_{\text{patch}} \ge C(T^3L^4 + L)$ suffices for a fixed time T, provided the external hypotheses hold on $[0, T]$.

Proof. Reflection reduces to positive vorticity and preserves the norms and external hypotheses. The map $\mathcal{C}_{\text{u}}$ of Lemma 3.3 satisfies $\mathcal{C}_{\text{u}}(\eta, 0) = E(\eta)$ and has bounded derivatives and inverse derivatives. The additional change in Lemma 3.4 is $O(\varepsilon)$. Hence the final coordinates satisfy

$$\|z(0)\| \le C\varepsilon, \qquad \|\eta(0) - \eta_0\| \le C\varepsilon.$$

Put $\rho = \varepsilon^{2/3}$ and use the equivalent norm $\|\cdot\|_*$ defined in the remark following Lemma 3.2. By Duhamel's formula,

$$\|z(\tau)\|_* \le C\varepsilon + C\int_0^\tau (\|z(\sigma)\|_*^3 + \varepsilon^2)\, d\sigma.$$

Under the bootstrap assumptions $\|z\|_* \le C_*\rho$ and $0 \le \tau \le c\rho^{-2}$, choose C_* large, then c small, and finally ε_0 small. Since $\rho^3 = \varepsilon^2$,

$$\|z(\tau)\|_* \le C\varepsilon + C(C_*^3 + 1)c\rho \le \frac{C_*\rho}{2}.$$

Also,

$$\|\eta(\tau) - \eta(0)\| \le C\int_0^{c\rho^{-2}} (C_*^2\rho^2 + \varepsilon^2)\, d\sigma \le C(C_*^2 + 1)c.$$

Choose c so that $C(C_*^2 + 1)c \le \delta_0/8$. Returning to the original coordinates changes (η, z) by $O(\rho^2 + \varepsilon) = O(\varepsilon)$. Decrease ε_0 so that the initial and coordinate-change errors together are at most $\delta_0/8$ and $C\rho < \delta_0/2$. In the original coordinates of Lemma 3.2, this gives

$$\|\eta(t) - \eta_0\|_{C^{1,1/2}} \le \delta_0/4, \qquad \|F(t) - E(\eta(t))\|_{C^{1,1/2}} \le C\rho < \delta_0/2.$$

Since $\|\eta_0\|_{C^{1,1/2}} \le \delta_0/2$, both inequalities are strictly inside (3.1), so local existence continues the solution. Since $\tau = \Omega_{\text{patch}} t$, the time interval is the one stated. The radial displacement is bounded by the contour distance, which gives the support estimate. □

For $\Omega_{\text{patch}} = A\Omega^4$ and $L = C_0\Omega$, Lemma 3.6 gives time $cA^{1/3}C_0^{-4/3}$ and deformation $C(C_0/A)^{2/3}\Omega^{-2}$. Thus choosing A large and then Ω large gives the following consequence.

Corollary 3.7. *For an initial disk with standard labels $F(0,\theta) = e^{i\theta}$, $\Omega_{\text{patch}} = A\Omega^4$, and $L = C_0\Omega$, choose A large and then Ω large. On every initial time interval $[0,T] \subset [0,2]$ where the normalized external coefficients satisfy the bounds of Lemma 3.4, the original contour coordinates satisfy*

$$\|\eta(t)\|_{C^{1,1/2}} \le \delta_0/2, \qquad \|F(t) - e^{i(\cdot+\eta(t))}\|_{C^{1,1/2}} \le C_A\Omega^{-2} < \delta_0/2.$$

Thus the contour cannot first exit through (3.1).

For later use, the hypotheses for each patch are, in the physical spatial axes,

$$\begin{aligned} \frac{u_{\text{ext}}(t, w(t) + a\zeta) - u_{\text{ext}}(t, w(t))}{a} &= \sum_{k\ge 1} a_k(t)\bar{\zeta}^k, \\ \sum_{k\ge 1} 2^k |a_k(t)| \le C_0\Omega, \qquad & \sum_{k\ge 1} 2^k |\dot{a}_k(t)| \le C_0^2\Omega^2. \end{aligned} \tag{3.3}$$

Here $w(t)$ is the patch centroid, $\dot{a}_k$ differentiates along $w(t)$, and C_0 is fixed. The weight 2^k controls the series on $|\zeta| \le 2$, corresponding to $B(w(t), 2a)$, where the external field is curl-free and divergence-free. These coefficients exclude the internal rotation $A\Omega^4/2$. The same A works for a larger set of quadrupole configurations provided (3.3) holds with the same C_0.

3.4 Relative estimates in common coordinates

We compare two distinct patch solutions under different external velocity field in the coordinates of Lemma 3.4 constructed from the first one's external field. Consider two patches with the same signed circulation Γ, area πa^2, and vorticity magnitude Ω_{patch}. Center each normalized contour at its centroid, use the same initial boundary-label convention, and rotate both frames at the same signed internal rate. Suppose both patches satisfy the hypotheses of Lemma 3.6, with the same bound L for their normalized external coefficients. Denote these coefficients by $a_k^{(j)}$, $j = 1, 2$, as defined in Lemma 3.4 at the respective centroids with the common radius a.

Lemma 3.8. *Put $\rho = (L/\Omega_{\text{patch}})^{2/3}$ and apply the coordinate change of Lemma 3.4, constructed from the first patch's normalized external coefficients, to both contours. In these coordinates $(\eta^{(j)}, z^{(j)})$, $j = 1, 2$, write $\triangle$ for the second value minus the first at the same physical time. Define*

$$\triangle z(t) = z^{(2)}(t) - z^{(1)}(t), \qquad W_{\text{bdry}} = \|\triangle z\|_* + \rho\|\triangle\eta\|,$$

where $\|\cdot\|_*$ is the norm defined in the remark following Lemma 3.2. Then, on the common time interval from Lemma 3.6, $0 \le t \le c\Omega_{\text{patch}}^{1/3}/L^{4/3}$,

$$W_{\text{bdry}}(t) \le e^{C\Omega_{\text{patch}}\rho^2 t} W_{\text{bdry}}(0) + C\int_0^t e^{C\Omega_{\text{patch}}\rho^2(t-r)} \sum_{k\ge 1} 2^k |\triangle a_k(r)|\, dr. \tag{3.4}$$

Identical initial normalized embeddings give $W_{\text{bdry}}(0) = 0$. The estimate requires no time derivative of $\triangle a_k$.

Proof. Let $\tau = \Omega_{\text{patch}} t$ and let $\Phi(\tau, F)$ be the coordinate change of Lemma 3.4 constructed from the first list of normalized external coefficients. Denote by $f_j(\tau, F)$ the centered external contour field determined by the normalized external coefficients $a_k^{(j)}$. At the same contour F, the difference of the transformed fields is

$$D_F\Phi(\tau,F)\big(f_2(\tau,F)-f_1(\tau,F)\big), \qquad \|D_F\Phi(f_2-f_1)\| \le \frac{C}{\Omega_{\text{patch}}}\sum_{k\ge1} 2^k|\triangle a_k|.$$

Indeed, the external contour field, including subtraction of its patch average, is linear in the coefficients. Both equations contain the same $\partial_\tau\Phi(\tau, F)$. Its change with F is included in the state derivatives of the first transformed field, so no derivative of $\triangle a_k$ occurs.

Choose a smaller convex coordinate ball. Confinement and the $O(L/\Omega_{\text{patch}})$ forcing-dependent change give $\|z\| \le C\rho$ at both states and on the segment joining them. The first transformed field is

$$\eta_\tau = R_\eta, \qquad z_\tau = -\tfrac{1}{2}Hz + R_0.$$

By Lemma 3.4, $L/\Omega_{\text{patch}} = \rho^{3/2}$ gives

$$\|D_\eta R_\eta\| \le C\rho^2, \qquad \|D_z R_\eta\| \le C\rho, \qquad \|D_\eta R_0\| \le C\rho^3, \qquad \|D_z R_0\| \le C\rho^2.$$

Integrating these derivatives along the segment gives

$$D^+\|\triangle\eta\| \le C\rho^2\|\triangle\eta\| + C\rho\|\triangle z\|_* + \frac{C}{\Omega_{\text{patch}}}\sum_{k\ge1} 2^k|\triangle a_k|,$$

$$D^+\|\triangle z\|_* \le C\rho^3\|\triangle\eta\| + C\rho^2\|\triangle z\|_* + \frac{C}{\Omega_{\text{patch}}}\sum_{k\ge1} 2^k|\triangle a_k|.$$

Here $D^+h(\tau) = \limsup_{s\downarrow0}(h(\tau+s)-h(\tau))/s$. For the second inequality we used Duhamel's formula and $\|e^{-\tau H/2}z\|_* = \|z\|_*$ from the remark following Lemma 3.2. Multiplying the first inequality by ρ and adding yields

$$D^+W_{\text{bdry}} \le C\rho^2 W_{\text{bdry}} + \frac{C}{\Omega_{\text{patch}}}\sum_{k\ge1} 2^k|\triangle a_k|.$$

Gronwall's inequality and $\tau = \Omega_{\text{patch}} t$ prove (3.4), with prefactor one on the initial value because $e^{-\tau H/2}$ preserves $\|\cdot\|_*$. The differential inequality applies from any later time in the interval. Since both contours use the same map, identical initial embeddings give $W_{\text{bdry}}(0) = 0$. Reflection as in Lemma 3.6 gives the assertion for negative vorticity. □

Lemma 3.9. *For the patches of Lemma 3.8, let $d^{(j)}$ denote their centroids and set*

$$M_k^{(j)} = \int (z-d^{(j)})^k \omega^{(j)}(z)\,dA(z), \qquad I^{(j)} = \int |z-d^{(j)}|^2\omega^{(j)}(z)\,dA(z).$$

Then, for $k \ge 2$,

$$|\triangle M_k| \le C_k|\Gamma|a^k W_{\text{bdry}}, \qquad |\triangle I| \le C|\Gamma|a^2\rho W_{\text{bdry}}.$$

Each patch satisfies $|I^{(j)} - \Gamma a^2/2| \le C|\Gamma|a^2\rho^2$. The constants may be chosen so that $C_k \le C(k+1)^2(3/2)^k$, where C depends only on the fixed contour neighborhood and coordinate maps, not on k, a, or Γ. For the same harmonic field U on a fixed disk larger than both centered patches,

$$\left|\frac{1}{\Gamma}\int U(z-d^{(2)})\omega^{(2)}(z)\,dA(z) - \frac{1}{\Gamma}\int U(z-d^{(1)})\omega^{(1)}(z)\,dA(z)\right| \le Ca^2\sup|D^2U|W_{\text{bdry}}.$$

Proof. For fixed $k \geq 2$, Green's formula gives the normalized moment functional

$$\mathcal{M}(F) = \frac{1}{\pi} \int_{D_F} w^k \, dA(w) = \frac{1}{2\pi i} \int_0^{2\pi} F^k \overline{F} \, \partial_\theta F \, d\theta.$$

The common rotation of the two frames multiplies both moments by the same factor of modulus one, so it does not affect their difference in absolute value. On the fixed contour neighborhood, $\|F\|_{L^\infty} \leq 3/2$ and $\|F\|_{C^{1,1/2}} \leq C$. Differentiating the displayed formula once or twice gives

$$\|D\mathcal{M}(F)\| + \|D^2\mathcal{M}(F)\| \leq C(k+1)^2(3/2)^k.$$

Indeed, each derivative of F^k contributes at most a factor k, while $\overline{F}$ and $\partial_\theta F$ depend linearly on F. The coordinate maps of Lemma 3.4 have bounded first two derivatives, so the same bound holds in contour coordinates. This functional vanishes on every $E(\eta)$. In the unforced coordinates it therefore satisfies

$$\mathcal{M}(\eta, z) = \int_0^1 D_z\mathcal{M}(\eta, rz) z \, dr, \qquad \|D_z\mathcal{M}\| \leq C_k, \qquad \|D_\eta\mathcal{M}\| \leq C_k\|z\|.$$

The forcing-dependent change is $O(L/\Omega_{\text{patch}}) = O(\rho^{3/2})$ in C^2. Thus the z and η derivatives of the normalized kth moment are bounded by C_k and $C_k\rho$ on $\|z\| \leq C\rho$. Integrating along the segment between the states gives

$$\frac{|\triangle M_k|}{|\Gamma| a^k} \leq C_k(\|\triangle z\|_* + \rho\|\triangle\eta\|) = C_k W_{\text{bdry}}.$$

For the averaging error, subtract $U(0) + DU(0)x$. The linear term has zero patch average by the centroid constraint, and the remainder has zero disk average by the mean-value property. Taylor's formula and Cauchy estimates give z and η derivatives bounded by $Ca^2 \sup|D^2U|$ and $Ca^2\rho \sup|D^2U|$. Integrating along the segment gives the asserted bound. Here U is fixed, and its difference is estimated separately in the centroid equation.

For the radial moment, closeness in C^1 gives $\partial_\theta \arg F = \operatorname{Im}(F'/F) > 0$. The boundary is therefore a radial graph $a(1 + h(\theta))e^{i\theta}$ in centered physical coordinates, with $\|h\|_{L^\infty} \leq C\rho$. Area conservation and polar integration give

$$\int_0^{2\pi} (2h + h^2) \, d\theta = 0, \qquad I = \frac{\Gamma a^2}{4\pi} \int_0^{2\pi} (1+h)^4 \, d\theta.$$

Consequently,

$$I - \frac{\Gamma a^2}{2} = \frac{\Gamma a^2}{\pi} \int_0^{2\pi} \left(h + \frac{h^2}{2}\right)^2 d\theta.$$

The normalized impulse $I/(\Gamma a^2) = (4\pi i)^{-1} \int F\overline{F}^2 F' \, d\theta$ is an analytic contour functional. In the unforced coordinates, $\|h\|_{L^\infty} \leq C\|z\|$, so $I/(\Gamma a^2) - 1/2 = O(\|z\|^2)$. Its z and η derivatives are therefore $O(\|z\|)$ and $O(\|z\|^2)$. The forcing-dependent change is $O(\rho^{3/2})$ in C^2 and adds at most $C\rho\rho^{3/2} \leq C\rho^2$ to the η derivative. The z derivative remains bounded by $C\rho$. Thus

$$\frac{|\triangle I|}{|\Gamma| a^2} \leq C(\rho\|\triangle z\|_* + \rho^2\|\triangle\eta\|) = C\rho W_{\text{bdry}}.$$

□

3.5 The centroid and moment theorem

Consider four patches with circulations $\Gamma_1 = \Gamma_2 = \Gamma$ and $\Gamma_3 = \Gamma_4 = -\Gamma$, where

$$\Gamma = 2\pi\Omega\ell^2, \qquad 0 < \ell \le 1, \qquad a^2 = \frac{2\ell^2}{A\Omega^3}.$$

Write ω_h for the vorticity of patch h, $\omega_{\text{quad}} = \sum_{h=1}^4 \omega_h$, and ω for the total vorticity. Let ζ_h be their centroids, $d = \frac{1}{4}\sum_h \zeta_h$, and $U = K * (\omega - \omega_{\text{quad}})$ the velocity from all other quadrupoles. Write the positive centroids as $d + \delta \pm z_1$ and the negative centroids as $d - \delta \pm z_2$. Recall $D = |z_1|^2 - |z_2|^2$ and define the moments M_k and the impulse I

$$M_1 = \int z\omega_{\text{quad}}(z)\, dA(z) = 4\Gamma\delta, \qquad M_k = \int (z-d)^k \omega_{\text{quad}}(z)\, dA(z), \qquad k \ge 2,$$

$$I = \int |z-d|^2 \omega_{\text{quad}}(z)\, dA(z).$$

The integrals include all four patches with their signs. Since $\sum_{h=1}^4 \Gamma_h = 0$, M_1 is independent of the origin. Put $\rho = C_A\Omega^{-2}$, with C_A large enough for Corollary 3.7.

For part (ii) and the relative estimate in part (iii) below, fix $c, R > 0$ and suppose that, for $j = 1, 2$ and throughout the comparison interval,

$$\max_{1\le h\le 4} \frac{|\zeta_h^{(j)} - d^{(j)}|}{\ell} \le \frac{R}{2}, \qquad \min_{h\ne g} \frac{|\zeta_h^{(j)} - \zeta_g^{(j)}|}{\ell} \ge c.$$

For $j = 1, 2$, assume $U^{(j)}$ is anti-holomorphic on $B(d^{(j)}, 2R\ell)$ and satisfies $|DU^{(j)}| \le C\mathsf{S}$ and $|D^2U^{(j)}| \le C\mathsf{T}$ on $B(d^{(j)}, R\ell)$, with $\mathsf{S}, \mathsf{T} \le 1$. Define

$$\begin{aligned} |Z| &= \ell^{-1}\sum_{h=1}^4 |\triangle(\zeta_h - d)|, \qquad \|\triangle A\|_R = \sum_{k\ge 1} R^k |\triangle A_k|, \\ \ell^{-1}[U^{(j)}(t, d^{(j)} + \ell z) - U^{(j)}(t, d^{(j)})] &= \sum_{k\ge 1} A_k^{(j)}(t)\bar{z}^k. \end{aligned} \tag{3.5}$$

The expansions use the same physical axes and their respective centers. Constants in the relative estimates may depend on c and R, but not on the scale or the number of quadrupoles.

Theorem 3.10. *Consider four patches in an Euler evolution of a finite collection of disjoint uniform patches with $C^{1,1/2}$ boundaries on an initial time interval $[0, T] \subset [0, 2]$. Suppose these four patches start from disjoint disks with the parameters above and the standard labels $F_h(0, \theta) = e^{i\theta}$. Assume their centroids have mutual distances at least $c\ell$ and their contours satisfy* (3.1)*. For each patch h, assume* (3.3) *with $w = \zeta_h$ and*

$$u_{\text{ext}} = K * (\omega - \omega_h) = U + \sum_{g\ne h} K * \omega_g.$$

Thus (3.3) *controls the field induced by the other three patches together with U.*

Suppose U is anti-holomorphic on a neighborhood of the convex hull of $\bigcup_h \overline{B(\zeta_h, 2a)}$, where $\sup|DU| \le C\mathsf{S}$ and $\sup|D^2U| \le C\mathsf{T}$ with $\mathsf{S}, \mathsf{T} \le 1$.

Choose A and the lower threshold for Ω as in Corollary 3.7. The constants below may depend on the fixed contour charts, separation and analytic margins, C_0, and A, but not on the scale or the number of other patches.

For (ii) and the relative estimate in (iii), assume also the normalized size, separation, and analyticity bounds stated before the theorem. Then:

(i) For each patch h, the label coordinate η_h and the normalized contour F_h satisfy

$$\|\eta_h(t)\|_{C^{1,1/2}} \le \delta_0/2, \qquad \|F_h(t) - e^{i(\cdot+\eta_h(t))}\|_{C^{1,1/2}} \le \rho < \delta_0/2, \qquad 0 \le t \le T.$$

These bounds improve (3.1)*. The exact centroid equations are*

$$\dot\zeta_h = \sum_{g\neq h} \Gamma_g K(\zeta_h - \zeta_g) + U(\zeta_h) + E_h, \qquad |E_h| \le C\Omega\ell\frac{a^2}{\ell^2}\rho + Ca^2\rho\mathsf{T} \le C\ell\Omega^{-4}. \tag{3.6}$$

Each patch has zero first centered moment and centered harmonic moments bounded by $C_k\Gamma a^k\rho$ for $k \ge 2$.

(ii) Consider two such evolutions with the same radii and signed circulations and identical initial normalized disks. On an initial time interval in $[0,2]$ satisfying the comparison bounds above, use $s = \Omega t$ and put $F(s) = \Omega^{-1}\|\triangle A(s/\Omega)\|_R$. Define

$$W(s) = C\int_0^s e^{\sigma_c(s-r)}\big(|Z(r)| + F(r)\big)\,dr, \qquad \sigma_c = C\left(\Omega^{-1} + \frac{a^2}{\ell^2}\right). \tag{3.7}$$

Here F is a nonnegative scalar measuring the external-field difference; the patch contours are denoted by F_h. The constant C can be chosen so that

$$\sum_{h=1}^4 \big(\|\triangle z_h\|_* + \rho\|\triangle\eta_h\|\big) \le W,$$

where the differences use the common contour coordinates of Lemma 3.8. With $|\triangle E| = \sum_h |\triangle E_h|$, we then have

$$\frac{|\triangle E|}{\Omega\ell} \le C\frac{a^2}{\ell^2}(\rho|Z| + W + \rho F). \tag{3.8}$$

For $k \ge 2$, the centered complex moments satisfy $|\triangle M_k| \le C_k\Gamma\ell^k(|Z| + (a^2/\ell^2)W)$. For every later s_0,

$$W(s) = e^{\sigma_c(s-s_0)}W(s_0) + C\int_{s_0}^s e^{\sigma_c(s-r)}\big(|Z(r)| + F(r)\big)\,dr. \tag{3.9}$$

In particular $W(0) = 0$, and no derivative of $\triangle A$ is required.

(iii) The first moment and angular impulse satisfy

$$\begin{aligned} \dot M_1 &= \int U(z)\omega_{\mathrm{quad}}(z)\,dA(z), \\ \dot I &= 2\,\mathrm{Re}\int \overline{z-d}[U(z) - U(d)]\omega_{\mathrm{quad}}(z)\,dA(z) + 2\,\mathrm{Re}\big((U(d) - \dot d)\overline{M_1}\big). \end{aligned} \tag{3.10}$$

Expanding about each patch centroid gives

$$I - 2\Gamma D = \sum_{h=1}^4 \int |z - \zeta_h|^2\omega_h(z)\,dA(z).$$

Initially each disk contributes $\Gamma_h a^2/2$, so this sum is zero because $\sum_h \Gamma_h = 0$. It satisfies

$$|I - 2\Gamma D| \le C\Gamma a^2\rho^2, \qquad |\triangle(I - 2\Gamma D)| \le C\Gamma a^2\rho W, \tag{3.11}$$

where the second estimate assumes the comparison hypotheses of (ii). Its time derivative satisfies

$$\left|\frac{d}{dt}(I-2\Gamma D)\right| \le C\Gamma a^2\Omega\rho. \tag{3.12}$$

The second complex moment satisfies

$$\begin{aligned}\dot M_2 = \frac{i}{2\pi}\iint \frac{z-w}{\bar z-\bar w}\,\omega_{\mathrm{quad}}(z)\omega_{\mathrm{quad}}(w)\,dA(z)dA(w)\\ +2\int (z-d)[U(z)-\dot d]\omega_{\mathrm{quad}}(z)\,dA(z).\end{aligned} \tag{3.13}$$

Each same-patch integral contributes at most $C\Gamma^2\rho$. Replacing all different-patch integrals by their centroid expressions has total error at most $C\Gamma^2a^2/\ell^2$.

(iv) The contour bounds cannot cause a first exit while the geometric and external hypotheses retain their margins. To verify (3.3) *for patch h, it suffices that the supports of $\omega-\omega_h$ have distance at least $c\ell$ from ζ_h and*

$$\int \frac{|(\omega-\omega_h)(y)|}{|\zeta_h-y|^2}\,dA(y) \le C\Omega.$$

For a/ℓ sufficiently small, the coefficient and material-derivative bounds then hold with fixed C_0, since $|\Gamma|/(c\ell)^2 = O(\Omega)$. Local existence and continuous dependence hold for every finite collection before a geometric or contour exit.

If the quadrupole is contained in $B(d,r/4)$, the support of $\omega-\omega_{\mathrm{quad}}$ lies outside $B(d,r)$, and $\int|(\omega-\omega_{\mathrm{quad}})(y)|/|d-y|^2\,dA(y)+\Gamma/r^2 \le C\mathsf{S}$, then

$$\left|\frac{d}{dt}DU(t,d(t))\right| \le C\mathsf{S}^2 + C\mathsf{T}|\dot d(t)-U(t,d(t))|. \tag{3.14}$$

The separation radius r in this assertion does not enter the choice of A.

Proof. (i) Corollary 3.7 gives the boundary bounds. Each patch differs from its centered disk on a set of area at most $Ca^2\rho$. By the centroid constraint and the vanishing disk moments,

$$M_{1,\mathrm{patch}} = 0, \qquad |M_{k,\mathrm{patch}}| \le C\Gamma a^k(1+C\rho)^k\rho, \qquad k\ge 2.$$

For $|z-\zeta_h| \ge c\ell/2$,

$$u_{\mathrm{patch}}(z) = \frac{i\Gamma_h}{2\pi(\bar z-\bar\zeta_h)} + \frac{i}{2\pi}\sum_{k\ge2}\frac{\overline{M_{k,\mathrm{patch}}}}{(\bar z-\bar\zeta_h)^{k+1}},$$

$$|u_{\mathrm{patch}}(z)-\Gamma_hK(z-\zeta_h)| \le \frac{C\Gamma a^2\rho}{|z-\zeta_h|^3}.$$

The self-field has zero patch average by antisymmetry of K. For the external field, subtract its constant and linear Taylor terms. The centroid constraint and the mean-value property give

$$\left|\frac{1}{\Gamma_h}\int u_{\mathrm{ext}}(z)\omega_h(z)\,dA(z) - u_{\mathrm{ext}}(\zeta_h)\right| \le Ca^2\rho\sup|D^2u_{\mathrm{ext}}| \le Ca^2\rho\left(\frac{\Gamma}{\ell^3}+\mathsf{T}\right).$$

Combining the two errors proves (3.6).

(ii) The derivative bounds for the external series give

$$\sum_{k\ge1}k^2R^{2k-2}|A_k|^2 \le C\mathsf{S}^2, \qquad \sum_{k\ge2}k^2(k-1)^2R^{2k-4}|A_k|^2 \le C\ell^2\mathsf{T}^2.$$

By Cauchy–Schwarz,

$$\sum_{k\ge1} R^k|A_k| \le C_R\mathsf{S}, \qquad \sum_{k\ge2} R^k|A_k| \le C_R\ell\mathsf{T}.$$

The contribution of U to the individual coefficient a_m is

$$\left(\frac{a}{\ell}\right)^{m-1} \sum_{k\ge m} \binom{k}{m} A_k \left(\frac{\overline{\zeta_h - d}}{\ell}\right)^{k-m}.$$

Since $|\zeta_h - d|/\ell \le R/2$ and $2a/\ell \le R/4$, summing with weight 2^m, also after one normalized centroid derivative, gives a bound $C_R \sum R^k|A_k|$. Its difference is therefore bounded by $C_R(\mathsf{S}|Z| + \|\triangle A\|_R)$.

Let W_{bdry} be the sum of the four quantities $\|\triangle z\|_* + \rho\|\triangle\eta\|$, one for each patch in the common contour coordinates of Lemma 3.8. The weight in that lemma is $(L/\Omega_{\mathrm{patch}})^{2/3} = (C_0/A)^{2/3}\Omega^{-2}$. Replacing it by $\rho = C_A\Omega^{-2}$ changes the distance and its differential inequality only by fixed factors. For the other three patches, the point fields contribute $C\Gamma\ell^{-2}|Z|$. Their moment differences start at order two and are bounded by Lemma 3.9. Summing the convergent moment series gives

$$\begin{aligned}\sum_{k\ge1} 2^k|\triangle a_k| &\le C\left(\frac{\Gamma}{\ell^2} + \mathsf{S}\right)|Z| + C\frac{\Gamma a^2}{\ell^4}W_{\mathrm{bdry}} + C\|\triangle A\|_R \\ &\le C\Omega\left(|Z| + \frac{a^2}{\ell^2}W_{\mathrm{bdry}} + F\right).\end{aligned}$$

The differential inequality in Lemma 3.8, $\Omega_{\mathrm{patch}}\rho^2 = AC_A^2$, and $s = \Omega t$ imply

$$D_s^+ W_{\mathrm{bdry}} \le C\left(\Omega^{-1} + \frac{a^2}{\ell^2}\right)W_{\mathrm{bdry}} + C(|Z| + F), \qquad W_{\mathrm{bdry}}(0) = 0.$$

The initial value is zero because both normalized disks and their labels agree. Choosing C in (3.7) sufficiently large, Gronwall gives

$$W_{\mathrm{bdry}}(s) \le C\int_0^s e^{\sigma_c(s-r)}(|Z(r)| + F(r))\,dr = W(s).$$

The centroid error is

$$E_h = \sum_{g\ne h}\left[\frac{1}{\Gamma_h}\int (K*\omega_g)(z)\omega_h(z)\,dA(z) - \Gamma_g K(\zeta_h - \zeta_g)\right] + \frac{1}{\Gamma_h}\int [U(z) - U(\zeta_h)]\omega_h(z)\,dA(z).$$

Both terms vanish for disks, and their moment expansions start at order two. By (i) and Lemma 3.9, each moment is bounded by $C_k\Gamma a^k\rho$ and its difference by $C_k\Gamma a^k W_{\mathrm{bdry}}$. Thus changes of the kernel coefficients retain ρ, while changes of the moments give W_{bdry}. For the external term, Cauchy's estimates give

$$\sup|D^2U| \le C_R\mathsf{S}/\ell, \qquad \sup|D^3U| \le C_R\mathsf{S}/\ell^2.$$

The centered external-field difference has Hessian bounded by $C_R\|\triangle A\|_R/\ell$. Combining the internal and external bounds gives

$$\begin{aligned}|\triangle E| &\le C\frac{\Gamma a^2}{\ell^3}(\rho|Z| + W_{\mathrm{bdry}}) \\ &\quad + C_R\frac{a^2}{\ell}\left[\mathsf{S}(\rho|Z| + W_{\mathrm{bdry}}) + \rho\|\triangle A\|_R\right].\end{aligned}$$

For nearby centroid configurations, apply the derivative bounds along their connecting segment. Otherwise $|Z|$ is bounded below, and the absolute estimates give the same bound. Since $\Gamma = 2\pi\Omega\ell^2$ and $\mathsf{S} \le \Omega$,

$$\frac{|\triangle E|}{\Omega\ell} \le C\frac{a^2}{\ell^2}(\rho|Z| + W_{\mathrm{bdry}} + \rho F) \le C\frac{a^2}{\ell^2}(\rho|Z| + W + \rho F).$$

This proves (3.8).

Expanding $(z-d)^k$ about each patch centroid and using the same moment bounds gives

$$|\triangle M_k| \le C_k\Gamma\ell^k|Z| + C_k\Gamma a^2\ell^{k-2}(\rho|Z| + W) \le C_k\Gamma\ell^k\left(|Z| + \frac{a^2}{\ell^2}W\right).$$

Splitting the integral defining W at s_0 proves (3.9).

(iii) Differentiate M_1 and I. The internal terms cancel by

$$K(z-w) + K(w-z) = 0, \qquad \mathrm{Re}(\overline{z-w}K(z-w)) = 0.$$

Differentiating the moving center gives the last term in (3.10). The centroid contribution to I is $2\Gamma D$, and the four signed disk impulses cancel. Lemma 3.9 and $W_{\mathrm{bdry}} \le W$ therefore give (3.11).

For each patch, the centroid term and self-field term again vanish. The centered external series gives

$$\frac{d}{dt}\int |z-\zeta_h|^2\omega_h(z)\,dA(z) = 2\,\mathrm{Re}\sum_{k\ge1} a_k a^{1-k}\overline{M_{k+1,\mathrm{patch}}}.$$

Since $(1+C\rho)^k < 2^k$, the moment bound in (i) yields

$$\left|\frac{d}{dt}\int |z-\zeta_h|^2\omega_h(z)\,dA(z)\right| \le C\Gamma a^2\rho\sum_{k\ge1}2^k|a_k| \le C\Gamma a^2\Omega\rho.$$

Summing proves (3.12).

For the second complex moment, symmetrize using

$$(z-d)K(z-w) + (w-d)K(w-z) = \frac{i(z-w)}{2\pi(\bar z - \bar w)}.$$

Together with the external and moving-center terms, this proves (3.13). The quotient has modulus one off the diagonal and zero integral over two copies of a disk, by rotation. Replacing one patch by its disk changes the vorticity measure by at most $C\Gamma\rho$ in total variation, so each same-patch integral is $O(\Gamma^2\rho)$. For distinct patches, the quotient has second derivatives bounded by $C\ell^{-2}$. Taylor expansion and the zero first centered moments give error $C\Gamma^2a^2/\ell^2$.

(iv) Lemma 3.5 gives (3.3) under the stated geometric criterion, with C_0 independent of the number and vorticity magnitudes of the other patches. For (3.14), its symmetrization bounds the external sources' contribution to $(\partial_t + U(d)\cdot\nabla)DU(d)$ by $C\mathsf{S}^2$. The four patches induce velocity at most $C\Gamma/|d-y|$ on the external supports, and hence contribute at most

$$C\Gamma\int\frac{|(\omega-\omega_{\mathrm{quad}})(y)|}{|d-y|^4}\,dA(y) \le C\frac{\Gamma}{r^2}\int\frac{|(\omega-\omega_{\mathrm{quad}})(y)|}{|d-y|^2}\,dA(y) \le C\mathsf{S}^2.$$

Replacing $U(d)$ by $\dot d$ adds $D^2U(d)[\dot d - U(d)]$, bounded by $C\mathsf{T}|\dot d - U(d)|$. This proves (3.14).

Local existence and continuous dependence follow from Lemma 3.1. Part (i) strictly improves the contour bounds, so continuation fails only if a geometric or external bound loses its margin. □

We record how the estimate is used when the centroid coordinates or comparison region change. Near a rotating rhombus, (p, q), D/ℓ^2, θ, and δ/ℓ are local coordinates for the centered centroids, so their difference norm is equivalent to $|Z|$. Replacing D/ℓ^2 by $I/(2\Gamma\ell^2)$ introduces an error at most $C(a^2/\ell^2)\rho W$ by (3.11). Gronwall then increases σ_c by at most $C(a^2/\ell^2)\rho$. Fix these constants in the rhombus neighborhood before fixing how far to follow the separating point-vortex trajectory.

On a subsequent fixed region of bounded, separated centroid configurations, continue W by $W_s = \sigma_c W + C(|Z| + F)$, using the incoming value of W and the constants required in that region. Formula (3.9) holds on each interval, and Lemma 3.8 preserves $W_{\mathrm{bdry}} \le W$. Across successive intervals the exponential factor is $\exp(\int_r^s \sigma_c(v)\,dv)$, with the input constant chosen on each interval. A fixed normalized duration gives a fixed amplification, without changing the constants on earlier intervals.

Once the normalized diameter grows like $1 + \Omega t$, use the absolute conclusions (i), (iii), and (iv), while their separation and external-field assumptions hold. They apply on the original interval starting from disks at time zero, including all later subintervals. No relative comparison with a rhombus is required there.

The following consequence bounds the accumulated patch error when the centroid and external-field differences grow at the unstable rate $2\sqrt{2}$.

Corollary 3.11. *Use the notation and fixed constants of Theorem 3.10(ii), with Ω sufficiently large that $\sigma_c < \sqrt{2}$. Let $0 < \kappa < 1$. On a normalized interval $[s_0, s_1]$, suppose*

$$W(s_0) \le C\kappa, \qquad |Z(s)| + F(s) \le C\kappa e^{2\sqrt{2}(s-s_0)}.$$

Then $W(s) \le C\kappa e^{2\sqrt{2}(s-s_0)}$ and

$$\frac{1}{\kappa}\int_{s_0}^{s_1} e^{-2\sqrt{2}(s-s_0)}\,\frac{|\triangle E(s)|}{\Omega\ell}\,ds \le C\frac{a^2}{\ell^2}(s_1 - s_0).$$

For an interval of length $O(\log(1/\kappa))$, this is $O(\Omega^{-3}\log(1/\kappa))$. The normalized angular-impulse correction satisfies

$$\frac{1}{\kappa}\int_{s_0}^{s_1} e^{-2\sqrt{2}(s-s_0)}\,\frac{|\triangle(I - 2\Gamma D)(s)|}{2\Gamma\ell^2}\,ds \le C\frac{a^2}{\ell^2}\rho(s_1 - s_0).$$

Proof. Substitute the assumed bound into (3.9) and use

$$\int_{s_0}^{s} e^{\sigma_c(s-r)}\kappa e^{2\sqrt{2}(r-s_0)}\,dr = \frac{\kappa\big(e^{2\sqrt{2}(s-s_0)} - e^{\sigma_c(s-s_0)}\big)}{2\sqrt{2} - \sigma_c} \le C\kappa e^{2\sqrt{2}(s-s_0)}.$$

The initial term $e^{\sigma_c(s-s_0)}W(s_0)$ has the same bound. Equations (3.8) and (3.11) give the two weighted integrals. Finally, $a^2/\ell^2 = 2/(A\Omega^3)$ gives the stated accumulated error. □

4 First solution: rotating quadrupoles at all scales

We choose the initial unstable shape variables in the exact centroid equations of Theorem 3.10 so that every quadrupole stays close to a rotating rhombus about its moving center for $0 \le t \le 2$. The estimates on $[0, 1]$ will be sharper because the unstable variables remain bounded through time 2.

Use the scales (1.1) and the signed circular patches of Section 1.2, with $B > 2$. First fix $\delta_0 > 0$ sufficiently small for the contour and shape coordinates and the estimates below. Next choose A large enough for Theorem 3.10 on $[0, 2]$, and finally choose Λ large. Constants may

depend on A, α, B, but are independent of n, N and the prescribed phases. We distinguish the constant C_{pv} in the quadratic point-vortex remainder, which is independent of A, from constants C_A that may depend on A.

For quadrupole n, use the centroid coordinates $d_n, \delta_n, z_{1,n}, z_{2,n}, D_n$ of Theorem 3.10 and the shape variables (p_n, q_n) of Section 2.2. Let $\theta_n = \arg z_{1,n}$ be continuous, with $\theta_n(0) = \varphi_n$. The displacement δ_n is complex-valued, whereas $\delta_0 > 0$ is the fixed contour and shape radius.

The unstable equation is

$$\dot{q}_n = 2\sqrt{2}\Omega_n \frac{\ell_n^2}{D_n} q_n + f_n,$$

where f_n contains the nonlinear terms and the forcing from the other patches. For small δ_0 and large Λ, the linear term dominates on $q_n = \pm\delta_0$ and points outward. Varying $(q_1(0), \dots, q_N(0))$ and applying Brouwer's theorem to the first exit gives a solution with $|q_n(t)| \le \delta_0$ through time 2. The bound at time 2 then gives an exponentially small terminal contribution on $[0, 1]$.

Prescribe $d_n(0) = d_n$, $\delta_n(0) = 0$, $D_n(0) = \ell_n^2$, $p_n(0) = 0$, and $\theta_n(0) = \varphi_n$, and vary $q_n(0)$ in $[-\delta_0, \delta_0]$. The corresponding initial positions relative to d_n are

$$z_{1,n}(0) = \frac{\ell_n e^{i\varphi_n}}{\sqrt{1 - R_*(1 + q_n(0))}}, \qquad z_{2,n}(0) = \frac{\ell_n \sqrt{R_*(1 + q_n(0))}}{\sqrt{1 - R_*(1 + q_n(0))}} e^{i(\varphi_n + \pi/2 + q_n(0)/\sqrt{2})}.$$

Set

$$\omega_N^{(1)}(0, x) = A \sum_{n=1}^{N} \Omega_n^4 \Big(\mathbf{1}_{B(d_n + z_{1,n}(0), a_n)}(x) + \mathbf{1}_{B(d_n - z_{1,n}(0), a_n)}(x) - \mathbf{1}_{B(d_n + z_{2,n}(0), a_n)}(x) - \mathbf{1}_{B(d_n - z_{2,n}(0), a_n)}(x) \Big).$$

The four centroid separations at scale n are comparable to ℓ_n. Since $a_n/\ell_n \to 0$ and $\ell_n/|d_n - d_j| \to 0$ uniformly for $j \ne n$, these disks are disjoint for sufficiently large Λ, uniformly over the initial cube.

Give each initial disk the normalized boundary labels $F(0, \theta) = e^{i\theta}$ and transport these labels with its Euler flow, as in Theorem 3.10.

Let I_n be the angular impulse in Theorem 3.10(iii). The difference $I_n - 2\Gamma_n D_n$ is the correction to the centroid impulse from the four patch interiors. It vanishes for the initial equal disks, so $I_n(0) = 2\Gamma_n \ell_n^2$.

The external velocity of quadrupole n is the velocity induced by all other quadrupoles. Near this quadrupole it is divergence-free and curl-free, so its gradient is symmetric and trace-free. Set

$$\mathsf{S} = \sum_{j \ge 1} \frac{\Gamma_j}{d_j^2} \le 8\Gamma_1, \qquad \mathsf{T} = \sum_{j \ge 1} \frac{\Gamma_j}{d_j^3} \le 16\Gamma_1.$$

Under the separation bounds below, the gradients and Hessians of the external velocities are bounded by $C\mathsf{S}$ and $C\mathsf{T}$, respectively. Both sums tend to zero as $\Lambda \to \infty$ and give bounds independent of N.

Proposition 4.1. *Fix $B > 2$, a sufficiently small $\delta_0 > 0$, and a sufficiently large $A > 0$. There exists Λ_0, independent of N, such that for every $\Lambda \ge \Lambda_0$, every $N \ge 1$, and every $(\varphi_1, \dots, \varphi_N) \in (\mathbb{R}/2\pi\mathbb{Z})^N$, some choice $(q_1(0), \dots, q_N(0)) \in [-\delta_0, \delta_0]^N$ gives an exact Euler patch solution $\omega_N^{(1)}$ on $[0, 2]$, with $u_N^{(1)} = K * \omega_N^{(1)}$ and the initial disks prescribed above. In particular, $p_n(0) = 0$, $\delta_n(0) = 0$, $D_n(0) = \ell_n^2$, and $\theta_n(0) = \varphi_n$. The following constants are independent of N, n and the phases.*

(i) For every $1 \le n \le N$ and $0 \le t \le 2$,

$$|q_n(t)|, |p_n(t)| \le \delta_0, \qquad \frac{1}{2} \le \frac{D_n(t)}{\ell_n^2} \le 2, \qquad |\delta_n(t)| \le C\mathsf{T}\ell_n^2 t e^{C\mathsf{S}t}.$$

Each normalized patch boundary has $C^{1,1/2}$ distance at most $C\Omega_n^{-2}$ from a parameterized circle. For $i \neq j$,

$$\frac{1}{2}|d_i - d_j| \le |d_i(t) - d_j(t)| \le 2|d_i - d_j|, \qquad 0 \le t \le 2.$$

Thus all patches remain disjoint, and every quadrupole stays near a rhombus about its moving center.

(ii) For every $1 \le n \le N$ and $0 < T \le 1$,

$$\sup_{0\le t\le T}\left(|q_n(t)| + |p_n(t)| + \left|\frac{I_n(t)}{2\Gamma_n\ell_n^2} - 1\right| + \left|\frac{D_n(t)}{\ell_n^2} - 1\right|\right) \le C\left(\frac{\mathsf{S} + T\mathsf{S}^2}{\Omega_n} + \Omega_n^{-5}\right).$$

The phase satisfies

$$\sup_{0\le t\le T}|\theta_n(t) - \varphi_n + \Omega_n t| \le CT(\mathsf{S} + T\mathsf{S}^2 + \Omega_n^{-4}), \qquad 0 < T \le 1. \tag{4.1}$$

In particular, $|q_n(0)| \le C(\mathsf{S}\Omega_n^{-1} + \Omega_n^{-5})$, and the phase error on $[0,1]$ tends to zero uniformly over $n \le N$ as $\Lambda \to \infty$.

(iii) The outer quadrupole satisfies

$$\sup_{0\le t\le 2}\frac{|d_1(t) - d_1|}{\ell_1} \le C\left(\frac{\sum_{j\ge 2}\Gamma_j}{\ell_1} + \mathsf{T}\Omega_1\ell_1 + \mathsf{T}\ell_1 + \Omega_1^{-4}\right) \longrightarrow 0 \qquad \text{as } \Lambda \to \infty.$$

Parts (ii) and (iii) hold for every initial choice whose solution satisfies part (i) through time 2.

Theorem 3.10(iv) gives local existence and continuous dependence for each initial choice. On an initial time interval $[0,T] \subset [0,2]$, impose the following *bootstrap assumptions* for every $1 \le n \le N$ and $i \neq j$,

$$|q_n(t)|, |p_n(t)| \le \delta_0, \qquad \tfrac{1}{2} \le D_n(t)/\ell_n^2 \le 2, \qquad |\delta_n(t)| \le \delta_0\ell_n, \qquad |d_i(t) - d_j(t)| \ge \tfrac{1}{2}|d_i - d_j|,$$

and require every contour boundary to satisfy (3.1). All these conditions hold for the initial disks. The next two lemmas improve (3.1) and the bounds on δ_n, D_n and $|d_i(t) - d_j(t)|$, and derive the shape equations.

Lemma 4.2. *On every initial time interval in $[0,2]$ satisfying the bootstrap assumptions, the geometric hypotheses of Theorem 3.10 hold. Each centroid satisfies* (3.6) *with $|E_i| \le C\ell_n\Omega_n^{-4}$. Every normalized patch boundary stays within $C\Omega_n^{-2}$ of a parameterized circle. The constants are uniform in n, N, the phases, and the initial vector in $[-\delta_0, \delta_0]^N$.*

Proof. Up to the first possible exit from (3.1), each patch lies in $B(\zeta_i, 2a_n)$. For sufficiently small δ_0, the bootstrap assumptions give centroid separations at least $c\ell_n$ within quadrupole n and at least $c|d_n - d_j|$ between quadrupoles n and j. Since $a_n/\ell_n = \sqrt{2/A}\,\Omega_n^{-3/2}$ is uniformly small, the supports remain separated.

For a centroid w at scale n, let ω_{other} denote all vorticity except its own patch. Since $|d_n - d_j| \ge d_j/2$ for $j \neq n$,

$$\int \frac{|\omega_{\text{other}}(y)|}{|w-y|^2}\,dA(y) \le C\frac{\Gamma_n}{\ell_n^2} + C\sum_{j\neq n}\frac{\Gamma_j}{|d_n - d_j|^2} \le C(\Omega_n + \mathsf{S}) \le C\Omega_n.$$

By Theorem 3.10(iv) and Lemma 3.5, its normalized external coefficients satisfy (3.3),

$$\sum_{k\ge 1} 2^k|a_k(t)| \le C\Omega_n, \qquad \sum_{k\ge 1} 2^k|\dot a_k(t)| \le C\Omega_n^2.$$

The derivative follows $w(t)$ in the fixed physical axes.

The external field U of the quadrupole is analytic near the convex hull of the four disks $B(\zeta_i, 2a_n)$, which is separated from the other supports. The spatial kernel bounds give, throughout this neighborhood,

$$\sup|DU| \le C\sum_{j\neq n}\frac{\Gamma_j}{|d_n-d_j|^2} \le C\mathsf{S}, \qquad \sup|D^2U| \le C\sum_{j\neq n}\frac{\Gamma_j}{|d_n-d_j|^3} \le C\mathsf{T}.$$

Thus Theorem 3.10 applies on the stopped interval. Its boundary bounds are

$$\|\eta(t)\|_{C^{1,1/2}} \le \delta_0/2, \qquad \|F(t)-e^{i(\cdot+\eta(t))}\|_{C^{1,1/2}} \le C\Omega_n^{-2} < \delta_0/2.$$

Moreover, (3.6) gives

$$|E_i| \le C\Omega_n\ell_n\frac{a_n^2}{\ell_n^2}\Omega_n^{-2} + Ca_n^2\Omega_n^{-2}\mathsf{T} \le C\ell_n\Omega_n^{-4},$$

using $a_n^2/\ell_n^2 = 2/(A\Omega_n^3)$ and $\mathsf{T}\le 1$. The strict contour bounds and Theorem 3.10(iv) exclude a first contour exit. □

Lemma 4.3. *On every initial time interval in* $[0,2]$ *satisfying the bootstrap assumptions,*

$$|\delta_n(t)| \le C\mathsf{T}\ell_n^2 te^{C\mathsf{S}t}, \qquad \left|\frac{D_n(t)}{\ell_n^2}-1\right| \le C(\mathsf{S}+\Omega_n^{-7}), \qquad \left|\frac{\dot D_n(t)}{D_n(t)}\right| \le C(\mathsf{S}+\Omega_n^{-4}),$$

$$\frac34|d_i-d_j| \le |d_i(t)-d_j(t)| \le \frac32|d_i-d_j| \qquad (i\neq j),$$

after increasing Λ *if necessary. The shape equations are*

$$\dot q_n = 2\sqrt2\Omega_n\frac{\ell_n^2}{D_n}q_n + f_n, \qquad \dot p_n = -2\sqrt2\Omega_n\frac{\ell_n^2}{D_n}p_n + \widetilde f_n,$$

$$|f_n| + |\widetilde f_n| \le C_{\mathrm{pv}}\Omega_n(|q_n|+|p_n|)^2 + C_A(\mathsf{S}+\Omega_n^{-4}+\Omega_n\mathsf{T}^2\ell_n^2).$$

The remainders $f_n, \widetilde f_n$ *include the nonlinear shape terms and the forcing by the other patches, and depend on the entire finite solution.*

Proof. Write $U_{\mathrm{ext},n}$ for the exact velocity of the other quadrupoles and expand

$$U_{\mathrm{ext},n}(d_n(t)+\zeta) = U_{\mathrm{ext},n}(d_n(t)) + \sum_{k\ge1}a_{k,n}\overline{\zeta}^k.$$

The series converges on a disk containing quadrupole n. Its coefficients satisfy $A_{k,n} = \ell_n^{k-1}a_{k,n}$ in the notation of Theorem 3.10. In particular, the strain coefficient is $S_n = a_{1,n}$. The individual-patch coefficients in (3.3) are normalized by a_n instead.

The internal velocity preserves the signed first moment $M_{1,n} = 4\Gamma_n\delta_n$. Since the total circulation is zero, (3.10) gives

$$\dot M_{1,n} = \sum_{k\ge1}a_{k,n}\overline{M_{k,n}}. \tag{4.2}$$

The supports lie within $C\ell_n$ of $d_n(t)$, so $|M_{k,n}| \le C_k\Gamma_n\ell_n^k$ for $k\ge2$. The sum over $k\ge2$ is the integral of the external Taylor remainder after its affine part is subtracted, and is bounded by $C\Gamma_n\mathsf{T}\ell_n^2$. Dividing by $4\Gamma_n$ gives

$$\dot\delta_n = a_{1,n}\overline{\delta_n} + \frac{1}{4\Gamma_n}\sum_{k\ge2}a_{k,n}\overline{M_{k,n}}, \qquad \left|\dot\delta_n - a_{1,n}\overline{\delta_n}\right| \le C\mathsf{T}\ell_n^2, \qquad |a_{1,n}| \le C\mathsf{S}.$$

Since $\delta_n(0) = 0$, Gronwall's inequality yields

$$|\delta_n(t)| \le C\mathsf{T}\ell_n^2 \int_0^t e^{C\mathsf{S}(t-s)}\, ds \le C\mathsf{T}\ell_n^2 t e^{C\mathsf{S}t}.$$

This strictly improves $|\delta_n| \le \delta_0 \ell_n$ for large Λ.

The internal point velocity of the arithmetic center is odd in δ_n and vanishes at $\delta_n = 0$ by central symmetry. Differentiating the rational point-vortex velocities on the fixed noncollision neighborhood bounds it by $C\Omega_n|\delta_n|$. The four external linear Taylor terms cancel because the centroids average to $d_n(t)$. Together with Lemma 4.2, this gives

$$|\dot{d}_n(t) - U_{\mathrm{ext},n}(d_n(t))| \le r_n, \qquad r_n = C(\mathsf{T}\Omega_n\ell_n^2 + \mathsf{T}\ell_n^2 + \ell_n\Omega_n^{-4}). \tag{4.3}$$

The three terms bound the internal point velocity, the external Taylor remainder, and the centroid error, respectively.

To compare the center trajectories, multiply each quadrupole's velocity by a smooth cutoff which is zero on $B(d_n(t), \epsilon_0 d_n)$ and one outside $B(d_n(t), 2\epsilon_0 d_n)$. Choose the fixed $\epsilon_0 > 0$ so that the larger disks are disjoint under the bound $|d_i(t) - d_j(t)| \ge \frac{1}{2}|d_i - d_j|$. The smaller disks contain their quadrupoles for large Λ. The sum V of these fields satisfies

$$V(d_n(t)) = U_{\mathrm{ext},n}(d_n(t)), \qquad \|\nabla V\|_{L^\infty} \le C\mathsf{S}.$$

Indeed, on the cutoff annulus the velocity is bounded by $C\Gamma_n/d_n$, while the cutoff derivative is bounded by C/d_n. The derivative of the velocity is bounded by $C\Gamma_n/d_n^2$ wherever its cutoff is nonzero. Summing gives the stated bound. Hence

$$|\dot{d}_i(t) - \dot{d}_j(t)| \le C\mathsf{S}|d_i(t) - d_j(t)| + r_i + r_j.$$

Since $d_n = 2^{-n}$ gives $d_i + d_j \le 3|d_i - d_j|$, we have $r_i + r_j \le 3|d_i - d_j| \sup_n(r_n/d_n)$. The upper and lower differential inequalities for the distance imply

$$e^{-C\mathsf{S}t} - 3t\sup_n(r_n/d_n) \le \frac{|d_i(t) - d_j(t)|}{|d_i - d_j|} \le e^{C\mathsf{S}t}(1 + 3t\sup_n(r_n/d_n)).$$

Since $d_n^{-1} = 2^n \le \Omega_n$ for $\Lambda \ge 1$ and $B > 2$,

$$\frac{r_n}{d_n} \le C(\mathsf{T}\Omega_n^2\ell_n^2 + \mathsf{T}\Omega_n\ell_n^2 + \ell_n\Omega_n^{-3}), \qquad \mathsf{S} + \sup_n \frac{r_n}{d_n} \longrightarrow 0.$$

Thus the distance ratio tends uniformly to one for $0 \le t \le 2$, proving the stated separation bounds.

The centroid contribution to the signed angular impulse is $2\Gamma_n D_n$, since the terms in $|\delta_n|^2$ cancel. The equal reference-disk radial moments also cancel. Theorem 3.10(iii) therefore gives

$$|I_n - 2\Gamma_n D_n| \le C\Gamma_n\ell_n^2\Omega_n^{-7}, \tag{4.4}$$

using $C\Gamma_n a_n^2\Omega_n^{-4} \le C\Gamma_n\ell_n^2\Omega_n^{-7}$. Expanding (3.10) yields

$$\dot{I}_n = 2\,\mathrm{Re}\Big((U_{\mathrm{ext},n}(d_n(t)) - \dot{d}_n(t))\overline{M_{1,n}} + \sum_{k\ge1} a_{k,n}\overline{M_{k+1,n}}\Big). \tag{4.5}$$

The internal contribution vanishes by antisymmetry of the kernel, and differentiation of the center contributes $-2\,\mathrm{Re}(\dot{d}_n\overline{M_{1,n}})$. The moment bounds and (4.3) imply

$$|\dot{I}_n| \le C\Gamma_n\ell_n^2(\mathsf{S} + \mathsf{T}\ell_n + \Omega_n\mathsf{T}^2\ell_n^2 + \mathsf{T}\ell_n\Omega_n^{-4}).$$

Since $I_n(0) = 2\Gamma_n \ell_n^2$, integration and (4.4) give

$$\left|\frac{D_n(t)}{\ell_n^2} - 1\right| \le C\big(\mathsf{S} + \mathsf{T}\ell_n + \Omega_n \mathsf{T}^2 \ell_n^2 + \mathsf{T}\ell_n \Omega_n^{-4} + \Omega_n^{-7}\big), \qquad 0 \le t \le 2.$$

For its derivative, use the patch impulse derivative bound in Theorem 3.10(iii) to obtain

$$|\dot{I}_n - 2\Gamma_n \dot{D}_n| \le C\Gamma_n a_n^2 \Omega_n \Omega_n^{-2}, \qquad \left|\frac{\dot{D}_n}{D_n}\right| \le C(\mathsf{S} + \Omega_n^{-4}) + C\mathsf{T}\ell_n + C\Omega_n \mathsf{T}^2 \ell_n^2.$$

Here internal patch rotation cancels, leaving the individual-patch external strain, bounded by $C\Omega_n$. Since $\ell_n = e^{-\Omega_n^\alpha}$ and $\mathsf{T} \le 1$, the additional terms in the bounds for D_n and $\dot{D}_n$ are at most $C\Omega_n^{-7}$ and $C\Omega_n^{-4}$, respectively. This proves both stated bounds and strictly improves the bootstrap bound on D_n.

Finally, taking the sum and difference of (2.4) at scale D_n gives the equations for q_n, p_n. Taylor expansion and the external and patch error bounds yield

$$|f_n| + |\widetilde{f}_n| \le C_{\mathrm{pv}} \Omega_n (|q_n| + |p_n|)^2 + C_A \left[\mathsf{S} + \Omega_n^{-4} + \Omega_n \left|\frac{\delta_n}{\ell_n}\right|^2\right].$$

The first term is the Taylor remainder of the point equations. Its constant C_{pv} depends only on the fixed centroid neighborhood and is independent of A. The second is the external strain, since common translation leaves the shape unchanged. The third follows by dividing the centroid error $C\ell_n\Omega_n^{-4}$ by ℓ_n. For the last term, reflection through the center followed by interchange of the two members of each equal-sign pair sends δ_n to $-\delta_n$ and leaves $z_{1,n}, z_{2,n}$ unchanged. Thus the internal shape equations are even in δ_n, and their correction is quadratic. Substituting the bound on δ_n proves the result. □

Lemma 4.4. *For every finite N and prescribed phase vector $(\varphi_1, \cdots, \varphi_N) \in (\mathbb{R}/2\pi\mathbb{Z})^N$, some $(q_1(0), \ldots, q_N(0)) \in [-\delta_0, \delta_0]^N$ gives a solution satisfying all bootstrap assumptions through time 2. Every such solution satisfies*

$$|q_n(t)| + |p_n(t)| \le C\left(\frac{\mathsf{S}}{\Omega_n} + \Omega_n^{-5}\right) + C\delta_0 e^{-c\Omega_n(2-t)}, \qquad 0 \le t \le 2, \tag{4.6}$$

where $c, C > 0$ are independent of n, N. In particular,

$$\sup_{0 \le t \le 1} (|q_n(t)| + |p_n(t)|) \le C(\mathsf{S}/\Omega_n + \Omega_n^{-5}).$$

Proof. On the bootstrap neighborhood,

$$\sqrt{2}\Omega_n \le 2\sqrt{2}\Omega_n \frac{\ell_n^2}{D_n(t)} \le 4\sqrt{2}\Omega_n.$$

By Lemma 4.3 and $\Omega_n \mathsf{T}^2 \ell_n^2 \le \Omega_n^{-4}$,

$$|f_n| + |\widetilde{f}_n| \le C_{\mathrm{pv}} \Omega_n (|q_n| + |p_n|)^2 + C_A(\mathsf{S} + \Omega_n^{-4}).$$

Choose δ_0 so that $4C_{\mathrm{pv}}\delta_0 \le \sqrt{2}/4$ and so that the kernel estimate below can be absorbed. This choice depends only on C_{pv} and universal kernel bounds. Next fix A as above, and then choose Λ so that

$$C_A \sup_{n \ge 1}(\mathsf{S}/\Omega_n + \Omega_n^{-5}) \le \tfrac{\sqrt{2}}{4}\delta_0.$$

The remainders are at most half the linear term on each shape face. Hence

$$q_n = \delta_0 \implies \dot{q}_n \geq \tfrac{\sqrt{2}}{2}\Omega_n\delta_0, \qquad q_n = -\delta_0 \implies \dot{q}_n \leq -\tfrac{\sqrt{2}}{2}\Omega_n\delta_0,$$
$$p_n = \delta_0 \implies \dot{p}_n \leq -\tfrac{\sqrt{2}}{2}\Omega_n\delta_0, \quad p_n = -\delta_0 \implies \dot{p}_n \geq \tfrac{\sqrt{2}}{2}\Omega_n\delta_0.$$

Both faces $p_n = \pm\delta_0$ point inward. Lemma 4.2 strictly improves (3.1), and Lemma 4.3 strictly improves the bounds on δ_n, D_n and $|d_i(t) - d_j(t)|$. Thus only $q_n = \pm\delta_0$ can be a first exit. The contours are regular and separated, and these faces lie inside the coordinate neighborhood, so Theorem 3.10(iv) gives continuation slightly beyond them.

Let $\mathbf{q} = (\mathbf{q}_1, \ldots, \mathbf{q}_N) \in [-\delta_0, \delta_0]^N$ prescribe $q_n(0) = \mathbf{q}_n$, with the other initial data fixed. Suppose no initial vector satisfies all bootstrap bounds through time 2. The preceding continuation and strict improvements imply that every trajectory first reaches $|q_n| = \delta_0$ for some n before time 2. For interior $\mathbf{q}$, let $\tau(\mathbf{q}) < 2$ be this first contact time. On the boundary of the cube set $\tau(\mathbf{q}) = 0$.

For fixed N, Theorem 3.10(iv) gives continuous dependence on the initial vector through $\tau(\mathbf{q})$ and for a short time beyond it. No uniform modulus in N is needed.

We claim that τ is continuous. On any nonempty interval $[0, \tau(\mathbf{q}) - \varepsilon]$, all $|q_n|$ have a positive margin below δ_0. Continuous dependence therefore prevents nearby trajectories from exiting on this interval. At $\tau(\mathbf{q})$, some coordinate q_n has a strictly outward derivative, so nearby trajectories also cross before time $\tau(\mathbf{q}) + \varepsilon$. These give the lower and upper bounds for continuity. If several faces are reached simultaneously, the lower bound uses all coordinates and the upper bound uses any outward coordinate. At an initial boundary point, the same upper bound gives $\tau \to 0$.

Consequently,

$$r(\mathbf{q}) = \big(q_1(\tau(\mathbf{q}); \mathbf{q}), \ldots, q_N(\tau(\mathbf{q}); \mathbf{q})\big)$$

is a continuous map from the cube to its boundary, equal to the identity on the boundary. By Brouwer's theorem, the cube self-map $\mathbf{q} \mapsto -r(\mathbf{q})$ has a fixed point. This point is on the boundary, where $r(\mathbf{q}) = \mathbf{q}$, so it must satisfy $\mathbf{q} = -\mathbf{q} = 0$, a contradiction. Thus some initial vector satisfies the bootstrap bounds through time 2, with first contact at time 2 allowed. The selected initial vector need not be unique or depend continuously on the phases.

Along any such solution, set

$$\lambda_n(t) = 2\sqrt{2}\Omega_n \frac{\ell_n^2}{D_n(t)}.$$

Duhamel's formula, forward from $p_n(0) = 0$ and backward from $q_n(2)$, gives

$$p_n(t) = \int_0^t \exp\left(-\int_r^t \lambda_n(s)\,ds\right) \widetilde{f}_n(r)\,dr,$$

$$q_n(t) = \exp\left(-\int_t^2 \lambda_n(s)\,ds\right) q_n(2) - \int_t^2 \exp\left(-\int_t^r \lambda_n(s)\,ds\right) f_n(r)\,dr.$$

In particular,

$$q_n(0) = -\int_0^2 \exp\left(-\int_0^r \lambda_n(s)\,ds\right) f_n(r)\,dr + \exp\left(-\int_0^2 \lambda_n(s)\,ds\right) q_n(2).$$

The last term is at most $\delta_0 e^{-2\sqrt{2}\Omega_n}$. Both f_n and D_n here belong to the actual coupled solution selected above.

The kernels decay at rate at least $c\Omega_n$, with $c = \sqrt{2}$, and have integrals at most C/Ω_n. Since $(|q_n| + |p_n|)^2 \leq 2\delta_0(|q_n| + |p_n|)$,

$$|q_n(t)| + |p_n(t)| \leq \delta_0 e^{-c\Omega_n(2-t)} + C_A(\mathsf{S}/\Omega_n + \Omega_n^{-5}) + 2C_{\mathrm{pv}}\delta_0\Omega_n \int_0^2 e^{-c\Omega_n|t-r|}(|q_n(r)| + |p_n(r)|)\,dr.$$

Fix $0 < c' < c$. Direct integration gives

$$\Omega_n \int_0^2 e^{-c\Omega_n|t-r|}\left(\frac{\mathsf{S}}{\Omega_n}+\Omega_n^{-5}+\delta_0 e^{-c'\Omega_n(2-r)}\right)dr \le \frac{C}{c-c'}\left(\frac{\mathsf{S}}{\Omega_n}+\Omega_n^{-5}+\delta_0 e^{-c'\Omega_n(2-t)}\right).$$

Divide the preceding inequality for $|q_n|+|p_n|$ by the positive expression in the last parentheses and take the supremum in t. The initial choice of δ_0 makes the coefficient of this supremum on the right at most $1/2$. Absorption proves (4.6), with c' renamed c. On $[0,1]$, the terminal term is at most $C\delta_0 e^{-c\Omega_n} \le C\Omega_n^{-5}$. □

Lemma 4.5. *Every initial choice whose solution satisfies the bootstrap assumptions on* $[0,2]$ *obeys, for* $0 < T \le 1$,

$$\sup_{0\le t\le T}\left|\log\frac{I_n(t)}{2\Gamma_n\ell_n^2}\right| \le C\left(\frac{\mathsf{S}+T\mathsf{S}^2}{\Omega_n}+T\Omega_n^{-5}\right).$$

Its shape variables, angular impulse, and phase satisfy part (ii) of Proposition 4.1.

Proof. By (4.4) and the bootstrap lower bound on D_n,

$$I_n \ge 2\Gamma_n D_n - C\Gamma_n\ell_n^2\Omega_n^{-7} \ge \tfrac{1}{2}\Gamma_n\ell_n^2 > 0.$$

Recall $S_n = a_{1,n}$. At the point rhombus, $z_{2,n}^2 = -R_* z_{1,n}^2$, so

$$\frac{M_{2,n}}{I_n} = \frac{z_{1,n}^2 - z_{2,n}^2}{|z_{1,n}|^2 - |z_{2,n}|^2} = \frac{1+R_*}{1-R_*}e^{2i\theta_n} = \sqrt{2}e^{2i\theta_n}.$$

The centroid terms in $M_{2,n}$ are $2\Gamma_n(z_{1,n}^2 - z_{2,n}^2)$, since the terms in δ_n^2 cancel. By Theorem 3.10(i), each centered second patch moment is bounded by $C\Gamma_n a_n^2\Omega_n^{-2} \le C\Gamma_n\ell_n^2\Omega_n^{-5}$. Together with (4.4), Taylor expansion in p_n, q_n gives

$$\frac{M_{2,n}}{I_n} = \sqrt{2}e^{2i\theta_n} + O(|q_n|+|p_n|+\Omega_n^{-5}).$$

Thus (4.5) gives

$$\left|\frac{\dot I_n}{I_n} - 2\sqrt{2}\,\mathrm{Re}(S_n e^{-2i\theta_n})\right| \le C\big[\mathsf{S}(|q_n|+|p_n|+\Omega_n^{-5}) + \mathsf{T}\ell_n + \Omega_n\mathsf{T}^2\ell_n^2 + \Omega_n^{-4}\mathsf{T}\ell_n\big].$$

For large Λ, $B(d_n(t), d_n/64)$ contains quadrupole n, and $B(d_n(t), d_n/16)$ excludes every other support. The weighted external absolute circulation is at most $C\mathsf{S}$, and $\Gamma_n/(d_n/16)^2 \le C\mathsf{S}$. By (3.14) and (4.3),

$$|\dot S_n| \le C\mathsf{S}^2 + C\mathsf{T}r_n.$$

The point phase equation in Section 2, expanded at the rhombus with scale D_n, and the centroid error give

$$\dot\theta_n = -\Omega_n\frac{\ell_n^2}{D_n} + e_{\theta,n}, \qquad |e_{\theta,n}| \le C\big(\Omega_n(|q_n|+|p_n|) + \mathsf{S} + \Omega_n^{-4} + \Omega_n\mathsf{T}^2\ell_n^2\big).$$

Fix $0 < T \le 1$. Lemmas 4.4 and 4.3 imply

$$\sup_{0\le t\le T}(|q_n(t)|+|p_n(t)|) \le C(\mathsf{S}/\Omega_n + \Omega_n^{-5}),$$
$$\sup_{0\le t\le T}\left|\dot D_n(t)/D_n(t)\right| + \sup_{0\le t\le T}|e_{\theta,n}(t)| \le C(\mathsf{S}+\Omega_n^{-4}),$$
$$\sup_{0\le t\le T}|\dot S_n(t)| \le C(\mathsf{S}^2+\Omega_n^{-4}), \qquad \sup_{0\le t\le T}|S_n(t)| \le C\mathsf{S}.$$

Here we used $\mathsf{T} \le 1$ and $\ell_n = e^{-\Omega_n^\alpha}$ to absorb the terms containing ℓ_n.

It remains to integrate the oscillatory term in $\dot{I}_n/I_n$. The phase equation gives

$$(e^{-2i\theta_n}\dot{}) = \left(\frac{2i\Omega_n \ell_n^2}{D_n} - 2ie_{\theta,n} \right) e^{-2i\theta_n}.$$

Solving for $e^{-2i\theta_n}$ and integrating by parts, we obtain

$$\begin{aligned} \int_0^t S_n(s) e^{-2i\theta_n(s)}\, ds &= \left[\frac{D_n(s) S_n(s) e^{-2i\theta_n(s)}}{2i\Omega_n \ell_n^2} \right]_{s=0}^{s=t} \\ &\quad - \int_0^t \frac{D_n(s)\dot{S}_n(s) + S_n(s)\dot{D}_n(s)}{2i\Omega_n \ell_n^2} e^{-2i\theta_n(s)}\, ds \\ &\quad + \int_0^t \frac{D_n(s) S_n(s) e_{\theta,n}(s)}{\Omega_n \ell_n^2} e^{-2i\theta_n(s)}\, ds. \end{aligned}$$

Since $D_n/\ell_n^2 \asymp 1$, the preceding bounds yield

$$\begin{aligned} \sup_{0\le t\le T} \left| \int_0^t S_n(s) e^{-2i\theta_n(s)}\, ds \right| &\le \frac{C}{\Omega_n} \left[\mathsf{S} + T(\mathsf{S}^2 + \Omega_n^{-4}) + T\mathsf{S}(\mathsf{S} + \Omega_n^{-4}) \right] \\ &\le C \left[\frac{\mathsf{S} + T\mathsf{S}^2}{\Omega_n} + T\Omega_n^{-5} \right]. \end{aligned}$$

The remaining terms in $\dot{I}_n/I_n$ are bounded by $C(\mathsf{S}^2/\Omega_n + \Omega_n^{-5})$. Since $I_n(0) = 2\Gamma_n \ell_n^2$, integration gives

$$\sup_{0\le t\le T} \left| \log \frac{I_n(t)}{2\Gamma_n \ell_n^2} \right| \le C \left[\frac{\mathsf{S} + T\mathsf{S}^2}{\Omega_n} + T\Omega_n^{-5} \right].$$

The right side is uniformly small. By (4.4) and Lemma 4.4,

$$\sup_{0\le t\le T} (|q_n(t)| + |p_n(t)|) \le C \left[\frac{\mathsf{S} + T\mathsf{S}^2}{\Omega_n} + \Omega_n^{-5} \right],$$

$$\sup_{0\le t\le T} \left[\left| \frac{I_n(t)}{2\Gamma_n \ell_n^2} - 1 \right| + \left| \frac{D_n(t)}{\ell_n^2} - 1 \right| + \left| \frac{\ell_n^2}{D_n(t)} - 1 \right| \right] \le C \left[\frac{\mathsf{S} + T\mathsf{S}^2}{\Omega_n} + \Omega_n^{-5} \right].$$

Finally, integrating the phase equation gives

$$\sup_{0\le t\le T} |\theta_n(t) - \theta_n(0) + \Omega_n t| \le CT(\mathsf{S} + T\mathsf{S}^2 + \Omega_n^{-4}).$$

These are the estimates in part (ii). □

Proof of Proposition 4.1. Apply Lemma 4.4 to the prescribed phases. Lemma 4.2 and Theorem 3.10(iv) give the exact patch solution on $[0, 2]$ and its boundary estimates. Lemma 4.3 gives the bounds on δ_n, D_n and $|d_i(t) - d_j(t)|$. Together with Lemmas 4.4 and 4.5, these prove (i) and (ii).

For (iii), the other quadrupoles stay at a fixed positive distance from quadrupole 1, uniformly in N. Their velocity at $d_1(t)$ is therefore bounded by $C\sum_{j\ge2} \Gamma_j$. Integrating (4.3), we get

$$\sup_{0\le t\le 2} \frac{|d_1(t) - d_1|}{\ell_1} \le C \left(\frac{\sum_{j\ge2} \Gamma_j}{\ell_1} + \mathsf{T}\Omega_1 \ell_1 + \mathsf{T}\ell_1 + \Omega_1^{-4} \right).$$

The last three terms tend to zero. For the first, $\Omega_j = \Omega_1 B^{j-1}$ and $\ell_j = e^{-\Omega_j^\alpha}$ imply

$$\frac{\sum_{j\ge2} \Gamma_j}{\ell_1} \le C\Omega_2 \exp(-(2B^\alpha - 1)\Omega_1^\alpha) \longrightarrow 0.$$

All estimates apply to every initial choice that remains within the bootstrap assumptions through time 2. □

5 Second solution: cascade of separating dipoles

We change only the four initial disk centers at scale N in the reference solution of Section 4. They are placed in a fixed configuration of separating dipoles, with the same radii and signed circulations. At every scale $n < N$, the initial patches of $\omega_N^{(1)}$ and $\omega_N^{(2)}$ agree. Both solutions then evolve under their own Biot–Savart velocities. No patch is moved or replaced at a later time.

The objective is to make scales $N-1, \dots, 1$ undergo the transition to separating dipoles successively, with scale 1 separating before time $1/2$. The field of the modified N-th scale acts on every scale from time zero. Thus each scale has already moved when the preceding scale separates, and the proof must retain that earlier motion. We use τ_n for the time when scale n reaches a fixed dipole separation, with $\tau_N = 0$. The intended motion at scale $n < N$ is

$[0, \tau_{n+1}]$	$[\tau_{n+1}, \tau_n]$	$[\tau_n, 1]$
near the rotating rhombus	transition and separation	separating dipoles.

The difference from the reference remains small before τ_{n+1} and grows exponentially during the first part of $[\tau_{n+1}, \tau_n]$. The second configuration then follows the fixed separating trajectory. After τ_n, the dipole centers separate at speed comparable to $\Omega_n \ell_n$. The second moment of scale $n+1$ supplies the strain that starts this growth. A large frequency ratio $\Omega_{n+1}/\Omega_n = B$ keeps the effects of the earlier motion and the responses of slower scales smaller than the interaction between adjacent scales.

We use two conclusions from Section 4. The reference exists for every prescribed initial phase vector, and, uniformly in n, N and $0 \le t \le 1$,

$$\theta_n^{(1)}(t) = \varphi_n - \Omega_n t + O(\mathsf{S} + \mathsf{S}^2 + \Omega_n^{-4}).$$

Thus its phase remains close to the prescribed uniform rotation even after many rotations. The scales satisfy $0 < \alpha < 1$, $\Omega_{n+1} = B\Omega_n$, and $\ell_n = e^{-\Omega_n^\alpha}$. We first choose B large and then Λ large, independently of N.

Section 6 proves the time, angle, and moment estimates for one quadrupole under bounds on its forcing and initial differences. Section 7 verifies those bounds for the coupled system, controls every $i < n$ together with n, and obtains the differences needed at the next scale. Figure 2 shows this induction.

5.1 Initial configurations and phases

We choose the initial phases so that separation at scale $n+1$ produces a positive growing coefficient at scale n.

Take the separating trajectory of Proposition 2.2 with $\ell = \Omega = 1$, write its time as s, and normalize its time and rotation by

$$\lim_{s \to -\infty} e^{-2\sqrt{2}s} q(s) = 1, \qquad \lim_{s \to -\infty} (\theta(s) + s) = 0.$$

Choose K sufficiently large for a fixed small tolerance $\varepsilon_* > 0$, following the parameter order in Section 7.1. It is independent of the scale and of N. Let θ_∞ be the limiting angle of the negative-to-positive dipole vector in (2.6). Pair the nearby opposite signs, let X_1, X_2 be their pair centers, and set

$$r_{\mathrm{out}} = |X_1(K) - X_2(K)|, \qquad \beta = \theta_\infty + K.$$

The rhombus approached as $s \to -\infty$ has phase $-s$. Thus $-K + \beta = \theta_\infty$ relates its phase to the outgoing dipole angle, with the same K and β at every scale. Choose ϑ_N arbitrarily and put the four initial disk centers at scale N at

$$d_N + \ell_N e^{i(\vartheta_N - \theta_\infty)} \{\pm z_1(K), \pm z_2(K)\}.$$

Using the same pairing for the patch centroids, define the actual separation time and associated dipole angle, whenever the prescribed distance is reached, by

$$\tau_n = \inf\{t \geq 0 : |X_1(t) - X_2(t)| = r_{\mathrm{out}}\ell_n\},$$
$$\theta_{d,n} = \arg z^{(2)}_{1,n}(\tau_n) + \theta_\infty - \theta(K) \pmod{\pi}.$$

For a rotated copy of the fixed shape, this angle is its limiting dipole angle. In particular, $\tau_N = 0$ and $\theta_{d,N} = \vartheta_N$. Later angle differences use their small representatives modulo π.

For $t \geq \tau_{n+1}$, the linear part of the source second moment has size $\Gamma^2_{n+1}(t-\tau_{n+1})$, inducing strain of size $\Gamma^2_{n+1}(t-\tau_{n+1})/|d_n - d_{n+1}|^4$. For the prescribed affine strain, Proposition 2.3 gives the coefficient κ_n from (2.12), the leading delay Δ_n, and the associated outgoing angle when the phases maximize the cosine.

$$\kappa_n = \frac{\sqrt{3}\,\Gamma^2_{n+1}}{2\sqrt{2}\pi^2\Omega_n^2|d_n - d_{n+1}|^4}, \qquad \Delta_n = \frac{1}{\Omega_n}\left(\frac{\log(1/\kappa_n)}{2\sqrt{2}} + K\right). \tag{5.1}$$

Define the predicted separation times by

$$\tau_{n,N} = \sum_{j=n}^{N-1} \Delta_j, \qquad \tau_{N,N} = 0.$$

The times $\tau_{n,N}$ depend only on the scales and K, so they can be computed before choosing any phases. Suppose the predicted source angle ϑ_{n+1} is known. At $\tau_{n+1,N}$, the receiving phase is predicted to be $\varphi_n - \Omega_n\tau_{n+1,N}$. Since $d_n - d_{n+1} > 0$, the cosine in (2.12) is maximized when

$$-2(\varphi_n - \Omega_n\tau_{n+1,N}) - 2\vartheta_{n+1} + \arctan(1/\sqrt{2}) - \pi = 0 \pmod{2\pi}.$$

Thus we choose the initial phases and predicted outgoing angles by

$$\begin{aligned} \varphi_n &= \Omega_n\tau_{n+1,N} + \frac{\arctan(1/\sqrt{2}) - \pi}{2} - \vartheta_{n+1} \pmod{\pi}, \\ \vartheta_n &= \varphi_n - \Omega_n\tau_{n,N} + \beta \pmod{\pi}, \qquad n = N-1, \dots, 1. \end{aligned} \tag{5.2}$$

This recursion includes the rotation $-\Omega_n\Delta_n$ during the delay and uses only the predicted times.

Choose φ_N arbitrarily and choose representatives modulo 2π for the phases in (5.2); changing a representative by π only exchanges the equal-sign patches. With all phases now fixed, Proposition 4.1 chooses $(q_1(0), \dots, q_N(0))$ and gives the reference solution $\omega_N^{(1)}$. Its applicability to every phase vector is what permits this order of choices. For $\omega_N^{(2)}$, retain its initial disks at every scale $n < N$ and use the prescribed separating shape at scale N, with unchanged radii, signs, and vorticity values. Give every disk the labels $F_i(0,\theta) = e^{i\theta}$. Theorem 3.10(iv) gives local existence. The phases may depend on N, while all subsequent estimates are uniform in these choices.

Finally, the choice of scales (1.1) gives

$$\log(1/\kappa_n) = 4\Omega_{n+1}^\alpha + O(n + \log B + 1), \qquad \sum_{n\geq 1}\Delta_n \leq C_{\alpha,B}\Lambda^{\alpha-1}.$$

For fixed B, choose Λ large so that $0 < \kappa_n < 1$, $\Delta_n > 0$, and $\sum_n \Delta_n < 1/4$. The later estimates prove continuation through time 1 and control the actual errors $\tau_n - \tau_{n,N}$ and $\theta_{d,n} - \vartheta_n$.

5.2 Growth and continued separation at each scale

Suppose scale $n+1$ reaches its prescribed dipole separation at $t_0 = \tau_{n+1}$, and set $s = \Omega_n(t - t_0)$. The estimates in this subsection assume initial differences of size $O(\kappa_n)$, positive weighted forcing, and the stated bounds for the other quadrupoles. The next subsection explains how the induction verifies these assumptions. All estimates are made up to the first possible failure of a shape, separation, or patch boundary bound. They then give continuation through time 1.

5.2.1. Differences from the reference. Before scale j reaches its prescribed separation, write Y_j for its dimensionless difference from the reference, including the integral W_j in (3.7) that controls boundary differences. Section 7.2 gives the precise equivalent norms, which satisfy

$$Y_j \asymp \frac{|\triangle z_{1,j}| + |\triangle z_{2,j}|}{\ell_j} + \frac{d_j|\triangle M_{1,j}|}{\Gamma_j \ell_j^2} + \frac{|\triangle d_j|}{d_j} + W_j.$$

The first term controls shape, impulse, and phase. The first moment $M_{1,j} = 4\Gamma_j\delta_j$ controls the offset between the positive and negative pairs. Its weight d_j/ℓ_j relative to the centroid norm is needed to estimate its far-field contribution. Here $\triangle d_j$ is the difference between the moving quadrupole centers, whereas d_j in the denominator is the fixed initial location. In particular,

$$|\triangle M_{1,j}| \le C\frac{\Gamma_j \ell_j^2}{d_j} Y_j, \qquad |\triangle M_{2,j}| \le C\Gamma_j \ell_j^2 Y_j.$$

These bounds convert differences of configurations into differences of the velocity acting on another scale. Small Y_j keeps the second solution's quadrupole near its reference counterpart. Along the subsequent fixed trajectory, only a uniform bound on Y_j is needed.

5.2.2. Why a relative estimate is needed. By the preceding estimate for $\log(1/\kappa_n)$, the coefficient κ_n is smaller than every fixed negative power of Ω_n. An absolute normalized centroid error $O(\Omega_n^{-5})$ therefore cannot determine the sign of this unstable coefficient. Theorem 3.10(ii) instead bounds the difference of the two centroid errors. With $F(s) = \Omega_n^{-1}\|\triangle A_n(t_0 + s/\Omega_n)\|_R$, its relevant consequence is

$$\frac{|\triangle E_n(t_0 + s/\Omega_n)|}{\Omega_n \ell_n} \le C\frac{a_n^2}{\ell_n^2}[Y_n(t_0 + s/\Omega_n) + F(s)], \qquad \frac{a_n^2}{\ell_n^2} = O(\Omega_n^{-3}).$$

There is no additive error independent of the differences. The integral W_n controlling the boundary difference retains its actual value at t_0. Its growth rate $\sigma_c < 2\sqrt{2}$ in (3.9) is smaller than the unstable rate. Thus $W_n(t_0) = O(\kappa_n)$ and inputs bounded by $C\kappa_n e^{2\sqrt{2}s}$ give the same bound for W_n. Over the required interval $S = O(\log(1/\kappa_n))$, the resulting relative error in the unstable coefficient is

$$\frac{1}{\kappa_n}\int_0^S e^{-2\sqrt{2}s}\frac{|\triangle E_n(t_0 + s/\Omega_n)|}{\Omega_n \ell_n}\, ds \le C\Omega_n^{-3}\log(1/\kappa_n) = O_{\alpha,B}(\Omega_n^{\alpha-3}).$$

The induction proves the growth bound and this error bound together. It does not assume an absolute patch error smaller than κ_n.

5.2.3. From positive forcing to the separating trajectory. Proposition 2.3 gives the time and outgoing angle for the prescribed-strain point-vortex motion. For the patches, Section 6.1 uses $(\widehat{p}, \widehat{q}, \widehat{\Theta})$ in which the separating point-vortex trajectory satisfies

$$\widehat{p} = 0, \qquad \widehat{q}_s = 2\sqrt{2}\widehat{q}, \qquad \widehat{\Theta}_s = -1.$$

Here $\widehat{q}/q \to 1$ and $\widehat{\Theta} - \theta \to 0$ at the rhombus. The equation $\widehat{q}_s = 2\sqrt{2}\widehat{q}$ retains the exact unstable rate, and $\widehat{\Theta}_s = -1$ accounts for the change of phase caused by the changing shape. Both are needed for time and angle estimates through the logarithmic interval.

Fix $M_{\mathrm{hist}} > 0$ as the constant in the bound

$$Y_j(t) \le M_{\mathrm{hist}} e^{c\Omega_j(t-\tau_j)}, \qquad 0 \le t \le \tau_j, \qquad 0 < c < 2\sqrt{2},$$

for scales whose transition has been completed. The next subsection explains how the same constant works at every scale. Put $Q_n(t) = \triangle\widehat{q}_n(t)$. The common initial patches give $Q_n(0) = 0$, regardless of the unknown values $q_n^{(1)}(0)$ chosen by shooting. The next subsection bounds the motion before t_0 by $|Q_n(t_0)|/\kappa_n \le CM_{\mathrm{hist}}B^{-2} + o_{\Lambda\to\infty}(1)$, with M_{hist} fixed before B, Λ. In the normalized equation for Q_n, let $\kappa_n f_q$ collect the forcing from scales $j > n$ with $\tau_j \le t_0$, their subsequent influence through scales $i < n$, and the slower-scale differences already present at t_0. The additional forcing produced when n perturbs the slower scales after t_0 is estimated separately. Neglecting the relative errors for the moment, Duhamel's formula gives

$$Q_n(t_0 + s/\Omega_n) \simeq e^{2\sqrt{2}s}\left[Q_n(t_0) + \kappa_n \int_0^s e^{-2\sqrt{2}r} f_q(r)\, dr\right].$$

The resulting coefficient is

$$\mathcal{A}_n = \frac{Q_n(t_0)}{\kappa_n} + \int_0^\infty e^{-2\sqrt{2}s} f_q(s)\, ds.$$

Here $\mathcal{A}_n$ is the normalized coefficient of unstable growth. The forcing may change sign. Under the completed-scale bounds below, the chosen phases give $\int_0^\infty e^{-2\sqrt{2}s} f_q(s)\, ds = 1 + O(\varepsilon_*)$. Together with the small value $Q_n(t_0)/\kappa_n$, this determines the sign independently of the common initial $q_n(0)$. If the motion is stopped at $s = S$, use the actual f_q on $[0, S]$ and then continue the leading strain obtained from $\dot{M}_{2,n+1} = -(2i/\pi)\Gamma_{n+1}^2 e^{2i\theta_{d,n+1}}$. The integral from S to infinity is subtracted in the finite-time formula.

Here ε_* bounds the errors accumulated over $s = O(\log(1/\kappa_n))$, not an error allowed at each unit of normalized time. If these accumulated relative errors are at most ε_*, Section 6.2 gives, after the initial forcing tail has decayed,

$$Q_n(t_0 + s/\Omega_n) = \kappa_n e^{2\sqrt{2}s}\big[\mathcal{A}_n + O(\varepsilon_*) + O((1+s)^3 e^{-\sqrt{2}s})\big].$$

Fix a small $q_* > 0$, independently of n, N, and let T_n be the first physical time when $Q_n(T_n) = q_*$. If $\mathcal{A}_n \ge 3/4$ and the other bounds do not fail first, then

$$\Omega_n(T_n - t_0) = \frac{1}{2\sqrt{2}} \log \frac{q_*}{\kappa_n \mathcal{A}_n} + O(\varepsilon_*).$$

The stable shape difference decays under its linear equation, while impulse and phase have at most polynomial unforced growth. Their forced estimates give, at T_n,

$$|\widehat{p}_n^{(2)}| + \left|\frac{I_n^{(2)}}{2\Gamma_n \ell_n^2} - 1\right| + \frac{|\delta_n^{(2)}|}{\ell_n} \le C\varepsilon_*.$$

The corrected phase difference $\triangle\widehat{\Theta}_n(T_n)$ is also $O(\varepsilon_*)$. The reference shape is much smaller than q_*. Thus, after matching its phase, the second configuration is close to the positive separating trajectory at $\widehat{q} = q_*$. The remaining normalized point-vortex duration is the fixed number $K - \log q_*/(2\sqrt{2})$. The vector field is Lipschitz on this collision-free segment, so the normalized centroid error stays $O(\varepsilon_*)$. The normalized pair-center distance crosses r_{out} with

derivative at least one, so the crossing time also changes by $O(\varepsilon_*)$ in normalized time. Adding the two durations and comparing phases yields

$$\begin{aligned} \tau_n - \tau_{n+1} &= \frac{1}{\Omega_n}\left[\frac{\log(1/(\kappa_n \mathcal{A}_n))}{2\sqrt{2}} + K + O(\varepsilon_*)\right], \\ \theta_{d,n} &= \theta_n^{(1)}(\tau_n) + \beta + O(\varepsilon_*). \end{aligned} \tag{5.3}$$

The $O(\varepsilon_*)$ error in the first line is small in the receiver's time unit Ω_n^{-1}. The second line then determines the outgoing angle from the reference phase at the actual time τ_n. Both estimates are needed when n becomes the source for $n-1$.

5.2.4. Why the dipoles keep separating. Each opposite-sign pair has length close to ℓ_n and translates with speed close to $\Omega_n \ell_n$. The two leading velocities are opposite. At pair-center distance R, the other pair changes its relative vector at rate $O(\Gamma_n \ell_n^2/R^3)$. The fractional change accumulated along the expected separation is bounded by

$$\int_0^{1-\tau_n} \frac{\Gamma_n \ell_n}{[\ell_n(r_{\text{out}} + \Omega_n t)]^3}\, dt \le C r_{\text{out}}^{-2}.$$

Over the remaining physical interval, the external strain and patch correction add at most $C(\mathsf{S} + \Omega_n^{-4})$ to this change. Thus the pair lengths and directions stay close to their values at τ_n when r_{out} and then Λ are large. Section 6.3 makes this a bootstrap estimate: the relative pair-center velocity has projection at least $\Omega_n \ell_n$ in the separating direction, and

$$|X_1(t) - X_2(t)| \asymp \ell_n\big(r_{\text{out}} + \Omega_n(t - \tau_n)\big), \qquad \tau_n \le t \le 1.$$

The same control gives

$$\dot{M}_{2,n}^{(2)}(t) = -\frac{2i}{\pi}\Gamma_n^2 e^{2i\theta_{d,n}} + O(\varepsilon_* \Gamma_n^2).$$

This is the force that scale n supplies to scale $n-1$. These conclusions hold up to the common stopping time until the geometric and boundary estimates give continuation.

5.3 The cascade by induction

At $t = \tau_{n+1}$, assume the stages $j > n$ are complete. Each completed quadrupole supplies the separation and moment estimates above, a time and angle close to their prescribed values, and the bound

$$Y_j(t) \le M_{\text{hist}} e^{c\Omega_j(t-\tau_j)}, \qquad 0 \le t \le \tau_j, \qquad 0 < c < 2\sqrt{2}.$$

The constant M_{hist} is independent of j, N. During $[\tau_{n+1}, \tau_n]$, we estimate n and all $i < n$ together, while the completed scales $j > n$ keep separating and retain their bounds on $[0, \tau_j]$. At the first stage $n = N-1$, $t_0 = 0$ and all differences at scales $j < N$ vanish. The bounds for scale N follow from its prescribed configuration.

5.3.1. Force from faster scales. The second moment of $n+1$ is its value at τ_{n+1}, of size $O(\Gamma_{n+1}\ell_{n+1}^2)$, plus an approximately linear term in $t - \tau_{n+1}$ with coefficient of size Γ_{n+1}^2. Integration against $e^{-2\sqrt{2}\Omega_n(t-\tau_{n+1})}$ gives one factor Ω_n^{-1} for a constant term and two for a linear term. Hence the constant moment and the reference second moment contribute at most $C\kappa_n/B$, since

$$\frac{\Gamma_{n+1}\ell_{n+1}^2/\Omega_n}{\Gamma_{n+1}^2/\Omega_n^2} \asymp B^{-1}.$$

The linearly growing term supplies the coefficient of size κ_n whose sign is determined by the phases.

The motion before τ_{n+1} has a smaller effect. By the assumed history bound, its effective duration is $O(\Omega_{n+1}^{-1})$, giving a contribution at most $CM_{\mathrm{hist}}\kappa_n B^{-2}$. Section 7.5, Step 3, proves the corresponding bound on the actual differences:

$$\sup_{0\le t\le\tau_{n+1}} e^{2\sqrt{2}\Omega_n(\tau_{n+1}-t)}Y_n(t) \le CM_{\mathrm{hist}}\kappa_n B^{-2} + C(1+M_{\mathrm{hist}})\kappa_n e^{-c\Omega_{n+2}^{\alpha}}.$$

This includes $W_n(\tau_{n+1})$ and controls the whole earlier interval. It supplies the small inherited state required in Section 5.2.

The last term bounds the sources $j \ge n+2$. They have been separating longer, but their circulations are much smaller. Section 7.3 compares this decrease with the extra time available for unstable growth and shows that their total contribution, divided by κ_n, is at most $C(1+M_{\mathrm{hist}})e^{-c\Omega_{n+2}^{\alpha}}$. All these contributions are bounded in absolute value; only the leading term from $n+1$ needs a phase choice.

5.3.2. Errors $\tau_n-\tau_{n,N}, \theta_{d,n}-\vartheta_n$ in time and angle. Put $h_j=\Omega_j(\tau_j-\tau_{j,N})$, so the timing error is measured in scale j's own time unit. The already completed scale $n+1$ supplies $|h_{n+1}|\le C_h\varepsilon_*$ and

$$\theta_{d,n+1}-\vartheta_{n+1} = -h_{n+1}+O(\varepsilon_*).$$

The angle error follows from (5.3) and the reference phase estimate: a delay h_{n+1}/Ω_{n+1} adds rotation $-h_{n+1}$. During the same delay the receiver rotates by only $-h_{n+1}/B$. Thus at τ_{n+1} its reference phase is

$$\theta_n^{(1)}(\tau_{n+1}) = \varphi_n - \Omega_n\tau_{n+1,N} - B^{-1}h_{n+1} + O(\varepsilon_*).$$

Both angles enter the cosine in (2.12) with coefficient -2. Its argument therefore changes from the chosen maximum by $2(1+B^{-1})h_{n+1}+O(\varepsilon_*)$, giving

$$\mathcal{A}_n = \cos\bigl(2(1+B^{-1})h_{n+1}\bigr)+O(\varepsilon_*) = 1+O(h_{n+1}^2+\varepsilon_*).$$

The maximum is important: the angle error is linear in h_{n+1}, but its effect on $\mathcal{A}_n$ is quadratic. The other coefficient errors, estimated above and below, are made at most $O(\varepsilon_*)$ by choosing B and then Λ large. Hence $\mathcal{A}_n\ge 3/4$. This positivity uses only the completed stages and the small inherited state. Replacing κ_n by $\kappa_n\mathcal{A}_n$ changes the normalized delay by $-(2\sqrt{2})^{-1}\log\mathcal{A}_n$. Subtracting the prescribed delay from (5.3) therefore gives

$$h_n = B^{-1}h_{n+1} - \frac{\log\mathcal{A}_n}{2\sqrt{2}} + O(\varepsilon_*), \qquad |h_n|\le B^{-1}|h_{n+1}| + C|h_{n+1}|^2 + C\varepsilon_*.$$

The linear term contracts by B^{-1}, and the quadratic term is small when h_{n+1} is small. Fix C_h and then ε_* using the universal constants in this recurrence, as specified in Section 7.1. For large B, the recurrence improves $|h_n|\le C_h\varepsilon_*$. Starting from $h_N=0$, the same timing and angle bounds are available for the next coefficient.

5.3.3. The response of slower scales. The motion of n also forces every $i<n$, which then acts back on n. The interaction estimates in Section 7.2 use $\max_j d_j^4 Y_j$ and give the bound

$$\Xi = C\sum_{j\ge1}\frac{\Omega_j\ell_j^4}{d_j^5} + C\mathsf{S}.$$

Thus $\Xi\to0$ as $\Lambda\to\infty$. The slower subsystem has growth rate at most $C\Omega_{n-1}+C\Xi<\sqrt{2}\Omega_n$ for large B. Hence

$$\int_{\tau_{n+1}}^{t} e^{\sqrt{2}\Omega_n(t-r)}e^{2\sqrt{2}\Omega_n(r-\tau_{n+1})}\,dr \le \frac{1}{\sqrt{2}\Omega_n}e^{2\sqrt{2}\Omega_n(t-\tau_{n+1})}.$$

On the common stopped interval, assume $Y_n(t) \le C\kappa_n e^{2\sqrt{2}\Omega_n(t-\tau_{n+1})}$ with a sufficiently large fixed constant. Let $f_i(t)$ bound the forcing on scale $i < n$ from scales $j > n$, in the physical-time equation for Y_i. Duhamel's formula then gives

$$\max_{i<n}\left(\frac{d_i}{d_n}\right)^4 Y_i(t) \le Ce^{\sqrt{2}\Omega_n(t-t_0)}\max_{i<n}\left(\frac{d_i}{d_n}\right)^4 Y_i(t_0) + C\int_{t_0}^{t} e^{\sqrt{2}\Omega_n(t-r)}\max_{i<n}\left(\frac{d_i}{d_n}\right)^4 f_i(r)\,dr + \frac{C\Xi}{\Omega_n}\kappa_n e^{2\sqrt{2}\Omega_n(t-t_0)},$$

where $t_0 = \tau_{n+1}$. The product $\kappa_n e^{2\sqrt{2}\Omega_n(T_n-\tau_{n+1})}$ is $O(q_*)$, and the remaining transition takes bounded normalized time. Since $d_i > d_n$, this estimate also controls each Y_i. Acting back on n costs another Ξ, and converting to normalized time gives another Ω_n^{-1}. Lemma 7.1 bounds the resulting feedback norm by $C\Xi^2/\Omega_n^2$, including all mutual interactions among slower scales. Their actual states at τ_{n+1} and responses to completed sources remain in $\kappa_n f_q$. The feedback contains only their response to the subsequent motion of n.

The estimates for the stable shape and the remaining coordinates give the following schematic bound on the common stopped interval, for $S \le C\log(1/\kappa_n)$:

$$\sup_{0\le s\le S}\frac{e^{-2\sqrt{2}s}Y_n(\tau_{n+1}+s/\Omega_n)}{\kappa_n} \le C + C\left(\frac{\mathsf{S}}{\Omega_n} + \Omega_n^{-3} + \frac{\Xi^2}{\Omega_n^2}\right)\log(1/\kappa_n) \times \sup_{0\le s\le S}\frac{e^{-2\sqrt{2}s}Y_n(\tau_{n+1}+s/\Omega_n)}{\kappa_n}.$$

The three small terms come from the reference and external fields, the relative patch error, and the feedback through slower scales. Their product with $\log(1/\kappa_n)$ is the error accumulated over the long growth interval. Since $\log(1/\kappa_n) = O_{\alpha,B}(\Omega_n^{\alpha})$ and $\alpha < 1$, it tends to zero uniformly in n as $\Lambda \to \infty$. The other local terms are controlled by the fixed small shape threshold and the scale choices. Thus the multiplier of the last supremum is less than $1/2$ for large Λ. Absorption then improves this bootstrap bound. Including the slower scales' initial values and forcing from $j > n$, Section 7.5, Step 4, obtains $\sup_{i<n,\,\tau_{n+1}\le t\le\tau_n} Y_i(t) = o_{\Lambda\to\infty}(1)$, uniformly in n, N. They therefore cannot leave their rhombus neighborhoods first. These strict improvements prove the current and slower bounds together. For $n = 1$, there are no slower scales.

5.3.4. The estimates passed to the next stage. The bound on the differences, including the weighted past before τ_{n+1}, gives

$$Y_n(t) \le C\kappa_n e^{2\sqrt{2}\Omega_n(t-\tau_{n+1})} \quad (0 \le t \le T_n), \qquad \kappa_n e^{2\sqrt{2}\Omega_n(T_n-\tau_{n+1})} = \frac{q_*}{\mathcal{A}_n}(1+O(\varepsilon_*)).$$

Combining these bounds controls every earlier time by its distance from T_n. The interval from T_n to τ_n has bounded length in normalized time and bounded linear evolution. Hence

$$Y_n(t) \le M_{\mathrm{hist}} e^{c\Omega_n(t-\tau_n)}, \qquad 0 \le t \le \tau_n.$$

To keep the same constant at every stage, the proof separates the leading source from the terms depending on the previously assumed M_{hist}. The coefficient in the new bound is at most

$$C + C\big(B^{-1} + B^{-2} + o_{\Lambda\to\infty}(1)\big)M_{\mathrm{hist}} \le \tfrac{3}{4}M_{\mathrm{hist}}.$$

The constants on the left are fixed by the one-quadrupole estimates before B, Λ are chosen. Section 7.1 first fixes M_{hist} larger than the leading constant, then chooses B and Λ to obtain this strict improvement.

The slower-scale estimate supplies the actual state of the next scale. The main factor is

$$\frac{\Gamma_n \ell_n^2}{\Omega_n |d_{n-1} - d_n|^4} \asymp \kappa_{n-1} \left(\frac{\Omega_{n-1}}{\Omega_n} \right)^2 = \kappa_{n-1} B^{-2}.$$

Consequently, for $n \geq 2$,

$$Y_{n-1}(\tau_n) \leq C M_{\mathrm{hist}} \kappa_{n-1} B^{-2} + C(1 + M_{\mathrm{hist}}) \kappa_{n-1} e^{-c\Omega_{n+1}^{\alpha}}.$$

These estimates, together with the time, angle, and moment bounds for scale n and the rhombus bounds for $i < n$, provide the inputs for the next stage.

Finally, the geometric estimates give

$$\mathrm{diam}(\text{quadrupole } j) \leq C\ell_j(1 + \Omega_j), \qquad |d_i^{(k)}(t) - d_j^{(k)}(t)| \geq \tfrac{1}{2}|d_i - d_j|.$$

Since $\ell_j(1 + \Omega_j) \ll d_j$, quadrupoles remain separated. Their minimum internal distances stay bounded below by $c\ell_j$, while the lengths within each dipole remain comparable to ℓ_j, and Theorem 3.10(iv) keeps each normalized patch boundary within $C\Omega_j^{-2}$ of a circle. These bounds exclude the remaining failures on the stopped interval. Descending induction therefore reaches scale 1 and continues every dipole through time 1, with constants independent of N. Moreover,

$$\tau_1 \leq \sum_{n \geq 1} \Delta_n + \frac{C_h \varepsilon_*}{\Omega_1} < \frac{1}{2}.$$

5.4 Conclusion

Proposition 5.1. *For the fixed choices above and every $N \geq 2$, the prescribed initial configurations give Euler solutions $\omega_N^{(1)}, \omega_N^{(2)}$ on $[0, 1]$, with $u_N^{(k)} = K * \omega_N^{(k)}$. Their initial patches agree at every scale $n < N$, and the first solution satisfies Proposition 4.1. In the second solution, scale N starts in the prescribed separating configuration and the remaining scales reach that separation in order, with*

$$0 = \tau_N < \tau_{N-1} < \cdots < \tau_1 < \tfrac{1}{2}, \qquad |\tau_n - \tau_{n,N}| \leq C_h \varepsilon_* / \Omega_n.$$

All patches remain disjoint. Each normalized boundary has $C^{1,1/2}$ distance at most $C\Omega_n^{-2}$ from a parameterized circle. Distances between quadrupoles remain comparable to their initial distances, and the supports lie in one bounded set independent of N.

Proposition 7.2, proved in Section 7.5, establishes this statement from the reference construction and the initial data above. By Section 7.6, at time 1 the first solution's outer patches lie within $C\ell_1$ of d_1, and the second solution's outer patches lie at distances comparable to $\Omega_1 \ell_1$. In each solution, the outer center moves by $o(\ell_1)$, uniformly in N. A fixed annulus centered at d_1 contains all four outer patches of the second solution and no other patches of either solution at time 1. Choose a smooth $0 \leq \chi \leq 1$ supported in this annulus and equal to one on those four patches, uniformly in N. Then

$$\int \chi |\omega_N^{(1)}(1)| \, dx = 0, \qquad \int \chi |\omega_N^{(2)}(1)| \, dx = 4\Gamma_1. \tag{5.4}$$

Since A, B, Λ are fixed, $4\Gamma_1 > 0$ is independent of N. The initial difference, confined to scale N, tends to zero in every finite L^p by (1.4). Section 8 extracts a common subsequence whose initial data converge to the same ω_0 and whose vorticities converge strongly in $C([0, 1]; L^1)$. Thus $\omega^{(1)}(0) = \omega^{(2)}(0)$ and $\|\omega^{(2)}(1) - \omega^{(1)}(1)\|_{L^1} \geq 4\Gamma_1 > 0$.

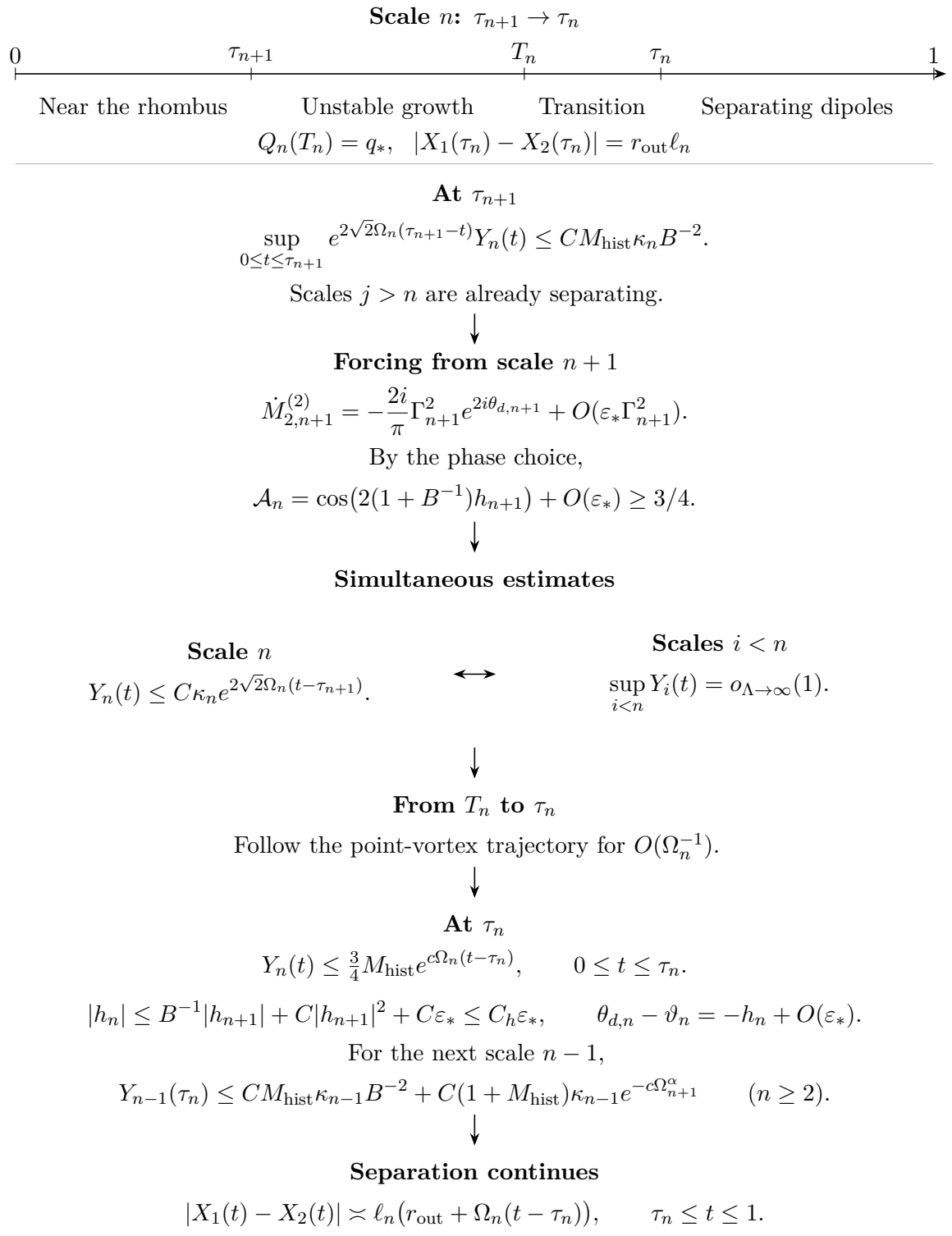


Figure 2: $h_j = \Omega_j(\tau_j - \tau_{j,N})$ measures the timing error in scale j's time unit. The estimates for $n, n-1, \cdots, 1$ are proved together in each induction step. The bounds at τ_n supply the same inputs for the next step. Patch boundaries and geometry are controlled by Theorem 3.10(iv) and §7.1.

6 Transition in quadrupole configurations

We compare one quadrupole with the prepared reference, starting at a physical time $t_0 \geq 0$. In Section 7, $t_0 = \tau_{n+1}$ is the time when quadrupole $n+1$ reaches the prescribed dipole separation. Both solutions have already evolved on $[0, t_0]$, and we retain their centroid, moment, and boundary differences at t_0. We first estimate the growth of the unstable shape variable, then the separation and second moment of the resulting dipoles. Section 7 verifies the external-field bounds used here.

Suppress the quadrupole index and write $\Gamma = 2\pi\Omega\ell^2$, $a^2/\ell^2 = 2/(A\Omega^3)$, and $\rho = C_A\Omega^{-2}$. The external velocity U is generated by all other quadrupoles. We use the centroid and moment equations (3.6) and (3.10). The quantity W is the integral in (3.7), retaining its value at t_0 as in (3.9). To estimate $D = |z_1|^2 - |z_2|^2$, we evolve the patch angular impulse I. Equation (3.11) gives

$$\left|\frac{D}{\ell^2} - \frac{I}{2\Gamma\ell^2}\right| \leq C\frac{a^2}{\ell^2}\rho^2, \qquad \left|\triangle\left(\frac{D}{\ell^2} - \frac{I}{2\Gamma\ell^2}\right)\right| \leq C\frac{a^2}{\ell^2}\rho W.$$

Thus $I/(2\Gamma\ell^2)$ determines D/ℓ^2 up to the displayed patch error.

6.1 The exact unstable rate

Consider first the four point vortices of Section 2, at $\pm z_1, \pm z_2$ with circulations $\Gamma, \Gamma, -\Gamma, -\Gamma$. Their angular impulse is $2\Gamma D$, where $D = |z_1|^2 - |z_2|^2$ is conserved. The orbit in Proposition 2.2 has $D = \ell^2$. In normalized time $s = \Omega t$, the shape variables (p, q) have linear rates $-2\sqrt{2}, 2\sqrt{2}$ at the rhombus.

We first express the separating orbit as $p = h(q)$. Put $r = \sqrt{R}$ and $r_* = \sqrt{2} - 1$. The sine formula in the proof of Proposition 2.2 is analytic near r_*. The branch $\phi(r) = \pi - \arcsin(\sin\phi(r))$ gives

$$\frac{d\sin\phi}{dr}\bigg|_{r=r_*} = -\frac{2\sqrt{2}}{r_*}, \qquad \frac{dq}{dr}\bigg|_{r=r_*} = \frac{2}{r_*}, \qquad \frac{dp}{dr}\bigg|_{r=r_*} = 0.$$

Consequently $p = h(q)$ near zero, with h analytic and $h(0) = h'(0) = 0$. Along the separating trajectory, $q > 0$ and

$$p_s - h'(q)q_s = 0 \qquad \text{when } p = h(q).$$

After substituting $p = h(q)$, the left side is an analytic function of q. Since it vanishes for all small positive q, it also vanishes for all small negative q. Thus a solution starting on this graph stays on it, for either sign of q.

Use the coordinates $\widehat{q}, \widehat{p}, \widehat{\Theta}$ in (2.15)–(2.16). Their differential with respect to (q, p, Θ) is the identity at the rhombus. On $\widehat{p} = 0$, differentiation gives $\widehat{q}_s = 2\sqrt{2}\widehat{q}$ and $\widehat{\Theta}_s = -1$. Away from this graph,

$$\widehat{q}_s = 2\sqrt{2}\widehat{q} + \widehat{p}B_q, \qquad \widehat{p}_s = -2\sqrt{2}\widehat{p} + \widehat{p}B_p, \qquad |B_q| + |B_p| \leq C(|\widehat{q}| + |\widehat{p}|).$$

Recall that $\Theta_s = -1 + \psi(\widehat{q}, \widehat{p})$, with $\psi = O((|\widehat{q}| + |\widehat{p}|)^2)$, when $D = \ell^2$. The functions B_q, B_p are analytic. Indeed, subtracting the value at $\widehat{p} = 0$ factors out $\widehat{p}$, and the linearization makes the remaining coefficient vanish at zero. The phase equation is $\widehat{\Theta}_s = -1 + \widehat{p}B_\Theta$, where

$$B_\Theta = \int_0^1 \partial_{\widehat{p}}\psi(\widehat{q}, r\widehat{p})\, dr - \frac{\psi(\widehat{q}, 0)}{2\sqrt{2}\widehat{q}}B_q, \qquad |B_\Theta| \leq C(|\widehat{q}| + |\widehat{p}|).$$

The quotient is analytic at zero because $\psi(\widehat{q}, 0) = O(\widehat{q}^2)$.

For general $D > 0$ near ℓ^2, the common frequency in (2.3) is $\Gamma/(2\pi D) = \Omega\ell^2/D$, in place of Ω. Keeping $s = \Omega t$ gives

$$\widehat{q}_s = \frac{\ell^2}{D}(2\sqrt{2}\widehat{q} + \widehat{p}B_q), \qquad \widehat{p}_s = \frac{\ell^2}{D}(-2\sqrt{2}\widehat{p} + \widehat{p}B_p).$$

The phase satisfies $\widehat{\Theta}_s = (\ell^2/D)(-1 + \widehat{p}B_\Theta)$, and $D_s = 0$. Thus the nonlinear shape and phase terms vanish when $\widehat{p} = 0$, with no term depending quadratically on $\widehat{q}$ alone. The next subsection estimates both the stable difference and ℓ^2/D during the long growth interval.

For the orbit normalized in Section 5.1, $\widehat{q}/q \to 1$ and $\widehat{\Theta} - \theta \to 0$ at the rhombus. Its equations therefore give $\widehat{q}(s) = e^{2\sqrt{2}s}$ and $\widehat{\Theta}(s) = -s$ as long as these local coordinates are defined. We retain $K, \theta_\infty, \beta = \theta_\infty + K$ from that section.

6.2 Departure and dipole separation

We now compare two four-patch motions, the first being the reference in Proposition 4.1. At the original time $t = 0$, their radii and signed circulations agree and $F_i^{(1)}(0,\theta) = F_i^{(2)}(0,\theta) = e^{i\theta}$. Their centroids may differ. Starting at t_0, set $s = \Omega(t - t_0)$, $\iota^{(j)} = I^{(j)}/(2\Gamma\ell^2)$, $Q = \triangle\widehat{q}$, and $P = \triangle\widehat{p}$. Write

$$\nu = \left(\triangle\iota, \triangle\widehat{\Theta}, \operatorname{Re}\frac{\triangle\delta}{\ell}, \operatorname{Im}\frac{\triangle\delta}{\ell}\right), \qquad |Z| = |Q| + |P| + |\nu|.$$

All trajectory variables in this subsection are evaluated at $t = t_0 + s/\Omega$ when their argument is s. We use the sum of the absolute values of the components for $|\nu|$. This $|Z|$ is equivalent, in the fixed rhombus neighborhood and up to the impulse correction above, to the centered-centroid norm in (3.5). We write $W(s)$ for the restarted integral (3.9), so $W(0)$ retains the history up to physical time t_0. The normalized external input is $F(s) = \Omega^{-1}\|\triangle A(t_0 + s/\Omega)\|_R$.

At the rhombus with $D = \ell^2$, the point-vortex linearization is

$$Q_s = 2\sqrt{2}Q, \qquad P_s = -2\sqrt{2}P, \qquad (\triangle\iota)_s = 0, \qquad (\triangle\widehat{\Theta})_s = \triangle\iota, \qquad (\triangle\delta)_s = 0.$$

The phase equation follows from $\partial_\iota(-1/\iota) = 1$ at $\iota = 1$. Thus the linear operator on ν is simply

$$\mathcal{N}\nu = (0, \triangle\iota, 0, 0), \qquad e^{s\mathcal{N}} = \mathrm{Id} + s\mathcal{N}, \qquad \|e^{s\mathcal{N}}\| \le C_\sigma e^{\sigma s/2} \quad (s \ge 0),$$

for any fixed $0 < \sigma < \sqrt{2}/2$. The unstable shape difference grows exponentially. The other unforced differences decay, stay constant, or grow only linearly.

6.2.1. External input and initial differences. We specify the bounds that Section 7 verifies. At scale n, let g denote the signed input difference from slower quadrupoles $i < n$ between the two motions. It contains the analytic coefficient differences and their reference projections onto the physical-time equations for (Q, P, ν), including the receiving-patch averages. The norm $\|g\|$ is the sum of the R-weighted coefficient norm in (3.5) and the absolute values of these projections. Division by Ω gives the corresponding input in time s.

Suppose $\|g\| \le b_0 + b_1$, where $b_0, b_1 \ge 0$ bound, respectively, the contributions from the states at t_0 and scales $j > n$, and the contribution from scale n after t_0. The fixed projection and averaging constants are included in these bounds. Split

$$g = \frac{b_0 g}{b_0 + b_1} + \frac{b_1 g}{b_0 + b_1}, \qquad \left\|\frac{b_k g}{b_0 + b_1}\right\| \le b_k \quad (k = 0, 1),$$

with both terms zero when $b_0 + b_1 = 0$. This decomposition is made along the actual solution; its pieces are not separate evolutions, and no derivatives of them are used. The common scalar factors preserve the linear projections. Section 7.2 provides b_0, b_1.

The forcing from $j > n$ together with $b_0 g/(b_0 + b_1)$ has normalized contributions $\kappa f_q, \kappa f_p, \kappa f_\nu$ to the reference centroid and moment equations. Here $0 < \kappa \ll 1$ measures the initial perturbation and forcing. Assume

$$|Q(0)| + |P(0)| + |\nu(0)| + W(0) \le C\kappa, \tag{6.1}$$

$$|f_q(s)|+|f_p(s)|+|f_\nu(s)| \le C(1+s)^m e^{\sigma s/2}, \qquad \mathcal{A} = \frac{Q(0)}{\kappa} + \int_0^\infty e^{-2\sqrt{2}s} f_q(s)\, ds \ge A_* > 0. \tag{6.2}$$

The integer $m \ge 0$, A_*, and the input constants are fixed independently of κ. The displayed bound also gives $\mathcal{A} \le C$. For a stopped motion, $\mathcal{A} \ge A_*$ refers to an extension of f_q satisfying the same bound. Its tail after s has absolute value at most $C(1+s)^m e^{-(2\sqrt{2}-\sigma/2)s}$, which becomes a small power of κ at the departure time proved below.

Bound the normalized contribution of $b_1 g/(b_0+b_1)$ by a positive operator

$$\begin{gathered}(\mathcal{R}Y)(s) = r_0(s)Y(s) + \int_0^s r(s,u)Y(u)\, du, \qquad r_0, r \ge 0, \\ \sup_s \left[r_0(s) + \int_0^s r(s,u) e^{-2\sqrt{2}(s-u)}\, du \right] \le \eta_{\mathrm{return}}.\end{gathered} \tag{6.3}$$

Let $F_0(s) = C\kappa(1+s)^m e^{\sigma s/2}$ bound the normalized coefficient input from $j > n$ and $b_0 g/(b_0+b_1)$, as well as $\kappa(|f_q| + |f_p| + |f_\nu|)$. Assume

$$F \le F_0 + \mathcal{R}(|Z| + W), \qquad \sigma_c \le \sigma/2. \tag{6.4}$$

The inherited values at t_0 enter the initial state and f_q, f_p, f_ν. The operator $\mathcal{R}$ bounds the response to subsequent motion.

Choose $T \le 1$ so that the available interval contains

$$t_0 + \frac{1}{\Omega}\left[\frac{1}{2\sqrt{2}} \log \frac{4}{A_*\kappa} + K + 1\right] \le T \le 1. \tag{6.5}$$

Up to the displayed time or the first bootstrap exit, assume the geometric, external, and comparison hypotheses of Theorem 3.10 on the original interval. The comparison neighborhoods are a fixed small neighborhood of the rhombus and a fixed collision-free neighborhood of the subsequent point-vortex trajectory to pair-center distance $r_{\mathrm{out}}\ell$. Proposition 4.1(ii) gives

$$|q^{(1)}| + |p^{(1)}| + |\iota^{(1)} - 1| + \left| \frac{\ell^2}{D^{(1)}} - 1 \right| \le C\left(\frac{\mathsf{S} + T\mathsf{S}^2}{\Omega} + \Omega^{-5} \right), \qquad \frac{|\delta^{(1)}|}{\ell} \le C\mathsf{T}\ell T.$$

For the remainder of this section, η denotes the following scalar error bound, not the contour label coordinate:

$$\eta = C\left(\frac{\mathsf{S} + T\mathsf{S}^2}{\Omega} + \Omega^{-3} + \mathsf{T}\ell T + \eta_{\mathrm{return}} \right). \tag{6.6}$$

In particular, $a^2/\ell^2 \le \eta$ and the reference errors above are $O(\eta)$. We choose a fixed small $q_* > 0$ from the input bounds, then require κ and $\eta \log(1/\kappa)$ to be sufficiently small. Section 7 will exclude geometric and external-field failures in the coupled construction.

6.2.2. Difference equations. Subtracting the two motions defines the remainders by

$$Q_s = 2\sqrt{2}Q + \kappa f_q + r_q, \qquad P_s = -2\sqrt{2}P + \kappa f_p + r_p, \qquad \nu_s = \mathcal{N}\nu + \kappa f_\nu + r_\nu.$$

The coordinate change removes the nonlinear terms on the separating orbit. After the terms with small reference coefficients are included in $C\eta|Z|$, every remaining quadratic difference contains P or a component of ν. We derive the bounds

$$\begin{aligned} |r_q| &\le C\left[\eta|Z| + |P|(|Q| + |P|) + |\nu||Q| + |\nu|^2 + \frac{a^2}{\ell^2} W + F_0|Z| \right] + \mathcal{R}(|Z| + W), \\ |r_p| + |r_\nu| &\le C\left[\eta|Z| + (|P| + |\nu|)|Z| + \frac{a^2}{\ell^2} W + F_0|Z| \right] + \mathcal{R}(|Z| + W). \end{aligned} \tag{6.7}$$

The impulses $\iota^{(j)}$ stay bounded away from zero in the chosen neighborhood. By the patch impulse bounds above and $x^{-1}-y^{-1}=(y-x)/(xy)$,

$$\left|\triangle\left(\frac{\ell^2}{D}-\frac{1}{\iota}\right)\right| \le C\frac{a^2}{\ell^2}\rho W + C\frac{a^2}{\ell^2}\rho^2|\triangle\iota|.$$

Replacing ℓ^2/D by $1/\iota$ therefore costs at most $C(a^2/\ell^2)W+C\eta|Z|$. This includes the difference of the shape factors multiplying the absolute reference correction $O((a^2/\ell^2)\rho^2)$. The normalized centered centroid differences are bounded by $C|Z|+C(a^2/\ell^2)\rho W$, so the same replacement is allowed in the input to W.

For the point-vortex system with no external field, conservation of $M_1=4\Gamma\delta$ gives $\delta_s=0$. The equations for z_1 and z_2 are even in δ, since the cross-pair denominators occur in pairs $2\overline{\delta}\pm\overline{z}_1\pm\overline{z}_2$. The internal arithmetic-center velocity is odd in δ and bounded by $C\Omega|\delta|$. Its product with M_1 in (3.10) is therefore quadratic. Taylor's formula bounds the normalized differences of these corrections by

$$C\left[\frac{|\delta^{(1)}|}{\ell}\frac{|\triangle\delta|}{\ell}+\left|\frac{\triangle\delta}{\ell}\right|^2+\left(\frac{|\delta^{(1)}|}{\ell}\right)^2|Z|\right] \le C\eta|Z|+C\left|\frac{\triangle\delta}{\ell}\right|^2.$$

The moving-center term in the material impulse equation is $-2\,\mathrm{Re}(\dot{\overline{dM_1}})$. Its additional centroid-error contribution has relative bound $C\eta|Z|+C(a^2/\ell^2)W$. Common translation cancels from the centered internal equations and is estimated separately in Section 7.

The reference shape variables, $\iota^{(1)}-1$, and $\delta^{(1)}/\ell$ are $O(\eta)$. The coordinate derivatives are bounded uniformly in the reference phase. For the inverse-impulse terms,

$$\begin{aligned}
\frac{\widehat{q}^{(2)}}{\iota^{(2)}}-\frac{\widehat{q}^{(1)}}{\iota^{(1)}}-Q &= \left(\frac{1}{\iota^{(2)}}-1\right)Q-\frac{\triangle\iota\,\widehat{q}^{(1)}}{\iota^{(2)}\iota^{(1)}},\\
\frac{\widehat{p}^{(2)}}{\iota^{(2)}}-\frac{\widehat{p}^{(1)}}{\iota^{(1)}}-P &= \left(\frac{1}{\iota^{(2)}}-1\right)P-\frac{\triangle\iota\,\widehat{p}^{(1)}}{\iota^{(2)}\iota^{(1)}},\\
-\frac{1}{\iota^{(2)}}+\frac{1}{\iota^{(1)}}-\triangle\iota &= \triangle\iota\left(\frac{1}{\iota^{(2)}\iota^{(1)}}-1\right).
\end{aligned}$$

These expressions are bounded, respectively, by $C\eta|Z|+C|\nu||Q|$, $C\eta|Z|+C|\nu||P|$, and $C\eta|Z|+C|\nu|^2$. Since each B_q, B_p, B_Θ vanishes linearly and has bounded first derivatives, the difference of $\widehat{p}B/\iota$ is bounded by $C\eta|Z|+C|P|(|Q|+|P|)$. Together with the offset estimate, these give the quadratic terms in (6.7).

We next estimate the external terms. Pull back each external field about its own center. For a centered field U, put

$$E^{(j)}_{\mathrm{ext},i}[U]=\frac{1}{\Gamma_i}\int[U(z-d^{(j)})-U(\zeta_i^{(j)}-d^{(j)})]\omega_i^{(j)}(z)\,dA(z).$$

Here Γ_i is the signed circulation, and $E^{(j)}_{\mathrm{ext}}[U]$ denotes the vector of the four averages. By linearity,

$$\triangle E_{\mathrm{ext}}=E^{(1)}_{\mathrm{ext}}[\triangle U]+(E^{(2)}_{\mathrm{ext}}-E^{(1)}_{\mathrm{ext}})[U^{(2)}].$$

The averaging calculation in Theorem 3.10(i),(ii), applied to the fixed field $U^{(2)}$, gives

$$\frac{|E^{(1)}_{\mathrm{ext}}[\triangle U]|}{\Omega\ell}\le C\frac{a^2}{\ell^2}\rho F,\qquad \frac{|(E^{(2)}_{\mathrm{ext}}-E^{(1)}_{\mathrm{ext}})[U^{(2)}]|}{\Omega\ell}\le C\frac{a^2}{\ell^2}\frac{\mathsf{S}}{\Omega}(\rho|Z|+W).$$

The second estimate uses $\|A^{(2)}\|_R\le C\mathsf{S}$ without separate absolute bounds for the two input contributions. The same decomposition applies to the external moment integrals. Indeed, the

first integral in the equation for $\dot I$, divided by $2\Gamma\ell^2\Omega$, is

$$\operatorname{Re}\sum_{k\ge1}\frac{A_k}{\Omega}\frac{\overline{M_{k+1}}}{\Gamma\ell^{k+1}},$$

and the equation for $\dot M_1/(\Gamma\ell\Omega)$ has the corresponding series with $M_k/(\Gamma\ell^k)$, where its $k=1$ term is $M_1/(\Gamma\ell)$. The relative moment bounds and the convergent coefficient series bound the changes at fixed $U^{(2)}$ by $C(\mathsf{S}/\Omega)[|Z|+(a^2/\ell^2)W]$. The external contribution to $(U(d)-\dot d)\overline{M_1}$ obeys the same bound, by the four centroid averages and $M_1=4\Gamma\delta$.

Relative to evaluation at the centroids, the receiving-patch averages enlarge the bounds given by F_0 by at most a factor $1+C(a^2/\ell^2)\rho$ and contribute at most $C(a^2/\ell^2)\rho\kappa$ to $\kappa\mathcal{A}$. The bound given by $\mathcal{R}$ increases by the same factor.

Evaluating the input bounded by F_0 at the second state instead of the reference costs $CF_0|Z|$, and the corresponding terms from $b_1g/(b_0+b_1)$ are absorbed into $\mathcal{R}(|Z|+W)$ on the fixed neighborhood.

When converting the centroid errors to coordinate errors, the difference of the coordinate derivatives also multiplies the absolute reference error. Theorem 3.10(i) and the centered-coordinate bound above estimate this term by $C(a^2/\ell^2)\rho[|Z|+(a^2/\ell^2)\rho W]$, which is included in $C\eta|Z|+C(a^2/\ell^2)W$. Together with (3.8), these estimates prove (6.7), with no term CQ^2 independent of P,ν.

6.2.3. Growth of the unstable shape difference. Duhamel's formula gives

$$\begin{aligned}
Q(s)&=e^{2\sqrt2 s}\left[Q(0)+\int_0^s e^{-2\sqrt2 r}(\kappa f_q+r_q)(r)\,dr\right],\\
P(s)&=e^{-2\sqrt2 s}P(0)+\int_0^s e^{-2\sqrt2(s-r)}(\kappa f_p+r_p)(r)\,dr,\\
\nu(s)&=e^{s\mathcal{N}}\nu(0)+\int_0^s e^{(s-r)\mathcal{N}}(\kappa f_\nu+r_\nu)(r)\,dr.
\end{aligned}$$

Put $E(s)=\kappa e^{2\sqrt2 s}$. Stop at $Q=\pm q_*$, another local boundary, or

$$T_\kappa=\frac{1}{2\sqrt2}\log\frac{4q_*}{A_*\kappa}. \tag{6.8}$$

Then $E\le 4q_*/A_*$. We prove

$$|Q|\le CE,\qquad |P|+|\nu|\le C\eta E+C\kappa e^{\sigma s},\qquad W\le CE.$$

Choose the constants for $|Q|$, the $\kappa e^{\sigma s}$ term, W, and the ηE term in this order, then reduce η. The convolution estimates are

$$\begin{aligned}
&\int_0^s e^{-2\sqrt2(s-r)}E(r)\,dr\le\frac{E(s)}{4\sqrt2},\qquad
\int_0^s e^{\sigma_c(s-r)}E(r)\,dr\le\frac{E(s)}{2\sqrt2-\sigma_c},\\
&\int_0^s C_\sigma e^{\sigma(s-r)/2}E(r)\,dr\le\frac{C_\sigma E(s)}{2\sqrt2-\sigma/2}.
\end{aligned}$$

The initial stable and neutral terms and the Duhamel integrals of $\kappa f_p,\kappa f_\nu$ are bounded by $C\kappa e^{\sigma s}$, since $(1+s)^{m+1}e^{\sigma s/2}\le Ce^{\sigma s}$. Also $\kappa e^{\sigma s}\le E$ and $\mathcal{R}E\le\eta E$. Under the displayed bounds,

$$\mathcal{R}(|Z|+W)\le C\eta E,\qquad \frac{a^2}{\ell^2}W\le C\eta E.$$

Since $|Z| \le Cq_*$, Duhamel's formula gives

$$|P(s)| + |\nu(s)| \le C\kappa(1+s)^{m+1}e^{\sigma s/2} + C\int_0^s e^{\sigma(s-r)/2}\left[\eta E(r) + q_*(|P(r)| + |\nu(r)|)\right] dr.$$

Here $F_0|Z| \le Cq_*F_0$ is included in the first term. Choose q_* so that the rate added by Gronwall is less than $\sigma/2$. The preceding convolution estimates then give $|P| + |\nu| \le C\eta E + C\kappa e^{\sigma s}$. Equation (3.9) gives

$$\sup_{0\le r\le s}\frac{W(r)}{E(r)} \le C + C\eta \sup_{0\le r\le s}\frac{W(r)}{E(r)}.$$

The coefficient of ηE was fixed after the bound for W, so its contribution is made small by reducing η. The remaining constant depends only on the chosen bounds for Q, the $\kappa e^{\sigma s}$ term, and $W(0)/\kappa$. Absorbing the last term proves $W \le CE$.

Every quadratic term in r_q contains P or ν. Hence

$$|r_q| \le C\eta E + CE(|P| + |\nu| + F_0), \qquad \int_0^s (|P| + |\nu| + F_0)\, dr \le C\eta + C\int_0^s \kappa e^{\sigma r}\, dr.$$

Dividing the formula for Q by E gives

$$\frac{Q(s)}{\kappa e^{2\sqrt{2}s}} = \mathcal{A} + O\left(\eta(1+s) + \int_0^s \kappa e^{\sigma r}\, dr\right) + O\left((1+s)^m e^{-(2\sqrt{2}-\sigma/2)s}\right).$$

Since $\sigma < \sqrt{2}/2$, for $s \le T_\kappa$ we have

$$\kappa e^{\sigma s} + \int_0^s \kappa e^{\sigma r}\, dr \le C\kappa^{1-\sigma/(2\sqrt{2})} \le C\kappa^{3/4}.$$

The partial integral $\int_0^s e^{-2\sqrt{2}r} f_q(r)\, dr$ is uniformly bounded. For $\eta\log(1/\kappa)$ and κ small, the last two estimates improve the bound for Q. Taking q_* smaller keeps all other coordinates inside their neighborhood. This closes the continuity argument up to $Q = \pm q_*$ or T_κ.

Choose a fixed s_0 so that the forcing tail is at most $A_*/4$ for $s \ge s_0$. For small κ, $|Q| \le C\kappa e^{2\sqrt{2}s_0} < q_*$ on $[0, s_0]$. For $s \ge s_0$, $Q/E \ge A_*/2$, so the value $Q = -q_*$ cannot be reached. Reaching T_κ first would give $Q(T_\kappa) \ge 2q_*$. Thus, unless a geometric or external-field bound fails first, $Q = q_*$ is reached. Its time satisfies $s_* = \frac{1}{2\sqrt{2}}\log(1/\kappa) + O(1)$. At this time the forcing tail is $O(\kappa^{3/4})$. Taking a logarithm in the formula for Q/E and using the stable and neutral estimates gives

$$s_* = \frac{1}{2\sqrt{2}}\log\frac{q_*}{\kappa\mathcal{A}} + O(\eta\log(1/\kappa) + \kappa^{3/4}), \qquad |P(s_*)| + |\nu(s_*)| \le C(\eta + \kappa^{3/4}). \tag{6.9}$$

On this interval $|Z| + F + W \le C\kappa e^{2\sqrt{2}s}$. Since the relative centroid error contains $(a^2/\ell^2)W$, its accumulated contribution to the unstable coefficient, divided by κ, is at most

$$\frac{C}{\kappa}\int_0^{s_*} e^{-2\sqrt{2}s}\frac{a^2}{\ell^2}W(s)\, ds \le C\Omega^{-3}\log(1/\kappa).$$

6.2.4. Continuation to separating dipoles. At $s = s_*$, the second motion has $\widehat{q}^{(2)} = q_* + O(\eta)$, while its errors in $\widehat{p}$, ι, and δ/ℓ are $O(\eta + \kappa^{3/4})$. Moreover, $\triangle\widehat{\Theta} = O(\eta + \kappa^{3/4})$ and $\widehat{\Theta}^{(1)} = \theta^{(1)} + O(\eta)$. The normalized point-vortex orbit reaches $\widehat{q} = q_*$ at time $\log q_*/(2\sqrt{2})$, with $\widehat{\Theta} = -\log q_*/(2\sqrt{2})$. Rotate it by

$$\theta^{(1)}(s_*) + \frac{\log q_*}{2\sqrt{2}}.$$

Its centered configuration then agrees with the second motion up to $O(\eta+\kappa^{3/4})$. The remaining point-vortex duration is $K - \log q_*/(2\sqrt{2})$, a fixed number independent of κ.

Let $e(r)$ be the sum of the four centered centroid differences between the second patch motion and this rotated point-vortex orbit, divided by ℓ, where r is the elapsed normalized time after s_*. On the fixed collision-free neighborhood, the point-vortex field is Lipschitz. The centroid error estimate of Theorem 3.10(i) therefore gives, up to the first neighborhood exit,

$$e(r) \le C(\eta + \kappa^{3/4}) + C_{\mathrm{sec}} \int_0^r \left[e(u) + \frac{\mathsf{S}}{\Omega} + \frac{a^2}{\ell^2}\rho \right] du.$$

Here C_{sec} may depend on the fixed orbit segment from q_* to r_{out}, but is independent of the scale. Gronwall gives $e \le C_{\mathrm{sec}}(\eta + \kappa^{3/4})$ on this fixed interval. For small parameters this excludes the neighborhood exit, and Theorem 3.10(iv) continues the patch boundary bounds. At the prescribed separation, Proposition 2.2 gives

$$\frac{d}{ds}\frac{|X_1 - X_2|}{\ell} = 2 + O(r_{\mathrm{out}}^{-2}) \ge 1.$$

This positive lower bound persists for the nearby patch motion. Thus its crossing time and angle differ by $O(\eta + \kappa^{3/4})$ from those of the rotated point-vortex orbit. Adding the two durations gives

$$s_{\mathrm{out}} = \frac{1}{2\sqrt{2}} \log \frac{1}{\kappa \mathcal{A}} + K + O\big(\eta \log(1/\kappa) + \kappa^{3/4}\big). \tag{6.10}$$

The physical separation time is $t_0 + s_{\mathrm{out}}/\Omega$. It lies before the assumed upper time, since the local duration is less than T_κ and

$$T_\kappa + K - \frac{\log q_*}{2\sqrt{2}} + 1 = \frac{1}{2\sqrt{2}} \log \frac{4}{A_* \kappa} + K + 1.$$

The reference satisfies $\theta_s^{(1)} = -1 + O(\eta)$, so

$$\theta^{(1)}(s_{\mathrm{out}}) = \theta^{(1)}(s_*) - K + \frac{\log q_*}{2\sqrt{2}} + O(\eta + \kappa^{3/4}).$$

The associated limiting angle θ_d is defined in Section 5.1 by adding $\theta_\infty - \theta(K)$ to the angle of $z_1^{(2)}$ at crossing. For the rotated orbit it equals $\theta^{(1)}(s_*) + \log q_*/(2\sqrt{2}) + \theta_\infty$. Since $\beta = \theta_\infty + K$, the patch motion satisfies

$$\theta_d = \theta^{(1)}(s_{\mathrm{out}}) + \beta + O\big(\eta \log(1/\kappa) + \kappa^{3/4}\big). \tag{6.11}$$

We summarize the results of this subsection as follows.

Proposition 6.1. *Assume* (6.1)–(6.5) *and the hypotheses of Theorem 3.10 on the comparison neighborhoods specified after* (6.5). *Suppose* κ *and* $\eta \log(1/\kappa)$ *are sufficiently small, with* η *given by* (6.6). *Unless a geometric or external-field bound fails first,* Q *reaches* q_* *with* (6.9). *The pair-center distance then reaches* $r_{\mathrm{out}}\ell$ *at physical time* $t_0 + s_{\mathrm{out}}/\Omega$, *with* s_{out} *and* θ_d *given by* (6.10) *and* (6.11). *The constants are independent of the scale and* κ.

6.3 Separating dipoles and their second moment

Shift physical time so that $t = 0$ is the separation time obtained in Section 6.2. Thus t in this subsection is elapsed physical time after separation; the corresponding interval lies in the original interval $[0, 2]$. Continue the patch boundary estimates from the original disks, retaining the actual contours at the new time zero.

Pair each positive patch with the nearby negative patch. Let X_j be the center of pair j and v_j its positive centroid minus its negative centroid. Write

$$d = \frac{X_1 + X_2}{2}, \qquad R = |X_1 - X_2|, \qquad M_1 = \Gamma(v_1 + v_2).$$

Assume that at $t = 0$ the four centroids are within $\xi\ell$ of a translated and rotated copy of the prescribed point-vortex configuration at distance $r_{\mathrm{out}}\ell$. Let ϑ be the limiting dipole angle of that copy. On a neighborhood of the quadrupole's convex hull, assume

$$\|DU\|_{L^\infty} \le C\mathsf{S}, \qquad \|D^2U\|_{L^\infty} \le C\mathsf{T}.$$

Assume also the geometric criterion of Theorem 3.10(iv) from the original initial time whenever the distances between centroids within the quadrupole are at least $c\ell$. Section 7 verifies these hypotheses. We require

$$\xi + r_{\mathrm{out}}^{-2} + \mathsf{S}(T + r_{\mathrm{out}}/\Omega) + \Omega\frac{a^2}{\ell^2}\rho T \ll 1.$$

As before, a/ℓ and $(a^2/\ell^2)\rho$ are small by the choice of Ω.

6.3.1. Continued separation. For an isolated point dipole, the vector v is constant and the velocity is $-i\Gamma/(2\pi\overline{v})$. Proposition 2.2 and the initial error give

$$\frac{|v_1(0) - \ell e^{i\vartheta}| + |v_2(0) + \ell e^{i\vartheta}|}{\ell} \le C(\xi + r_{\mathrm{out}}^{-2}).$$

Thus the two self-induced velocities are close to the opposite vectors $\mp i\Omega\ell e^{i\vartheta}$. We prove that this remains so and that the pair centers keep separating. Until a first possible failure, impose

$$\frac{\ell}{2} \le |v_j(t)| \le 2\ell, \qquad \frac{\ell}{4}(r_{\mathrm{out}} + \Omega t) \le R(t) \le 4\ell(r_{\mathrm{out}} + \Omega t).$$

Between the two pairs, $|DK| \le C/R^2$ and $|D^2K| \le C/R^3$. Subtracting the kernels of the two opposite circulations therefore gives a pair-center velocity $O(\Gamma\ell/R^2)$ and a within-pair relative velocity $O(\Gamma\ell^2/R^3)$. These bounds are uniform for $R \ge 4\ell$. Coupling the two normalized area measures in a pair bounds the difference of their external velocity averages by $C\mathsf{S}(|v_j| + a) \le C\mathsf{S}\ell$. Theorem 3.10(i) bounds the internal patch correction by $C\Omega\ell(a^2/\ell^2)\rho$. Consequently,

$$\frac{|\dot v_j(t)|}{\ell} \le C\frac{\Gamma\ell}{R(t)^3} + C\mathsf{S} + C\Omega\frac{a^2}{\ell^2}\rho.$$

The first term is integrable uniformly in time, since

$$\int_0^\infty \frac{\Gamma\ell}{[\ell(r_{\mathrm{out}} + \Omega t)/4]^3}\,dt = \frac{64\pi}{r_{\mathrm{out}}^2}.$$

It follows that

$$\frac{|v_1(t) - \ell e^{i\vartheta}| + |v_2(t) + \ell e^{i\vartheta}|}{\ell} \le C\left[\xi + r_{\mathrm{out}}^{-2} + \mathsf{S}t + \Omega\frac{a^2}{\ell^2}\rho t\right].$$

This improves the bounds for $|v_j|$ and controls both dipole directions.

For sufficiently large r_{out} and small ξ, the point-vortex asymptotics also give

$$\mathrm{Re}\big(ie^{-i\vartheta}(X_1(0) - X_2(0))\big) \ge \frac{3}{4}\ell r_{\mathrm{out}}, \qquad R(0) \le \frac{5}{4}\ell r_{\mathrm{out}}.$$

The self-induced velocity difference has projection at least $3\Omega\ell/2$ in the direction $-ie^{i\vartheta}$. Using the preceding bound for v_j and the bootstrap upper bound for R,

$$\frac{d}{dt}\operatorname{Re}(ie^{-i\vartheta}(X_1-X_2)) \geq \frac{3}{2}\Omega\ell - C\mathsf{S}R - C\frac{\Gamma\ell}{R^2} - C\Omega\ell\frac{a^2}{\ell^2}\rho \geq \Omega\ell,$$
$$|\dot{X}_1-\dot{X}_2| \leq 3\Omega\ell.$$

Indeed, after division by $\Omega\ell$, the three errors are bounded by $C\mathsf{S}(T+r_{\mathrm{out}}/\Omega)$, Cr_{out}^{-2}, and $C(a^2/\ell^2)\rho$. Integrating yields

$$\frac{3}{4}\ell(r_{\mathrm{out}}+\Omega t) \leq R(t) \leq 3\ell(r_{\mathrm{out}}+\Omega t).$$

This improves the remaining bootstrap bounds. All four patches stay separated by at least $c\ell$, so Theorem 3.10(iv) continues the boundary estimates. Hence the bounds for v_j and R hold on $[0,T]$.

6.3.2. The complex second moment. In the exact identity (3.13), the same-patch terms are $O(\Gamma^2\rho)$. Replacing different-patch integrals by their centroid expressions costs $O(\Gamma^2a^2/\ell^2)$, since the linear Taylor terms vanish at the centroids and the second derivatives of $z/\bar{z}$ are bounded by $C|z|^{-2}$. Only the minimum pair distance $c\ell$ is needed for this bound.

The centroid second moment is $2\Gamma[(X_1-d)v_1+(X_2-d)v_2]$. Differentiating it using only the two self-induced dipole velocities, including their contribution to $\dot{d}$, gives

$$-\frac{i\Gamma^2}{2\pi}\left(\frac{1}{\overline{v}_1}-\frac{1}{\overline{v}_2}\right)(v_1-v_2).$$

For $v_1=\ell e^{i\vartheta}$ and $v_2=-\ell e^{i\vartheta}$ this is $-(2i/\pi)\Gamma^2e^{2i\vartheta}$. The bound for v_j changes it by at most

$$C\Gamma^2\left[\xi + r_{\mathrm{out}}^{-2} + \mathsf{S}t + \Omega\frac{a^2}{\ell^2}\rho t\right].$$

For the cross-pair terms, taking one difference in each opposite-sign pair gives $C\Gamma^2\ell^2/R^2 \leq C\Gamma^2r_{\mathrm{out}}^{-2}$. The corresponding moving-center term has the same bound, since its velocity is $O(\Gamma\ell/R^2)$ and $|M_1| \leq C\Gamma\ell$.

For the external contribution, the derivative of $(z-d)(U(z)-U(d))$ is at most $C\mathsf{S}R$. Coupling the normalized area measures of the two patches in each pair, whose supports are at distance $O(\ell)$, therefore gives $C\Gamma\mathsf{S}R\ell$. The external part of $\dot{d}-U(d)$ is at most $C\mathsf{S}R$, so its product with M_1 has the same bound. Finally, the internal centroid error in the moving-center term $-2\dot{d}M_1$ is at most $C\Gamma\ell\cdot\Omega\ell(a^2/\ell^2)\rho$. Using $\Gamma=2\pi\Omega\ell^2$ and the upper bound for R, these errors satisfy

$$\frac{C\Gamma\mathsf{S}R\ell}{\Gamma^2} \leq C\mathsf{S}(t+r_{\mathrm{out}}/\Omega), \qquad \frac{C\Gamma\ell\cdot\Omega\ell(a^2/\ell^2)\rho}{\Gamma^2} \leq C\frac{a^2}{\ell^2}\rho.$$

Since $\rho \leq 1$, summing gives

$$\dot{M}_2(t) = -\frac{2i}{\pi}\Gamma^2e^{2i\vartheta} + O\left(\Gamma^2\left[\xi + r_{\mathrm{out}}^{-2} + \mathsf{S}(t+r_{\mathrm{out}}/\Omega) + \Omega\frac{a^2}{\ell^2}\rho t + \rho + \frac{a^2}{\ell^2}\right]\right). \tag{6.12}$$

The constants in the separation and second-moment bounds are uniform for all sufficiently large r_{out} and independent of Γ,ℓ,Ω and the number of other quadrupoles. In particular, the coefficient of r_{out}^{-2} is uniform. For a quadrupole produced by Section 6.2, insert $\xi \leq C_{\mathrm{sec}}[\eta\log(1/\kappa)+\kappa^{3/4}]$, whose constant contains the dependence on the preceding fixed trajectory segment.

6.3.3. The first and higher moments. For the inherited first moment, assume the same S, T bounds also hold before separation, from the original initial time. In the construction, M_1 is initially zero and the quadrupole stays within $C_{\mathrm{sec}}\ell$ of its center for a physical time at most 1 before separation. Equation (3.10) gives $|\dot{M}_1| \le C\mathsf{S}|M_1| + C_{\mathrm{sec}}\Gamma\mathsf{T}\ell^2$, hence $|M_1(0)| \le C_{\mathrm{sec}}\Gamma\mathsf{T}\ell^2$ at the shifted time zero. For the initially separated top quadrupole, $M_1(0) = 0$ directly.

During separation, subtract the affine external field at d. The derivative of the remainder is at most $C\mathsf{T}R$. The same coupling of the opposite-sign patch measures gives

$$|\dot{M}_1| \le C\mathsf{S}|M_1| + C\Gamma\mathsf{T}R\ell,$$
$$|M_1(t)| \le e^{C\mathsf{S}t}\left[|M_1(0)| + C\Gamma\mathsf{T}\ell^2(r_{\mathrm{out}}t + \Omega t^2)\right].$$

The second inequality follows by integration and the bound for R. It also controls the pair offset, since $M_1 = 4\Gamma\delta$.

Fix $d_{\mathrm{obs}} > 0$ so that the observation distance is at least $d_{\mathrm{obs}} \ge 2R(t)$ throughout $0 \le t \le T$. The first-moment contribution to the external strain is then at most $C|M_1|/d_{\mathrm{obs}}^3$. Let $0 < \Omega_r \le \Omega$ be the frequency of the receiving quadrupole. Integrating against $e^{-2\sqrt{2}\Omega_r t}$ and dividing by $\Gamma^2/(\Omega_r^2 d_{\mathrm{obs}}^4)$ gives

$$\frac{\Omega_r^2 d_{\mathrm{obs}}}{\Gamma^2}\int_0^T e^{-2\sqrt{2}\Omega_r t}|M_1(t)|\,dt \le C\left[\frac{\Omega_r}{\Omega}\mathsf{T}d_{\mathrm{obs}} + \frac{\mathsf{T}d_{\mathrm{obs}}}{\Omega_r}\right].$$

Here C may depend on the fixed r_{out} and the preceding segment. Indeed, $e^{C\mathsf{S}t}$ is bounded on this physical interval, and the three integrals are bounded by $k!/(2\sqrt{2}\Omega_r)^{k+1}$ for $k = 0, 1, 2$.

For $k \ge 2$, all material points satisfy $|z - d| \le R$ when r_{out} is large. Pairing opposite signs and using $|(z-d)^k - (w-d)^k| \le kR^{k-1}|z-w|$ gives

$$|M_k| \le Ck\Gamma\ell R^{k-1}, \qquad \sum_{k\ge 3}\frac{(k+1)|M_k|}{d_{\mathrm{obs}}^{k+2}} \le \frac{C\Gamma\ell R^2}{d_{\mathrm{obs}}^5} \quad \text{if } R/d_{\mathrm{obs}} \le 1/2.$$

Thus (6.12) supplies the leading second moment, and the last two estimates bound the first and higher moments in the far field. The reference second moment contributes a bounded remainder of size $C\Gamma\ell^2$, whose absolute integral against $e^{-2\sqrt{2}\Omega_r t}$ is at most $C\Gamma\ell^2/\Omega_r$. All time integrals are restricted to the actual interval with the stated separation from the receiving quadrupole. If the ideal linear moment is integrated to infinity, its explicit exponentially small tail is subtracted as in Section 2.

7 Proof of Proposition 5.1

We apply the estimates of Section 6.2 successively to $n = N-1, \dots, 1$. At stage n, the quadrupoles $j > n$ have separated and those with $i < n$ remain near their reference rhombi. All estimates are made before the first geometric, patch boundary, or coordinate exit.

7.1 Parameter choices and continuation

Use the scales (1.1). All constants are chosen independently of the number N of quadrupoles, in the order shown below.

A	ε_*, M_0	q_*, κ_0	r_{out}, K	M_{hist}	B	Λ
patch boundaries	local input bounds	departure from the rhombus	dipole separation	bound on earlier motion	frequency ratio	small error terms

An increase of B or Λ does not change any preceding choice.

7.1.1. Patch boundaries. Proposition 2.2 gives a minimum point-vortex distance $c_0\ell$ along the entire separating trajectory. Fix a perturbation margin $c_0\ell/4$ and the resulting individual-patch external bound $C_0\Omega$. Choose A so that Theorem 3.10 keeps the normalized boundaries within $C_A\Omega_n^{-2}$ of circles on $[0,2]$. This choice uses the minimum distance, so it is independent of how far the dipoles are followed. Write

$$\varepsilon_n = \frac{a_n^2}{\ell_n^2} = \frac{2}{A\Omega_n^3}.$$

7.1.2. Departure from the rhombus. Fix the rhombus comparison neighborhood and its coefficient radius R in Theorem 3.10. On $|x| \le 1/2$, we have $\cos x \ge 7/8$ and $|\log\cos x| \le Cx^2$. Fix a universal $C \ge 1$ for these elementary estimates and the timing recurrence (7.9), for $B \ge 4$ and total normalized errors at most ε_*. Fix $C_h \ge 4C$, then choose $\varepsilon_* > 0$ so that $CC_h\varepsilon_* \le 1/4$, $(5/2)C_h\varepsilon_* \le 1/2$, and $C\varepsilon_* \le 1/8$. These constants are independent of the later choices q_*, r_{out}, K. All later constants multiplying forcing, phase, or delay errors are included before those errors are required to be at most ε_*. Fix also $A_* = 1/4$ and $0 < \sigma < \sqrt{2}/2$. In time $s = \Omega_n(t - t_0)$, the leading input from scale $n+1$ is bounded by $C_{\mathrm{dir}}\kappa_n s$, because

$$\frac{\Gamma_{n+1}^2 s}{\Omega_n^2 |d_n - d_{n+1}|^4} \asymp \kappa_n s.$$

The constant $C_{\mathrm{dir}} \ge 1$ includes the projections onto the centroid and moment equations. It also covers velocity divided by d_n and Hessian multiplied by d_n, since $|d_n - d_{n+1}| = d_n/2$. It is independent of q_* and r_{out}. Set

$$M_0 = 4C_{\mathrm{dir}} \max\left\{1, \int_0^\infty e^{-(2\sqrt{2}-\sigma/2)s}(1+s)^3\, ds\right\}.$$

Fix the input bounds of Section 6.2 by

$$|Z(0)| + W(0) \le 2M_0\kappa, \qquad F_0(s) \le 2M_0\kappa(1+s)^3 e^{\sigma s/2},$$
$$\int_0^\infty e^{-2\sqrt{2}s} F_0(s)\, ds \le 2M_0\kappa, \qquad \mathcal{A} \ge A_*.$$

Then $\mathcal{A} \le 4M_0$. Include the fixed coordinate constants for the first-moment and center estimates of Section 7.2 in the same bounds. Section 6.2 now fixes $q_* > 0$ and then $\kappa_0 > 0$ for departure at $Q = q_*$.

7.1.3. Dipole separation and earlier motion. Choose a point sufficiently far along the separating orbit that $Cr_{\mathrm{out}}^{-2} \le \varepsilon_*/4$. Here C is the uniform constant in (6.12), enlarged only by the fixed projections and elementary timing estimates. In particular, it does not depend on the segment chosen by r_{out}. This fixes r_{out}, K, and the trajectory segment from $Q = q_*$ to that distance. Fix a collision-free comparison neighborhood of this segment and its coefficient radius. In this section R is the fixed analytic radius of the comparison neighborhood currently used; the pair-center distance from Section 6.3 will be written explicitly. Enlarging the later neighborhood does not change the local input bounds above. Continue W from its incoming value by (3.9).

Fix also $0 < c < 2\sqrt{2}$ in the earlier-motion bound (7.5). Let C_{sec} bound the estimates on this segment and in Section 6.3. Let $C_{\mathrm{out}} \ge 1$ include the bounds for growth near the rhombus and along this segment, and the bound for the prescribed scale-N initial configuration. These constants depend only on the choices already made. Fix

$$M_{\mathrm{hist}} = 2C_{\mathrm{out}}A_*^{-1}M_0. \tag{7.1}$$

The inequalities in Section 7.4 close this bound in Step 6 of Section 7.5. The factor two leaves room for the interactions between quadrupoles. In particular, M_{hist} is fixed before B and Λ.

The error Cr_{out}^{-2} changes the forcing coefficient $\mathcal{A}$, which is retained in the logarithmic delay. The error from the preceding trajectory segment is $C_{\mathrm{sec}}[\eta\log(1/\kappa)+\kappa^{3/4}]$. It tends to zero with Λ^{-1} after the segment has been fixed. Thus the later dependence on r_{out} does not change its already chosen tolerance.

7.1.4. The frequency ratio and overall frequency. Choose $B>4$ sufficiently large, depending on α, for the frequency and source comparisons in Sections 7.2–7.3 and 7.5, and require

$$B^{\alpha}>2, \qquad B^{1-\alpha}\ge 2,$$
$$C_{\mathrm{sec}}(1+M_{\mathrm{hist}})(B^{-1}+B^{-2})\le \tfrac14\min\{M_0,\varepsilon_*\}.$$

The ratio $\Omega_{n-1}/\Omega_n=B^{-1}$ controls the slower quadrupoles. The factors B^{-1} and B^{-2} also control the constant second moment and the earlier motion of the nearest source, respectively. All constants in these requirements have been fixed independently of B.

With B fixed, choose Λ large. Formula (5.1) gives

$$\log(1/\kappa_n)=4\Omega_{n+1}^{\alpha}+O_{\alpha,B}(n+1), \qquad \sup_n\kappa_n\longrightarrow 0, \qquad \sum_n\Delta_n\longrightarrow 0.$$

The spatial estimates below make S,T and the interaction bounds tend to zero. The coefficient estimates in Sections 7.2–7.4 give $\sup_n[\eta_n\log(1/\kappa_n)+\kappa_n^{3/4}]\to 0$, where η_n is (6.6). Choose Λ so that these errors, including their fixed factors $C_{\mathrm{sec}}, M_{\mathrm{hist}}$, meet the stated smallness bounds. Require also

$$\sup_n\kappa_n\le\kappa_0, \qquad C(\Omega_1^{-1}+\Omega_1^{-3})\le\sigma/2, \qquad \sum_n\Delta_n<1/4.$$

The middle inequality ensures $\sigma_c\le\sigma/2$ in the local integral estimate. Increase Λ once more so that the total upper bound for the separation times in Section 6.2 satisfies

$$\sum_{n\ge1}\frac{1}{\Omega_n}\left[\frac{1}{2\sqrt2}\log\frac{4}{A_*\kappa_n}+K+1\right]=\sum_{n\ge1}\Delta_n+\frac{(2\sqrt2)^{-1}\log(4/A_*)+1}{\Lambda(B-1)}<\frac12.$$

The choices are now fixed as $N\to\infty$. For each N, construct the reference on $[0,2]$ and the second initial configuration as in Sections 4–5. Compare them on $[0,1]$.

7.1.5. Spatial bounds and continuation. For fixed $k,m\ge0$ and $r>0$,

$$\sum_{n\ge1}\Omega_n^k d_n^{-m}\ell_n^r\longrightarrow 0 \qquad (\Lambda\to\infty,\ B \text{ fixed}).$$

Indeed, the ratio of consecutive terms is $B^k2^m e^{-r(B^{\alpha}-1)\Omega_n^{\alpha}}\le 1/2$ for large Λ. The sum is then at most $2\Omega_1^k d_1^{-m}\ell_1^r$, which tends to zero. The corresponding supremum has the same limit.

Stop at the first patch boundary exit in (3.1) or failure of

$$|d_i^{(j)}(t)-d_k^{(j)}(t)|\ge\tfrac12|d_i-d_k| \qquad (i\ne k,\ j=1,2).$$

The geometric bootstrap bounds near the rhombus, along the fixed trajectory segment, and during dipole separation give diameter at most $C_{\mathrm{sec}}\ell_n(1+\Omega_n t)$ and minimum centroid distance at least $c_0\ell_n/2$. Sections 6.2–6.3 improve these bounds once their inputs are verified. For the latter section, the initial error is zero at scale N and small by Section 6.2 at subsequent scales. Its other smallness requirements are bounded by

$$r_{\mathrm{out}}^{-2}+\mathsf{S}(1+r_{\mathrm{out}}/\Omega_n)+C_A\Omega_n^{-4}.$$

These are small by the choices of r_{out} and Λ.

The series estimate gives

$$\sup_i \frac{C_{\mathrm{sec}}\ell_i(1+\Omega_i)+2R\ell_i+2a_i}{d_i} \longrightarrow 0.$$

Thus the comparison disks $B(d_i^{(j)}(t), 2R\ell_i)$ and the separating quadrupoles' convex hulls stay away from every other quadrupole. The external fields are analytic there, with

$$\sup|DU^{(j)}_{\mathrm{ext},i}| \le C\sum_{k\neq i}\frac{\Gamma_k}{|d_i-d_k|^2} \le C\mathsf{S}, \qquad \sup|D^2U^{(j)}_{\mathrm{ext},i}| \le C\sum_{k\neq i}\frac{\Gamma_k}{|d_i-d_k|^3} \le C\mathsf{T}.$$

We next control the quadrupole centers. For separating dipoles use X_1, X_2, v_1, v_2 from Section 6.3, so $M_1 = \Gamma(v_1+v_2) = 4\Gamma\delta$. Summing the four point-vortex velocities gives

$$\dot d_{\mathrm{point,int}} = -\frac{\Gamma}{2}\big[K(v_1)+K(v_2)+K(X_1-X_2+2\delta)+K(X_2-X_1+2\delta)\big].$$

Since $v_1+v_2 = 4\delta$, oddness of K and $|DK(x)| \le C|x|^{-2}$ imply

$$|\dot d_{\mathrm{point,int}}| \le C\Gamma|\delta|(\ell^{-2}+|X_1-X_2|^{-2}) \le C\Omega|M_1|/\Gamma.$$

Here, suppressing the scale index, $\varepsilon = a^2/\ell^2$. The internal patch correction is at most $C\Omega\ell\varepsilon\Omega^{-2}$. The linear external Taylor term cancels when averaged over the four patches about d, so

$$|\dot d - U(d)| \le C\Omega|M_1|/\Gamma + C\mathsf{T}(|X_1-X_2|^2+a^2) + C\Omega\ell\varepsilon\Omega^{-2}.$$

On the original interval $[0,1]$, Section 6.3 gives $|M_1| \le C_{\mathrm{sec}}\Gamma\mathsf{T}\Omega\ell^2$ and $|X_1-X_2| \le C_{\mathrm{sec}}\Omega\ell$. Near the rhombus and along the fixed segment, the same calculation uses diameter $C_{\mathrm{sec}}\ell$ and gives a smaller bound. Hence, in all three parts of the motion,

$$|\dot d_n - U_{\mathrm{ext},n}(d_n(t))| \le r_n, \qquad r_n = C_{\mathrm{sec}}(\mathsf{T}\Omega_n^2\ell_n^2 + \ell_n\Omega_n^{-4}), \qquad \sup_n r_n/d_n \longrightarrow 0.$$

The cutoff field V from Lemma 4.3 satisfies $V(d_n(t)) = U_{\mathrm{ext},n}(d_n(t))$ and $\|DV\|_{L^\infty} \le C\mathsf{S}$. Thus

$$|\dot d_i(t) - \dot d_j(t)| \le C\mathsf{S}|d_i(t)-d_j(t)| + r_i + r_j.$$

Using $d_i + d_j \le 3|d_i - d_j|$ for the fixed initial locations and integrating gives

$$\frac{|d_i(t)-d_j(t)-(d_i-d_j)|}{|d_i-d_j|} \le e^{C\mathsf{S}t} - 1 + 3te^{C\mathsf{S}t}\sup_k\frac{r_k}{d_k} \longrightarrow 0 \qquad (0\le t\le 1).$$

For large Λ this is less than $1/4$, improving the separation assumption and controlling the change in the arguments of all interquadrupole vectors.

For each individual patch, the other three patches in its quadrupole contribute at most $C\Gamma_n/\ell_n^2 = C\Omega_n$ to the weighted circulation integral in Theorem 3.10(iv). The other quadrupoles contribute at most $C\mathsf{S}$. The normalized external coefficient and material-derivative bounds are therefore $C\Omega_n$ and $C\Omega_n^2$. The theorem improves the patch boundary bounds from the original time zero. Consequently, while the centroid bounds hold, neither a patch boundary exit nor loss of separation between quadrupoles can occur first.

7.2 Relative estimates and slower quadrupoles

The linear shape rates are $2\sqrt{2}\Omega_i$ and $-2\sqrt{2}\Omega_i$, while the exponential rate in the physical-time integral W_i is bounded independently of i. We use the centroid decomposition of Theorem 3.10 and take second minus first as in Lemma 3.8. Thus $\triangle d_i(t) = d_i^{(2)}(t) - d_i^{(1)}(t)$, while $d_i = 2^{-i}$ is the fixed initial location. In addition to the shape, angular-impulse, and corrected-phase differences and the integral W_i, use

$$\widehat{M}_{1,i} = \frac{d_i \triangle M_{1,i}}{\Gamma_i \ell_i^2}, \qquad \widehat{d}_i = \frac{\triangle d_i}{d_i}.$$

In the coordinates of Section 6, set $Q_i = \triangle \widehat{q}_i$, $P_i = \triangle \widehat{p}_i$, and

$$Y_i = |Q_i| + |P_i| + \frac{|\triangle I_i|}{2\Gamma_i \ell_i^2} + |\triangle \widehat{\Theta}_i| + W_i + |\widehat{M}_{1,i}| + |\widehat{d}_i|.$$

Write $Z_i = Y_i - W_i$ for the sum of the finite-coordinate differences. Compared with $|Z|$ in Section 6.2, this norm includes translation and uses the stronger weight d_i/ℓ_i on the first moment. Both motions began at the original time zero from disks with the same radii, signed circulations, and standard normalized material labels $F(0,\theta) = e^{i\theta}$. Equation (3.11) bounds the difference between D_i/ℓ_i^2 and $I_i/(2\Gamma_i\ell_i^2)$, with relative error $C\varepsilon_i\Omega_i^{-2}W_i$. Enlarge the centroid input in (3.7) to include all these coordinates, as justified after Theorem 3.10. Each W_i starts from $W_i(0) = 0$ at the original time zero and retains its actual value at every later starting time and chart change. At $i < N$ the initial centroid configurations also agree, so $Y_i(0) = 0$. Since $\triangle\delta_i/\ell_i = (\ell_i/(4d_i))\widehat{M}_{1,i}$, the stronger first-moment normalization decreases its coefficient in the equations for $z_{1,i}, z_{2,i}$ and in the integral input.

At distance comparable to d_i, this normalization gives the same scale for the first- and second-moment strains.

$$\frac{|\triangle M_{1,i}|}{d_i^3} = \frac{\Gamma_i\ell_i^2}{d_i^4}|\widehat{M}_{1,i}|, \qquad \frac{|\triangle M_{2,i}|}{d_i^4} \le C\frac{\Gamma_i\ell_i^2}{d_i^4}Y_i.$$

The translation variable $\widehat{d}_i$ is normalized by the interquadrupole distance.

Choose the relative rhombus neighborhood to be a fixed small ball for Y_i. Lift the relative phase continuously from the identical initial data. The absolute reference phase may rotate freely. Stop at the first exit of any component of Y_i, or at loss of patch confinement or separation. A small bound on Y_i therefore excludes every rhombus-neighborhood exit.

On the fixed compact segment after $Q_i = q_*$, retain the four material labels and their representation $d + \delta \pm z_1, d - \delta \pm z_2$, and use instead

$$Y_i = \frac{|\triangle z_{1,i}| + |\triangle z_{2,i}|}{\ell_i} + W_i + |\widehat{M}_{1,i}| + |\widehat{d}_i|.$$

The two norms are uniformly equivalent near $Q_i = q_*$. Indeed, the four real components of $(z_{1,i}, z_{2,i})$ give local analytic coordinates for shape, angular impulse, and phase, with $|\triangle(I_i/(2\Gamma_i\ell_i^2) - D_i/\ell_i^2)| \le C\varepsilon_i\Omega_i^{-2}W_i$. The reference stays near a rotating rhombus, and the second motion stays near the fixed collision-free compact segment. The latter norm is defined throughout this passage, satisfies the same multipole bounds with constants depending on the segment, and continues the integral comparison of Theorem 3.10. Use the corresponding norm on each interval when estimating earlier motion.

Near $Q_i = q_*$, use the local relative estimates. On the rest of the outgoing segment, its shape has a fixed positive distance from the compact set of rotating rhombi, so $(|\triangle z_{1,i}| + |\triangle z_{2,i}|)/\ell_i \ge c_{\mathrm{sec}} > 0$. Each separated normalized point field and individual external coefficient list is bounded by C_{sec}. Their difference is therefore bounded by $2C_{\mathrm{sec}}c_{\mathrm{sec}}^{-1}(|\triangle z_{1,i}| + |\triangle z_{2,i}|)/\ell_i$. This

proves the relative coefficient estimate without requiring a collision-free straight segment between the two configurations.

Write the external expansion about each quadrupole's own center as

$$U^{(j)}_{\mathrm{ext},i}(d^{(j)}_i + z) - U^{(j)}_{\mathrm{ext},i}(d^{(j)}_i) = S^{(j)}_i \bar{z} + \sum_{k\geq 2} a^{(j)}_{k,i} \bar{z}^k.$$

Subtracting the exact first-moment equations gives

$$\triangle \dot{M}_{1,i} = S^{(1)}_i \overline{\triangle M_{1,i}} + \triangle S_i \overline{M^{(2)}_{1,i}} + \sum_{k\geq 2} \left(a^{(1)}_{k,i} \overline{\triangle M_{k,i}} + \triangle a_{k,i} \overline{M^{(2)}_{k,i}} \right).$$

Fix the time-independent bound

$$\mathsf{T}_i = C \sum_{j\neq i} \frac{\Gamma_j}{|d_i - d_j|^3},$$

where the geometric constant C is large enough to bound both external Hessians on the comparison disks throughout the stopped interval. It also bounds the reference Hessian on its original interval. By the first-moment equation, $\delta^{(1)}_i(0) = 0$ gives $|\delta^{(1)}_i(t)| \leq C\mathsf{T}_i \ell_i^2 t e^{C\mathsf{S}t} \leq C\mathsf{T}_i \ell_i^2$ on $[0,1]$. Use the radius R already fixed for the comparison neighborhood. In the rhombus neighborhood, $|\triangle M_{k,i}| \leq CR^k \Gamma_i \ell_i^k Y_i$. Also $d_i |M^{(2)}_{1,i}|/(\Gamma_i \ell_i^2) \leq C$, by the reference bound and the bound on $\widehat{M}_{1,i}$. Hence

$$|\dot{\widehat{M}}_{1,i}| \leq C\mathsf{S}|\widehat{M}_{1,i}| + Cd_i \mathsf{T}_i Y_i + C\left(|\triangle S_i| + d_i \sum_{k\geq 2} R^k \ell_i^{k-2} |\triangle a_{k,i}| \right).$$

Write $\triangle U_i(z) = U^{(2)}_{\mathrm{ext},i}(d^{(2)}_i + z) - U^{(1)}_{\mathrm{ext},i}(d^{(1)}_i + z)$. Cauchy's estimate for the coefficients of $\partial_{\bar{z}}^2 \triangle U_i$ gives

$$\sum_{k\geq 2} R^k \ell_i^{k-2} |\triangle a_{k,i}| \leq R^2 \sup_{|z|\leq 2R\ell_i} |D^2 \triangle U_i(z)| \sum_{k\geq 2} \frac{2^{2-k}}{k(k-1)}.$$

Since $|d_i - d_j| \geq \frac{1}{2}\max\{d_i, d_j\}$,

$$d_i \mathsf{T}_i \leq C \sum_{j<i} \frac{\Gamma_j d_i}{d_j^3} + C \sum_{j>i} \frac{\Gamma_j}{d_i^2} \leq C \sum_{j\neq i} \frac{\Gamma_j}{d_j^2} \leq C\mathsf{S}.$$

Thus the coefficient of a local shape or patch difference is at most $C\mathsf{S}$, and every forcing term is an actual external-field difference.

For the internal point field, direct summation of the four centroid equations gives

$$\dot{d}_{\mathrm{point,int}} = -\frac{\Gamma}{2} \sum_{\epsilon_1,\epsilon_2\in\{-1,1\}} K(2\delta + \epsilon_1 z_1 + \epsilon_2 z_2).$$

The expression is odd in δ. On the fixed separated normalized neighborhood, its δ derivative is bounded by $C\Omega$ and its shape derivative by $C\Omega|\delta|/\ell$. Since $|\delta^{(1)}_i| \leq C\mathsf{T}_i \ell_i^2$ and $|\triangle \delta_i| = \ell_i^2 |\widehat{M}_{1,i}|/(4d_i)$, the mean-value formula gives

$$\frac{|\triangle \dot{d}_{\mathrm{point,int}}|}{d_i} \leq C\frac{\Gamma_i}{d_i^2} |\widehat{M}_{1,i}| + C\frac{\Omega_i \mathsf{T}_i \ell_i^2}{d_i} Y_i.$$

The offset coefficient is $C\Gamma_i/d_i^2$. The shape coefficient contains the small reference offset and is small because ℓ_i/d_i decays superexponentially. The relative patch contribution to the arithmetic-center equation is bounded by

$$C\Omega_i\frac{\ell_i}{d_i}\varepsilon_i(W_i+\Omega_i^{-2}|Z_i|)+C\frac{\ell_i}{d_i}\varepsilon_i\Omega_i^{-2}\|\triangle A_i\|_R.$$

Here $Z_i=Y_i-W_i$, and $\triangle A_i$ is the actual external coefficient difference from Theorem 3.10(ii). The last term retains its instantaneous external input, with uniformly small factor $(\ell_i/d_i)\varepsilon_i\Omega_i^{-2}$. External averaging adds $C\mathsf{T}_i\ell_i^2/d_i$ times a local relative variable and the corresponding external-input difference. Since the point equations for $z_{1,i}, z_{2,i}$ are even in δ_i, their offset contribution is a small reference factor times $\triangle\delta_i/\ell_i$, plus a quadratic difference.

Indeed, Taylor's formula gives

$$C\frac{|\delta_i^{(1)}|}{\ell_i}\frac{|\triangle\delta_i|}{\ell_i}+C\left|\frac{\triangle\delta_i}{\ell_i}\right|^2\le C\mathsf{T}_i\ell_i\frac{|\triangle\delta_i|}{\ell_i}+C\left|\frac{\triangle\delta_i}{\ell_i}\right|^2.$$

The first term has a small coefficient, and the second is quadratic. Theorem 3.10(ii),(iii) bounds the remaining moment and centroid errors by the same finite-coordinate differences and W_i.

For an external velocity difference V at quadrupole i, use the norm

$$d_i^{-1}\|V\|_{L^\infty}+\|DV\|_{L^\infty}+d_i\|D^2V\|_{L^\infty},\qquad |z|\le 2R\ell_i,$$

in the centered coordinates above. A shape, angular-impulse, phase, or patch difference at quadrupole j changes its centered second moment by at most $C\Gamma_j\ell_j^2Y_j$. Its first-moment difference is at most $C\Gamma_j\ell_j^2|\widehat{M}_{1,j}|/d_j$. Translating its center differentiates the existing first and higher moment fields, since the total circulation remains zero. Since the reference satisfies $|M_{1,j}|\le C\Gamma_j\mathsf{T}\ell_j^2$, these translation terms satisfy the bounds below as well.

Use the weighted norm $\max_i d_i^4Y_i$, so the coefficient from j to i acquires the factor $(d_i/d_j)^4$.

Throughout the receiving disk the distance to source j is comparable to $|d_i-d_j|$. This also holds along the segment between the two relative center vectors, since each differs from d_i-d_j by at most $|d_i-d_j|/4$. In either fixed comparison neighborhood the higher source moments sum geometrically in $C_{\mathrm{sec}}\ell_j/|d_i-d_j|$. Before multiplication by $(d_i/d_j)^4$, the second- and first-moment coefficients are bounded respectively by

$$C\Gamma_j\ell_j^2\left(\frac{1}{d_i|d_i-d_j|^3}+\frac{1}{|d_i-d_j|^4}+\frac{d_i}{|d_i-d_j|^5}\right),$$
$$C\frac{\Gamma_j\ell_j^2}{d_j}\left(\frac{1}{d_i|d_i-d_j|^2}+\frac{1}{|d_i-d_j|^3}+\frac{d_i}{|d_i-d_j|^4}\right).$$

Let $A_{ij}(t)\ge 0$ be the sum of these interaction bounds, including the translation terms below. These real bounds are distinct from the complex Taylor coefficients $A_{k,i}$ in (3.5). For $j>i$, multiplication by $(d_i/d_j)^4$ bounds the two expressions by $C\Gamma_j\ell_j^2/d_j^4$ and $C\Gamma_j\ell_j^2d_i/d_j^5$, respectively. For $j<i$, both are bounded by $C\Gamma_j\ell_j^2/d_j^4$, since $d_i/d_j\le 1$. Thus

$$\sup_{t,i}\sum_{j\ne i}A_{ij}(t)\left(\frac{d_i}{d_j}\right)^4\le\Xi,\qquad \Xi=C\sum_{j\ge1}\frac{\Omega_j\ell_j^4}{d_j^5}+C\mathsf{S}. \tag{7.2}$$

For the same three components, translating the second-moment field gives a coefficient at most

$$C\Gamma_j\ell_j^2d_j\left(\frac{1}{d_i|d_i-d_j|^4}+\frac{1}{|d_i-d_j|^5}+\frac{d_i}{|d_i-d_j|^6}\right).$$

Translating the reference first-moment field has coefficient at most

$$C\mathsf{T}\Gamma_j\ell_j^2 d_j\left(\frac{1}{d_i|d_i-d_j|^3}+\frac{1}{|d_i-d_j|^4}+\frac{d_i}{|d_i-d_j|^5}\right).$$

Multiplication by $(d_i/d_j)^4$ and the same split into $j>i$ and $j<i$ give the majorant in (7.2), using $\mathsf{T}\le 1$ and $d_j\le 1$. The constants are independent of the truncation. Include the local impulse, phase, first-moment, and translation terms in the local evolution estimate, whose growth is bounded by $C\exp(C\Omega_i(t-s))$ in the rhombus neighborhood.

Equation (3.9) uses the external coefficient difference without its time derivative. In physical time, the centroid input to W_i has coefficient $C\Omega_i$, the W_i term in the centroid equation has coefficient $C\Omega_i\varepsilon_i$, and the exponential rate in the W_i integral is uniformly bounded. Include these terms in the same local growth and weighted interaction estimates.

For the target, replace $\triangle\delta_i/\ell_i$ in ν by $\widehat{M}_{1,i}=4d_i\triangle\delta_i/\ell_i^2$ and adjoin $\widehat{d}_i$. In recipient time their coefficients satisfy

$$\frac{d_i\mathsf{T}_i}{\Omega_i}\le\frac{C\mathsf{S}}{\Omega_i},\qquad\frac{\Gamma_i}{\Omega_i d_i^2}=\frac{2\pi\ell_i^2}{d_i^2}\le C\Omega_i^{-3},\qquad\frac{\ell_i}{d_i}\varepsilon_i\le C\varepsilon_i.$$

The remaining local center-error coefficients are smaller. After the displayed small coefficients are included in the remainders, the additional coordinates have zero unperturbed derivatives. Translation changes the shape equation by at most $d_i\mathsf{T}_i/\Omega_i$, since internal velocities depend only on relative positions. The reference offset also satisfies $|\delta_i^{(1)}|/\ell_i\le C\mathsf{T}_i\ell_i\le C\Omega_i^{-3}$. Thus the enlarged system satisfies the remainder inequalities and reference-offset bound of Section 6.2, with its stated η.

Slower quadrupoles. Fix a target n. The slower quadrupoles are $i<n$, which have smaller frequencies and remain in their local rhombus neighborhoods. Stop when the target reaches its prescribed dipole separation or a slower quadrupole leaves its neighborhood. All estimates below hold on this stopped interval.

For $i<n$, use the bound $e^{C_f\Omega_i t}$ and $\Omega_i\le\Omega_n/B$. Choose B so that $C_f\Omega_i<2\sqrt{2}\Omega_n$. The target estimate will retain the exact rate $2\sqrt{2}\Omega_n$, since a fixed change in that rate over the logarithmic departure time would change the effective coefficient by a power of κ_n.

Recall $Z_i=Y_i-W_i$. The change of receiving center in the velocity, strain, and Hessian components has coefficients bounded by $C\mathsf{S}$, $Cd_i\mathsf{T}_i$, and $Cd_i^2\sup|D^3U_{\mathrm{ext},i}|$, respectively. Kernel differentiation gives

$$d_i^2\sup|D^3U_{\mathrm{ext},i}|\le C\sum_{j\ne i}\frac{\Gamma_j d_i^2}{|d_i-d_j|^4}\le C\mathsf{S}.$$

Thus the terms caused by changing the receiving state are bounded by $C(\mathsf{S}+d_i\mathsf{T}_i)Y_i$. Include them in the local centroid and integral coefficients. Let F_i^{ext} be the remaining physical-time external input norm, due to changes in the other quadrupoles. Since $A_{k,i}=\ell_i^{k-1}a_{k,i}$ and $\ell_i\le d_i$, the coefficient estimate above gives

$$\|\triangle A_i\|_R\le CF_i^{\mathrm{ext}}+C\mathsf{S}Y_i.$$

Since $(\ell_i/d_i)\varepsilon_i\Omega_i^{-2}\le 1$, the instantaneous patch term above is included in CF_i^{ext} and the small local coefficients. Theorem 3.10 and (3.9) give, on every subinterval $[r,t]$ before the stop,

$$Z_i(t)\le Ce^{C\Omega_i(t-r)}Z_i(r)+C\int_r^t e^{C\Omega_i(t-s)}\big(\Omega_i\varepsilon_iW_i(s)+F_i^{\mathrm{ext}}(s)\big)\,ds,$$

$$W_i(t)\le Ce^{\mu(t-r)}W_i(r)+C\int_r^t e^{\mu(t-s)}\big(\Omega_iZ_i(s)+F_i^{\mathrm{ext}}(s)\big)\,ds,\qquad\mu\le C\Omega_i.$$

The constants here may depend on A and the fixed coordinate neighborhoods, but not on i, N. Since $\varepsilon_i \le 1$, addition and Gronwall give fixed constants C_G, C_f, chosen before B, such that

$$Y_i(t) \le C_G e^{C_f \Omega_i (t-r)} Y_i(r) + C_G \int_r^t e^{C_f \Omega_i (t-s)} F_i^{\mathrm{ext}}(s)\, ds. \tag{7.3}$$

This estimate includes the coefficient $C\Omega_i$ of the centroid input to W_i.

Lemma 7.1. *Let $n \ge 2$ and $0 \le t_0 \le T \le 1$, where T is a stopped endpoint as above. For every $i < n$, suppose the input in (7.3) is bounded on $[t_0, T]$ by*

$$F_i^{\mathrm{ext}}(t) \le f_i(t) + A_{in}(t) Y_n(t) + \sum_{j<n,\ j\neq i} A_{ij}(t) Y_j(t), \qquad f_i(t) \ge 0.$$

Here f_i contains the forcing from completed sources, and $A_{in} Y_n$ bounds the current target's contribution. Set

$$V_0 = \max_{i<n} \left(\frac{d_i}{d_n}\right)^4 Y_i(t_0), \qquad f(t) = \max_{i<n} \left(\frac{d_i}{d_n}\right)^4 f_i(t), \qquad \beta_n = C_f \Omega_{n-1} + C_G \Xi.$$

The forcing returned by the slower quadrupoles to the target is bounded by

$$\sum_{i<n} A_{ni}(t) Y_i(t) \le C_G \Xi e^{\beta_n (t-t_0)} V_0 + C_G \Xi \int_{t_0}^t e^{\beta_n (t-r)} f(r)\, dr + C_G \Xi^2 \int_{t_0}^t e^{\beta_n (t-r)} Y_n(r)\, dr.$$

The terms on the right come respectively from the slower-quadrupole states at t_0, new source inputs, and the target's contribution after t_0. For every $\gamma > \beta_n$, the last term defines a positive integral operator $\mathcal{K}_n$ on $[t_0, T]$ satisfying

$$\sup_{t_0 \le t \le T} \int_{t_0}^t C_G \Xi^2 e^{-(\gamma - \beta_n)(t-r)}\, dr \le \frac{C_G \Xi^2}{\gamma - \beta_n}.$$

The exponentially weighted integrals of the first and second terms are bounded by

$$\frac{C_G \Xi}{\gamma - \beta_n} V_0, \qquad \frac{C_G \Xi}{\gamma - \beta_n} \int_{t_0}^T e^{-\gamma (r - t_0)} f(r)\, dr,$$

respectively. These bounds use no continuation beyond the stopping time T.

Proof. Set

$$V(t) = \max_{i<n} (d_i/d_n)^4 Y_i(t).$$

By $\Omega_i \le \Omega_{n-1}$, (7.3), and (7.2),

$$V(t) \le C_G e^{C_f \Omega_{n-1}(t-t_0)} V_0 + C_G \int_{t_0}^t e^{C_f \Omega_{n-1}(t-r)} \big(f(r) + \Xi Y_n(r) + \Xi V(r)\big)\, dr.$$

Multiply by $e^{-C_f \Omega_{n-1}(t-t_0)}$ and apply Gronwall to obtain

$$V(t) \le C_G e^{\beta_n (t-t_0)} V_0 + C_G \int_{t_0}^t e^{\beta_n (t-r)} \big(f(r) + \Xi Y_n(r)\big)\, dr.$$

Equation (7.2) gives $\sum_{i<n} A_{ni} Y_i \le \Xi V$, proving the three terms.

For an input $e^{\gamma(t-t_0)}$, $\gamma > \beta_n$, division of the returned term by the input gives

$$C_G \Xi^2 \int_{t_0}^t e^{-(\gamma - \beta_n)(t-r)}\, dr \le \frac{C_G \Xi^2}{\gamma - \beta_n}.$$

This proves the operator estimate. Integration of the initial-state term against $e^{-\gamma(t-t_0)}$ gives at most $C_G\Xi V_0/(\gamma-\beta_n)$. For the source term, interchanging the nonnegative integrals gives

$$\int_{t_0}^{T} e^{-\gamma(t-t_0)} \int_{t_0}^{t} e^{\beta_n(t-r)} f(r)\, dr\, dt = \int_{t_0}^{T} e^{-\gamma(r-t_0)} f(r) \int_{r}^{T} e^{-(\gamma-\beta_n)(t-r)} dt\, dr.$$

Bound the inner integral by $(\gamma-\beta_n)^{-1}$. This proves the remaining estimate on the stopped interval. □

In Lemma 7.1, let b_0 be the sum of the first two terms and b_1 the last term on the right-hand side, including the fixed projection and receiving-patch averaging constants. Apply the decomposition of Section 6.2 to the actual slower-quadrupole input g. Then $b_0 g/(b_0+b_1)$ contributes to $\kappa_n f_q, \kappa_n f_p, \kappa_n f_\nu$, and $b_1 g/(b_0+b_1)$ to the remainders in (6.7). The receiving-state terms contribute $C\mathsf{S}Y_n/\Omega_n$ to the local part of $\mathcal{R}$.

The same construction applies with starting time zero.

Require B and then Λ to be large enough that $\beta_n \le \sigma\Omega_n/4$. Since $\sigma < 2\sqrt{2}/4$, the lemma applies at $\gamma = 2\sqrt{2}\Omega_n$, with physical forcing operator norm at most $C\Xi^2/\Omega_n$. Under $s = \Omega_n(t-t_0)$, a physical kernel $k_n(t,r)$ becomes $\Omega_n^{-2} k_n(t_0+s/\Omega_n, t_0+u/\Omega_n)$.

$$\frac{1}{\Omega_n}\int_{t_0}^{t_0+s/\Omega_n} C_G\Xi^2 e^{\beta_n(t_0+s/\Omega_n-r)} Y_n(r)\, dr = \frac{C_G\Xi^2}{\Omega_n^2}\int_0^s e^{(\beta_n/\Omega_n)(s-u)} Y_n(t_0+u/\Omega_n)\, du.$$

The normalized norm of the slower-quadrupole integral operator $\mathcal{K}_n$ is therefore $C\Xi^2/\Omega_n^2$, giving an accumulated relative contribution at most $C\Xi^2 T/\Omega_n$ over physical time T. Together with the local receiving-state term, $\eta_{\mathrm{return}} \le C(\mathsf{S}/\Omega_n + \Xi^2/\Omega_n^2)$ in Section 6.2. The source-driven weighted integral gains $C\Xi/\Omega_n$. For $n=1$, the slower-quadrupole subsystem is empty and $\mathcal{K}_1 = 0$.

Retain also the source-index factor in the forcing norm. If $j > n$ satisfies $Y_j(t) \le M_{\mathrm{hist}} e^{c\Omega_j(t-\tau_j)}$ for $t \le \tau_j$, then its first-moment difference is bounded by $M_{\mathrm{hist}}\Gamma_j\ell_j^2 d_j^{-1} e^{c\Omega_j(t-\tau_j)}$. Thus, in the weighted norm for all $i \le n$, the second-moment forcing bound is multiplied by $C(1+d_j^{-1})$. At a fixed recipient i, the factor is $C(1+d_i/d_j)$. For the nearest source,

$$\sup_{n\ge 1}\frac{1}{\Omega_n d_{n+1}} = \frac{2}{\Lambda}\sup_{n\ge 1}(2/B)^n \longrightarrow 0. \tag{7.4}$$

Hence the factor d_{n+1}^{-1} is offset by the gain Ω_n^{-1}, and the nearest source's contribution through slower quadrupoles is relatively bounded by $C\Xi/(\Omega_n d_{n+1})$. For more distant source indices, retain d_j^{-1} in the strength summation.

Since $\beta_n/\Omega_n \le \sigma/4$, the source estimates in Section 7.3, with the spatial factors retained, will bound their source-driven contribution by $C\kappa_n(1+s)^3 e^{\sigma s/2}$. Keep the target's returned contribution as the integral operator above.

At $t = \tau_{n+1}$, retain the actual slower-quadrupole states. Lemma 7.1 bounds their later response by contributions from these states, new source forcing, and target forcing after τ_{n+1}. For $n \ge 2$, put $j = n+1$ and

$$V_0 = \max_{i<n}(d_i/d_n)^4 Y_i(\tau_j).$$

The preceding stage, as verified in Step 6 of Section 7.5, gives

$$V_0 \le C M_{\mathrm{hist}}\kappa_n B^{-2}(1+d_j^{-1}) + C_{\mathrm{sec}}(1+M_{\mathrm{hist}})\kappa_n e^{-c\Omega_{n+2}^{\alpha}}.$$

For the nearest source, use $|d_i - d_j| \asymp d_i$, $d_j = d_n/2$, and $\Gamma_j\ell_j^2/\Omega_j = \Gamma_j^2/(2\pi\Omega_j^2)$ in (7.13); the sum from $k > j$ is bounded as in (7.8). By (7.2) and the slower-quadrupole growth estimate,

the resulting forcing in recipient time is at most $(C\Xi/\Omega_n)V_0e^{\sigma s/2}$. Its absolute weighted integral and coefficient in this bound are therefore at most $CM_{\mathrm{hist}}\kappa_nB^{-2}\Xi/(\Omega_nd_{n+1})$, plus the older-source contribution. Include these terms in the source input. The state at τ_j contains every earlier slower-quadrupole response, including that driven by the current target. This calculation requires no bound on the uncompleted target's entire previous motion. For the deepest source, $\tau_j = 0$ and every slower quadrupole agrees with the reference, so $V_0 = 0$. For $n = 1$, also set $V_0 = 0$ and omit the empty subsystem.

7.3 Forcing from separated quadrupoles

All estimates below are restricted to the current common existence interval, stopped at a geometric or patch-confinement exit. At stage n, suppose every quadrupole $j > n$ has first reached pair-center distance $r_{\mathrm{out}}\ell_j$ at time τ_j and satisfies

$$Y_j(t) \le M_{\mathrm{hist}}e^{c\Omega_j(t-\tau_j)}, \qquad 0 \le t \le \tau_j. \tag{7.5}$$

Here Y_j is the norm from Section 7.2 and c was fixed in Section 7.1. Write $\mathcal{F}_{i\leftarrow j}$ for the nonnegative physical-time input norm from quadrupole j to i, including the centroid and moment projections. In particular,

$$|\triangle M_{2,j}(t)| \le CM_{\mathrm{hist}}\Gamma_j\ell_j^2e^{c\Omega_j(t-\tau_j)}, \qquad |\triangle M_{1,j}(t)| \le M_{\mathrm{hist}}\frac{\Gamma_j\ell_j^2}{d_j}e^{c\Omega_j(t-\tau_j)}.$$

The initial quadrupole N already has pair-center distance $r_{\mathrm{out}}\ell_N$ at $\tau_N = 0$, so its bound is required only at time zero.

By Section 6.3, for $t \ge \tau_j$,

$$M_{2,j}^{(2)}(t) = M_{2,j}^{(2)}(\tau_j) - \frac{2i}{\pi}\Gamma_j^2e^{2i\theta_{d,j}}(t-\tau_j) + \mathcal{E}_j(t), \qquad |\dot{\mathcal{E}}_j(t)| \le \varepsilon_{\mathrm{sep}}\Gamma_j^2,$$

where $\mathcal{E}_j(\tau_j) = 0$ and $C\varepsilon_{\mathrm{sep}} \le \varepsilon_*/4$, with the fixed projection constant C used in Section 7.4. The reference second moment and the value at τ_j are bounded by $C_{\mathrm{sec}}\Gamma_j\ell_j^2$. The first-moment identity and cancellation within each dipole give

$$|M_{1,j}^{(2)}(t)| + |M_{1,j}^{(1)}(t)| \le C_{\mathrm{sec}}\mathsf{T}\Gamma_j\ell_j^2(1+\Omega_j(t-\tau_j)^2), \qquad \tau_j \le t \le 1.$$

The linear term in $t-\tau_j$ is included in this bound. Before τ_j, we use the relative estimate (7.5).

For a quadrupole $i < j$ near its rhombus, the resulting strain, velocity divided by d_i, and Hessian multiplied by d_i are bounded, for $t \le \tau_j$, by

$$CM_{\mathrm{hist}}\frac{\Gamma_j\ell_j^2}{|d_i-d_j|^4}\left(1+\frac{d_i}{d_j}\right)e^{c\Omega_j(t-\tau_j)}.$$

For $t \ge \tau_j$, they are bounded by

$$C_{\mathrm{sec}}\frac{\Gamma_j^2}{|d_i-d_j|^4}\left[t-\tau_j+\Omega_j^{-1}+\mathsf{T}d_i\big((t-\tau_j)^2+\Omega_j^{-1}\big)\right].$$

Since $\ell_j(1+\Omega_j) \ll |d_i-d_j|$ uniformly, these bounds include the finite spatial extent of the source. For $j \ge 2$, the higher-moment error has relative size at most $C\Omega_j\ell_j/d_j$. If $B^\alpha > 2$ and Λ is sufficiently large,

$$\sup_{j\ge2}\frac{\Omega_j\ell_j}{d_j} \le C\frac{\Omega_2\ell_2}{d_2} \le C_{\alpha,B}e^{-(B^\alpha-2)\Omega_1^\alpha}\mathsf{S} \le \mathsf{S}.$$

The geometric estimates also give a uniformly small change in the argument of the direct strain. Terms caused by the recipient's own displacement are included in its small diagonal coefficients.

For $n = j - 1$, we have $|d_n - d_j| = d_j$, $d_n/d_j = 2$, and $\Omega_n/\Omega_j = B^{-1}$. Hence

$$\begin{aligned} \frac{CM_{\mathrm{hist}}\Gamma_j\ell_j^2}{|d_n - d_j|^4}\int_0^{\tau_j} e^{(c\Omega_j - 2\sqrt{2}\Omega_n)(t-\tau_j)}\,dt &\le CM_{\mathrm{hist}}\kappa_n B^{-2}, \\ \frac{C_{\mathrm{sec}}\Gamma_j\ell_j^2}{|d_n - d_j|^4}\int_{\tau_j}^{\infty} e^{-2\sqrt{2}\Omega_n(t-\tau_j)}\,dt &\le C_{\mathrm{sec}}\kappa_n B^{-1}. \end{aligned} \tag{7.6}$$

Indeed, $c\Omega_j - 2\sqrt{2}\Omega_n \ge c\Omega_j/2$ for sufficiently large B, and $\Gamma_j\ell_j^2 = \Gamma_j^2/(2\pi\Omega_j)$. The relevant integrals are

$$\int_0^{\tau_j} e^{-2\sqrt{2}\Omega_n(t-\tau_j)}e^{c\Omega_j(t-\tau_j)}\,dt \le \frac{1}{c\Omega_j - 2\sqrt{2}\Omega_n},$$

$$\int_{\tau_j}^{\infty} e^{-2\sqrt{2}\Omega_n(t-\tau_j)}\,dt = \frac{1}{2\sqrt{2}\Omega_n}, \qquad \int_{\tau_j}^{\infty} e^{-2\sqrt{2}\Omega_n(t-\tau_j)}(t-\tau_j)\,dt = \frac{1}{8\Omega_n^2}.$$

The term linear in $t - \tau_j$ has coefficient $O(\Gamma_j^2)$ and weighted integral comparable to κ_n. Thus the motion before τ_j and the bounded second moment after τ_j gain B^{-2} and B^{-1}, respectively. The infinite integrals are nonnegative upper bounds. Actual signed forcing is integrated only to the current stopping time.

Integrating the constant and quadratic first-moment terms gives a further contribution, divided by κ_n, of at most

$$C_{\mathrm{sec}}\left(\frac{\mathsf{T}d_n}{\Omega_n} + \frac{\mathsf{T}d_n}{B}\right).$$

For forcing through slower quadrupoles, the spatially weighted input has the additional factor $1 + d_j^{-1}$ from Section 7.2. Its return is controlled by (7.4).

7.3.1. Earlier sources. Suppose the completed delays are at most $C\log(1/\kappa_k)/\Omega_k$. For $j \ge n+2$ and a common stopping time T, the preceding profiles give

$$\begin{aligned} &\frac{1}{\kappa_n}\int_0^T e^{-2\sqrt{2}\Omega_n(t-\tau_{n+1})}\mathcal{F}_{n\leftarrow j}(t)\,dt \\ &\quad\le C_{\mathrm{sec}}(1+M_{\mathrm{hist}})\left(1 + \frac{d_n}{d_j} + \frac{\Xi}{\Omega_n d_j}\right)\frac{\Gamma_j^2}{\Gamma_{n+1}^2}\exp\left(C_1\Omega_n\sum_{k=n+1}^{j-1}\frac{\log(1/\kappa_k)}{\Omega_k}\right). \end{aligned} \tag{7.7}$$

To obtain the exponential factor, split the input integral at τ_j and shift the weight from τ_{n+1} to τ_j. This gives $e^{2\sqrt{2}\Omega_n(\tau_{n+1}-\tau_j)}$, which is bounded using the completed delays. The factor d_n/d_j bounds the first-moment contribution before τ_j, and $\Xi/(\Omega_n d_j)$ bounds forcing through slower quadrupoles. By Lemma 7.1, the same right-hand side also bounds the input through slower quadrupoles. The constants include the bounded first-moment terms after τ_j and the small return to the target. The coordinate and $W_n(\tau_{n+1})$ estimates are proved in Steps 1 and 3 of Section 7.5. The larger comparison rate in Step 1 is used only for the preliminary bounds; Step 3 retains the exact rate $2\sqrt{2}\Omega_n$ in the weighted history estimate.

The delay and growth constants depend only on the fixed thresholds q_*, r_{out} once B exceeds a fixed threshold. For each such B, take Λ large enough that $\log(1/\kappa_k) \le 5\Omega_{k+1}^{\alpha}$ for all k. Then

$$\Omega_n\sum_{k=n+1}^{j-1}\frac{\log(1/\kappa_k)}{\Omega_k} \le \frac{5\Omega_{n+1}^{\alpha}}{B^{1-\alpha}-1}.$$

Also,

$$\log \frac{\Gamma_j^2}{\Gamma_{n+1}^2} = -4(\Omega_j^\alpha - \Omega_{n+1}^\alpha) + 2(j-n-1)\log B.$$

The logarithm of the spatial factor in (7.7) is at most $C + j\log 2 + \log(1 + \Xi/\Omega_n)$. Since $j \geq n+2$, the logarithm of the circulation ratio plus the exponent in (7.7) is at most

$$-\left(4 - \frac{4}{B^\alpha} - \frac{5C_1}{B^\alpha(B^{1-\alpha}-1)}\right)\Omega_j^\alpha + 2(j-n-1)\log B.$$

Choose B so that the parenthesis is at least three, then increase Λ to absorb the spatial and index terms, uniformly in n, j. Summing (7.7) over $j \geq n+2$ gives

$$\frac{1}{\kappa_n}\sum_{j\geq n+2}\int_0^T e^{-2\sqrt{2}\Omega_n(t-\tau_{n+1})}\mathcal{F}_{n\leftarrow j}(t)\,dt \leq C_{\mathrm{sec}}(1+M_{\mathrm{hist}})e^{-c\Omega_{n+2}^\alpha}. \tag{7.8}$$

This is uniform in n and N, and retains the first-moment factor 2^{j-n}. All these contributions are estimated in absolute value.

7.3.2. Pointwise bounds. Let $\mathcal{F}_n^{\mathrm{source}}$ bound the combined input from $j > n$, including its response through slower quadrupoles. The direct source norms $\mathcal{F}_{n\leftarrow j}$ were defined above. Set $t_0 = \tau_{n+1}$ and $s = \Omega_n(t - t_0)$. For $j = n+1$, the preceding profiles give

$$\frac{\mathcal{F}_{n\leftarrow j}(t_0 + s/\Omega_n)}{\Omega_n} \leq C_{\mathrm{dir}}\kappa_n s + C_{\mathrm{sec}}\kappa_n\left[B^{-1} + \mathsf{T}d_n\left(\frac{s^2}{\Omega_n} + B^{-1}\right)\right].$$

Here C_{dir} includes the small material and geometric errors in the linear term. The remaining terms are the constant second-moment term and the constant and quadratic first-moment terms. Since $\Gamma_j^2/(\Omega_n^2|d_n - d_j|^4) \asymp \kappa_n$, these remaining terms are at most $C_{\mathrm{sec}}(B^{-1} + \mathsf{T})\kappa_n(1+s)^2$.

For $j \geq n+2$, the completed delays give

$$0 \leq \Omega_n(\tau_{n+1} - \tau_j) \leq \frac{C\Omega_{n+1}^\alpha}{B^{1-\alpha}-1}.$$

Thus

$$\frac{\mathcal{F}_{n\leftarrow j}(t_0 + s/\Omega_n)}{\Omega_n} \leq C_{\mathrm{sec}}\kappa_n(1+s)^2(1+d_j^{-1})\frac{\Gamma_j^2}{\Gamma_{n+1}^2}\left[1 + \Omega_n(\tau_{n+1} - \tau_j)\right]^2.$$

The logarithms of the circulation ratio, spatial factor, and age polynomial are bounded by $-4(\Omega_j^\alpha - \Omega_{n+1}^\alpha) + 2(j-n-1)\log B$, $C + j\log 2$, and $C + 2\alpha\log\Omega_{n+1}$, respectively. The calculation proving (7.8) therefore gives

$$\sum_{j\geq n+2}\frac{\mathcal{F}_{n\leftarrow j}(t_0 + s/\Omega_n)}{\Omega_n} \leq C_{\mathrm{sec}}(1+M_{\mathrm{hist}})e^{-c\Omega_{n+2}^\alpha}\kappa_n(1+s)^2.$$

The same estimate applies to the weighted input to the slower quadrupoles. For $j = n+1$, retain the factor $1 + d_{n+1}^{-1}$. For $j \geq n+2$, this factor is already included in the sum.

Choose $\beta_n/\Omega_n \leq \sigma/4$. Lemma 7.1 bounds the return of these inputs after t_0, divided by Ω_n, by

$$C\kappa_n\left[\frac{\Xi}{\Omega_n d_{n+1}} + \frac{\Xi}{\Omega_n}C_{\mathrm{sec}}(1+M_{\mathrm{hist}})e^{-c\Omega_{n+2}^\alpha}\right](1+s)^3 e^{\sigma s/4}.$$

This follows by integrating $(1+s)^2$ against $e^{\beta_n(s-r)/\Omega_n}$. All interactions among slower quadrupoles are included in β_n.

The preceding stage bounds the actual norm V_0 from Lemma 7.1 by

$$V_0 \le CM_{\mathrm{hist}}\kappa_n B^{-2}(1+d_{n+1}^{-1}) + C_{\mathrm{sec}}(1+M_{\mathrm{hist}})\kappa_n e^{-c\Omega_{n+2}^{\alpha}}.$$

Its homogeneous return, divided by Ω_n, is at most $(C\Xi/\Omega_n)V_0 e^{\sigma s/4}$. The target norm at t_0 is at most $CM_{\mathrm{hist}}\kappa_n B^{-2}$ plus the same older-source remainder. The value V_0 includes every earlier response, including the response to quadrupole n.

Combining these bounds gives

$$\frac{\mathcal{F}_n^{\mathrm{source}}(t_0+s/\Omega_n)}{\Omega_n\kappa_n(1+s)^3e^{\sigma s/2}} \le C_{\mathrm{dir}} + C_{\mathrm{sec}}(1+M_{\mathrm{hist}})\left(B^{-1}+\mathsf{T}+\sup_k \frac{\Xi}{\Omega_k d_{k+1}} + e^{-c\Omega_3^{\alpha}}\right).$$

The target norm at t_0 is at most $C_{\mathrm{sec}}(1+M_{\mathrm{hist}})(B^{-2}+e^{-c\Omega_3^{\alpha}})\kappa_n$. Choose B, then Λ, so that the error coefficient in the preceding display is at most C_{dir} and this initial-value coefficient is at most M_0. The source input is then bounded by $2C_{\mathrm{dir}}\kappa_n(1+s)^3e^{\sigma s/2}$, and its absolute weighted integral is at most $2C_{\mathrm{dir}}\kappa_n\int_0^\infty e^{-(2\sqrt{2}-\sigma/2)s}(1+s)^3\,ds \le M_0\kappa_n/2$. These bounds lie strictly inside the input class fixed in Section 7.1.

7.4 The history constant and the phases

We record the constant inequalities needed in Steps 3–6 of Section 7.5. Put

$$\zeta_{\Lambda,B} = B^{-1}+B^{-2}+\mathsf{T}+\sup_n \frac{\Xi}{\Omega_n d_{n+1}} + e^{-c\Omega_3^{\alpha}}.$$

The leading nearest-source term has absolute weighted integral at most $M_0\kappa_n$, independently of M_{hist}. Its constant term, the motion before τ_{n+1}, sources $j \ge n+2$, and their forcing through slower quadrupoles add at most $C_{\mathrm{sec}}M_{\mathrm{hist}}\zeta_{\Lambda,B}\kappa_n$. The same coefficients bound the pointwise input, as shown in Section 7.3.

Choose B, then Λ, so that

$$C_{\mathrm{sec}}M_{\mathrm{hist}}\zeta_{\Lambda,B} \le \tfrac{1}{2}M_0$$

and the corresponding signed weighted errors are below the prescribed margin. The input norm is then below $2M_0\kappa_n$, and (7.1) gives

$$C_{\mathrm{out}}A_*^{-1}\big(M_0 + C_{\mathrm{sec}}M_{\mathrm{hist}}\zeta_{\Lambda,B}\big) \le \tfrac{3}{4}M_{\mathrm{hist}}.$$

Phase and timing. Use the phases, predicted times, and initial configurations fixed in Section 5.1. Recall $h_n = \Omega_n(\tau_n - \tau_{n,N})$. By (2.12), the normalized weighted forcing coefficient generated by the linear term in the second moment of scale $n+1$ is

$$\cos(4\arg(d_n - d_{n+1}) - 2\theta_n^{(1)}(\tau_{n+1}) - 2\theta_{d,n+1} + \arctan(1/\sqrt{2}) - \pi).$$

By (5.2), its argument vanishes at the ideal phases, since $d_n - d_{n+1} > 0$.

Make the choices in Section 7.1 so that

$$C\varepsilon_{\mathrm{sep}} + C_{\mathrm{sec}}\left(M_{\mathrm{hist}}\zeta_{\Lambda,B} + \sup_n\left[\eta_n\log(1/\kappa_n) + \kappa_n^{3/4}\right] + \mathsf{S} + \sup_n r_n/d_n\right) \le \varepsilon_*,$$

where η_n is (6.6), including the return, first-moment, and translation coefficients estimated above. The displayed C is universal, and C_{sec} includes every fixed segment factor. By (6.12), $C\varepsilon_{\mathrm{sep}}$ is bounded by the already chosen uniform multiple of r_{out}^{-2} plus terms tending to zero with Λ^{-1}, including $C_{\mathrm{sec}}[\eta_n\log(1/\kappa_n) + \kappa_n^{3/4}]$. All remaining terms are made small by choosing

B, then Λ. Thus the normalized forcing, phase, and delay errors are at most ε_*. In particular, Section 6.2 gives, at every completed stage,

$$\theta_{d,n} - \vartheta_n = -h_n + O(\varepsilon_*).$$

Both timing and angle errors vanish at scale N. At time τ_{n+1}, when quadrupole $n+1$ first reaches its prescribed dipole separation, the phases in the next weighted coefficient are

$$\begin{aligned}\theta_n^{(1)}(\tau_{n+1}) &= \vartheta_n + \Omega_n\Delta_n - \beta - B^{-1}h_{n+1} + O(\varepsilon_*),\\ \theta_{d,n+1} &= \vartheta_{n+1} - h_{n+1} + O(\varepsilon_*).\end{aligned}$$

Since $\Omega_n/\Omega_{n+1} = B^{-1}$, substitution into the cosine gives

$$\mathcal{A}_n = \cos\bigl(2(1+B^{-1})h_{n+1}\bigr) + O(\varepsilon_*).$$

For $|2(1+B^{-1})h_{n+1}| \le 1/2$, the choices above make the absolute $O(\varepsilon_*)$ error at most $1/8$. Hence $\mathcal{A}_n \ge 3/4$, and the delay formula yields

$$h_n = B^{-1}h_{n+1} - \frac{1}{2\sqrt{2}}\log\cos\bigl(2(1+B^{-1})h_{n+1}\bigr) + O(\varepsilon_*).$$

Since $|\log\cos x| \le Cx^2$ on this interval, we obtain

$$|h_n| \le B^{-1}|h_{n+1}| + C|h_{n+1}|^2 + C\varepsilon_*. \tag{7.9}$$

Here C is the elementary constant fixed before ε_* in Section 7.1. If $|h_{n+1}| \le C_h\varepsilon_*$, that choice keeps the cosine argument in $[-1/2, 1/2]$ and bounds the right side by $3C_h\varepsilon_*/4$. Starting from $h_N = 0$, this proves $|h_n| \le C_h\varepsilon_*$ at every completed stage. The preceding phase formula then gives the claimed angle error.

7.5 The stopped inductive step

We prove by descending induction that every quadrupole n first reaches pair-center distance $r_{\mathrm{out}}\ell_n$ within the deterministic duration of Section 6.2, satisfies (7.5) and (7.9), and supplies the actual values for the next stage. All estimates before completion are restricted to the stopped interval.

Step 1. Initial values and earlier times. At time zero, quadrupole N is in its prescribed separating configuration. At stage n, put $t_0 = \tau_{n+1}$ and assume, for every $j > n$,

$$Y_j(t) \le M_{\mathrm{hist}}e^{c\Omega_j(t-\tau_j)} \quad (0 \le t \le \tau_j), \qquad |h_j| \le C_h\varepsilon_*, \qquad \theta_{d,j} - \vartheta_j = -h_j + O(\varepsilon_*).$$

Assume also the separation and moment bounds of Section 6.3 on $[\tau_j, 1]$ up to the common stopping time. Retain (7.13) from every completed stage $j > n$ for all $i < j$; these estimates provide the slower-scale states at t_0. Every $i \le n$ remains in its rhombus neighborhood, and the preceding stage supplies

$$Y_n(t_0) \le CM_{\mathrm{hist}}\kappa_n B^{-2} + C_{\mathrm{sec}}(1+M_{\mathrm{hist}})\kappa_n e^{-c\Omega_{n+2}^{\alpha}}.$$

For $n = N-1$, $t_0 = 0$ and $Y_i(0) = 0$ for every $i < N$, since these quadrupoles have identical initial patches in the two solutions.

Starting at t_0, stop at $Q_n = \pm q_*$, a target or slower-quadrupole chart boundary, a geometric or patch boundary exit, or the physical time $t_0 + T_{\kappa_n}/\Omega_n$, with T_{κ_n} given by (6.8). Lemma 7.1 estimates all $i < n$. In the decomposition of Section 6.2, the b_0 term enters f_q, f_p, f_ν, and the b_1 term is bounded by $\mathcal{R}$.

For each completed stage retain its deterministic duration bound from Section 6.2. Since $\tau_N = 0$, the choice in Section 7.1 gives

$$\tau_{n+1} + \frac{1}{\Omega_n}\left[\frac{1}{2\sqrt{2}}\log\frac{4}{A_*\kappa_n} + K + 1\right] \le \sum_{k=n}^{N-1}\frac{1}{\Omega_k}\left[\frac{1}{2\sqrt{2}}\log\frac{4}{A_*\kappa_k} + K + 1\right] < \frac{1}{2}.$$

Thus the interval required by Section 6.2, including continuation up to τ_n, is contained in $[0, 1/2]$. The original disks have identical normalized labels, radii, and signed circulations, as required there.

On $[0, t_0]$, the completed stages keep every $i \le n$ near its rhombus. Their local rates are at most $C\Omega_n$, so the spatial estimate (7.2) bounds the linear evolution by $Ce^{\gamma_n t}$, where $\gamma_n = C_f\Omega_n + C\Xi$ and C_f is fixed. Choose B so that $c\Omega_{n+1} > 2\gamma_n$. The external inputs $k > n$ have the already proved profiles.

Convolution of the nearest source bound before τ_{n+1} costs C/Ω_{n+1}. Its direct spatial factor is $1 + d_n/d_{n+1}$. The indirect term has an additional Ξ/Ω_{n+1} applied to $1 + d_{n+1}^{-1}$. Thus its contribution, for every $t \le t_0$, is at most

$$CM_{\mathrm{hist}}\frac{\Gamma_{n+1}\ell_{n+1}^2}{\Omega_{n+1}|d_n - d_{n+1}|^4}\left(1 + \frac{d_n}{d_{n+1}} + \frac{\Xi}{\Omega_{n+1}d_{n+1}}\right) \le CM_{\mathrm{hist}}\frac{\kappa_n}{B^2}.$$

For $k \ge n+2$, the bound before τ_k has the factor $e^{\gamma_n(t_0-\tau_k)}$. After τ_k, set $v = t - \tau_k$. The profile is bounded by $C\Gamma_k^2[v + \Omega_k^{-1} + \mathsf{T}(v^2 + \Omega_k^{-1})]$ times its spatial factor. Its integral against $e^{-\gamma_n v}$ costs C/Ω_n^2, since $\gamma_n \asymp \Omega_n$, $\Omega_k \ge \Omega_n$, and $\mathsf{T} \le 1$. Hence the older sources contribute at most

$$\frac{C_{\mathrm{sec}}(1 + M_{\mathrm{hist}})}{\Omega_n^2 d_n^4}\sum_{k\ge n+2}(1 + d_k^{-1})\Gamma_k^2 e^{\gamma_n(\tau_{n+1}-\tau_k)}.$$

After division by κ_n/B^2, (7.7) applies with an additional fixed factor B^2 and spatial factor $1 + d_k^{-1}$. Its logarithm is at most $C + k\log 2$, and the completed delays bound $t_0 - \tau_k$ by the same sum as before. Increasing Λ therefore bounds this contribution by $C_{\mathrm{sec}}(1 + M_{\mathrm{hist}})(\kappa_n/B^2)e^{-c\Omega_{n+2}^{\alpha}}$. Consequently,

$$\sup_{0\le t\le\tau_{n+1}} Y_n(t) \le CM_{\mathrm{hist}}\frac{\kappa_n}{B^2}, \qquad \Omega_n\int_0^{\tau_{n+1}} Y_n(t)\,dt \le C_{\alpha,B}M_{\mathrm{hist}}\frac{\kappa_n\Omega_n^{\alpha}}{B^2} = o(\kappa_n^{3/4}). \tag{7.10}$$

The integral estimate uses the completed delay bound $\tau_{n+1} \le C_{\alpha,B}\Omega_n^{\alpha-1}$. The small-o bound is uniform in n, since $2^n \le \Omega_n$ and

$$\kappa_n^{1/4}\Omega_n^{\alpha} \le C_{\alpha,B}\Omega_n^{\alpha+1}e^{-\Omega_{n+1}^{\alpha}} \longrightarrow 0.$$

When $n = N-1$, $t_0 = 0$ and both left sides vanish. Since the quadratic point remainders are bounded by $C\Omega_n Y_n^2$, (7.10) also bounds the integral of their coefficients. The reference and patch coefficients have the bounds already proved.

Step 2. The signed weighted forcing. Let S be the current stopping time in normalized units. Using the decomposition after Lemma 7.1, let f_q^{act} denote the resulting f_q along the stopped motion. It includes the inherited and completed-source contributions; the b_1 term remains in the remainder. For the leading strain of the nearest source and uniform receiver rotation from $\theta_n^{(1)}(t_0)$, (2.11) gives

$$f_q^{\mathrm{id}}(s) = -2\sqrt{6}\,s\,\mathrm{Re}\left[(2 - i\sqrt{2})e^{i(2s+4\arg(d_n-d_{n+1})-2\theta_n^{(1)}(t_0)-2\theta_{d,n+1})}\right].$$

Define

$$f_q^{[S]}(s) = \begin{cases} f_q^{\mathrm{act}}(s), & 0 \le s \le S, \\ f_q^{\mathrm{id}}(s), & s > S. \end{cases}$$

$$A_S = \frac{Q_n(t_0)}{\kappa_n} + \int_0^\infty e^{-2\sqrt{2}s} f_q^{[S]}(s)\, ds, \qquad A_{\mathrm{id}} = \int_0^\infty e^{-2\sqrt{2}s} f_q^{\mathrm{id}}(s)\, ds.$$

Put $j = n+1$, so $|d_n - d_j| = d_j$. The term in $M_{2,j}^{(2)}$ linear in $t - t_0$ produces a velocity proportional to $\bar{z}^{-3}$ about the source. Its Hessian on the receiving quadrupole is bounded by $C\Gamma_j^2(t-t_0)/d_j^5$. The affine approximation at the receiving center therefore has error at most $C\Gamma_j^2(t-t_0)\ell_n^2/d_j^5$ at each reference centroid. Dividing by $\Omega_n \ell_n$ gives an error of at most $C\kappa_n s \ell_n/d_j$ in the normalized shape equation by (5.1).

At the rhombus, $\widehat{q}$ and q have the same differential, so the affine field contributes the signed strain term in (2.11). In units of ℓ_n, the centered reference centroids are within $C\eta_n$ of the rhombus at phase $\theta_n^{(1)}(t)$, and $\theta_n^{(1)}(t_0 + s/\Omega_n) = \theta_n^{(1)}(t_0) - s + O(\eta_n s)$ by Section 6.2. Since the projection depends smoothly on the centroids and the normalized strain is $O(\kappa_n s)$, these two errors cost at most $C\kappa_n s(1+s)\eta_n$. Replacing the moving center vector in $\bar{z}^{-4}$ by $d_n - d_j$ incurs a relative error $O(\mathsf{S} + \sup_i r_i/d_i)$ by Section 7.1.

For large Λ, $\ell_n/d_j \le \Omega_n^{-3}$. In the normalized weighted integral, the higher source moments contribute at most $C_{\mathrm{sec}}\Omega_j \ell_j/d_j \le C_{\mathrm{sec}}\mathsf{S}$ by Section 7.3, and averaging over the receiving patches adds $O(\Omega_n^{-5})$ by Section 6.2. Since $\int_0^\infty e^{-2\sqrt{2}s} s(1+s)\, ds < \infty$, combining these estimates with (6.12) and the bounds for the remaining contributions to f_q in Sections 7.3–7.4 gives

$$\int_0^S e^{-2\sqrt{2}s} |f_q^{\mathrm{act}}(s) - f_q^{\mathrm{id}}(s)|\, ds \le C\varepsilon_{\mathrm{sep}} + C_{\mathrm{sec}}\big(M_{\mathrm{hist}}\zeta_{\Lambda,B} + \eta_n + \mathsf{S} + \sup_i r_i/d_i\big).$$

The identity

$$A_S = A_{\mathrm{id}} + \frac{Q_n(t_0)}{\kappa_n} + \int_0^S e^{-2\sqrt{2}s}\big(f_q^{\mathrm{act}}(s) - f_q^{\mathrm{id}}(s)\big)\, ds$$

and the initial-value bound from Step 1 now give $|A_S - A_{\mathrm{id}}| \le C\varepsilon_*$, uniformly in S. The phase estimate, with cosine at least $7/8$ and total coefficient error at most $1/8$, gives $A_S \ge 3/4 > A_*$. Both pieces of $f_q^{[S]}$ satisfy the same polynomial and slow-exponential bound. For $0 \le r \le S$,

$$\frac{Q_n(t_0)}{\kappa_n} + \int_0^r e^{-2\sqrt{2}s} f_q^{\mathrm{act}}(s)\, ds = A_S - \int_r^\infty e^{-2\sqrt{2}s} f_q^{[S]}(s)\, ds.$$

$$\left| \int_r^\infty e^{-2\sqrt{2}s} f_q^{[S]}(s)\, ds \right| \le C(1+r)^3 e^{-(2\sqrt{2}-\sigma/2)r}.$$

By Section 6.2, these identities exclude $Q_n = -q_*$ and reaching the deterministic upper time before $Q_n = q_*$, provided the other exits are excluded below. All constants are independent of S. The extension after S is used only in the displayed integrals, while the return operator remains restricted to $[0, S]$. At $Q_n = q_*$, the tail is $O(\kappa_n^{3/4})$ and A_S is the coefficient in the delay formula.

At $Q_n = q_*$ set $\mathcal{A}_n = A_S$. To bound earlier motion, eliminate the slower quadrupoles from the original time zero, when their relative states vanish. Let $F_n(t) \ge 0$ bound all projected centroid, moment, and patch inputs from indices greater than n, including their responses through slower quadrupoles, and let $\mathcal{K}_n$ be the positive return operator starting at zero. It includes the earlier response to n, which is therefore omitted from F_n. In the formulation starting at t_0, the response from $[0, t_0]$ belongs to the initial slower-scale state. This follows by splitting each return integral as $\int_0^t = \int_0^{t_0} + \int_{t_0}^t$. Lemma 7.1 bounds the forcing-level return

norm by $C\Xi^2/\Omega_n$ and the weighted integral of a source-driven response by $C\Xi/\Omega_n$ times its weighted source norm. Thus, for every stopped time T,

$$\int_0^T e^{-2\sqrt{2}\Omega_n(t-\tau_{n+1})}F_n(t)\,dt \le \big(M_0 + C_{\mathrm{sec}}M_{\mathrm{hist}}\zeta_{\Lambda,B}\big)\kappa_n < 2M_0\kappa_n.$$

The bound includes the inputs to every component of Y_n. Together with the pointwise bounds and the ideal extension after S, it verifies the fixed input class without continuing the physical motion beyond the stop.

Step 3. A comparison bound for the recipient. We use the signed equation to control departure and a nonnegative comparison function to bound Y_n at every earlier time. In this step T denotes the absolute physical stopping time, so $[0,T]$ includes the motion before t_0. Here $Q = Q_n = \triangle\widehat{q}_n$, $P = P_n = \triangle\widehat{p}_n$, and $\nu = (\triangle I_n/(2\Gamma_n\ell_n^2), \triangle\widehat{\Theta}_n, \widehat{M}_{1,n}, \widehat{d}_n)$ collects the other finite differences defined in Section 7.2. Use the sum of their absolute values for $|\nu|$.

The changes of shape and phase in Section 6.1 remove the nonlinear terms depending only on the unstable shape variable. The terms QP and $Q\nu$ cost at most $\exp(Cq_*)$, since the normalized-time integral of $|Q|$ before $Q_n = q_*$ is $O(q_*)$. Their return to the unstable equation uses the estimate $|P| + |\nu| \le C\eta\kappa e^{2\sqrt{2}s} + C\kappa e^{\sigma s}$ in Section 6.2. The remaining accumulated coefficient and integral-error terms are bounded by

$$C_{\mathrm{sec}}\left[\mathsf{S}T + \Omega_n^{-3}\Omega_n T + \frac{\Xi^2 T}{\Omega_n} + \kappa_n^{3/4}\right] \tag{7.11}$$

while $\kappa_n e^{2\sqrt{2}\Omega_n(t-\tau_{n+1})} \le Cq_*$. The completed delays and current upper time give

$$T \le C\frac{\log(1/\kappa_n)}{\Omega_n} \le C_{\alpha,B}\Omega_n^{\alpha-1}.$$

Since $\alpha < 1$, the accumulated errors tend to zero uniformly as $\Lambda \to \infty$. More explicitly, (6.6) and the normalized return bound $C\Xi^2/\Omega_n^2$ give

$$\eta_n \log(1/\kappa_n) \le C_{\alpha,B}\left[(\mathsf{S}+\mathsf{S}^2)\Omega_n^{\alpha-1} + \Omega_n^{\alpha-3} + \mathsf{T}\ell_n\Omega_n^{\alpha} + \Xi^2\Omega_n^{\alpha-2}\right] = o_{\Lambda\to\infty}(1).$$

The term containing ℓ_n is small by the series estimate in Section 7.1. The four terms in (7.11) come from the external and reference coefficients, patch feedback, slower-quadrupole return, and forcing of P and ν, respectively. In particular,

$$\varepsilon_n\Omega_n T \le C\Omega_n^{-3}\log(1/\kappa_n) = O_{\alpha,B}(\Omega_n^{\alpha-3}), \qquad \frac{\Xi^2 T}{\Omega_n} \le C_{\alpha,B}\Xi^2\Omega_n^{\alpha-2}.$$

Before t_0, the nonlinear coefficient integral is bounded by (7.10). The fixed factor $\exp(Cq_*)$ is included in C_{out}.

In normalized time the unperturbed linear operator is $\mathrm{diag}(2\sqrt{2}, -2\sqrt{2}, \mathcal{N})$, where $\mathcal{N}^2 = 0$ describes the impulse-to-phase coupling in Section 6. The first-moment and translation coordinates have zero unperturbed equations. Their small coupling is included in α_n below. Since impulse-to-shape terms vanish at the rhombus, the linear evolution is bounded by $C[e^{2\sqrt{2}s} + 1 + s] \le C_Z e^{2\sqrt{2}s}$ for $s \ge 0$. Recall $Z_n = Y_n - W_n = |Q| + |P| + |\nu|$, and set $E_a(t) = e^{at}$ for $t \ge 0$, with $(E_a * f)(t) = \int_0^t e^{a(t-r)}f(r)\,dr$. Then

$$\begin{aligned} Z_n &\le C_Z E_{2\sqrt{2}\Omega_n} * [F_n + \alpha_n Z_n + C\varepsilon_n\Omega_n W_n + \mathcal{K}_n(Y_n)],\\ W_n &\le C_W E_\mu * [\Omega_n Z_n + F_n + \mathcal{K}_n(Y_n)], \qquad \mu = O(1). \end{aligned}$$

The nonnegative coefficient $\alpha_n(t)$ contains the reference, source-evaluation, and nonlinear centroid terms. By (7.10) before t_0 and the estimates of Section 6.2 afterwards,

$$\int_0^T \alpha_n(t)\,dt \le Cq_* + C_{\mathrm{sec}}\left[\mathsf{S}T + \Omega_n^{-3}\Omega_n T + \frac{\Xi^2 T}{\Omega_n} + \kappa_n^{3/4}\right].$$

The kernel rate μ is bounded independently of n.

Substitute the inequality for Z_n into that for W_n. The identity

$$\Omega_n E_\mu * E_{2\sqrt{2}\Omega_n} = \frac{\Omega_n}{2\sqrt{2}\Omega_n - \mu}(E_{2\sqrt{2}\Omega_n} - E_\mu) \le C E_{2\sqrt{2}\Omega_n}$$

holds with a uniform constant. Since $E_\mu \le E_{2\sqrt{2}\Omega_n}$, we obtain

$$Y_n(t) \le C\int_0^t e^{2\sqrt{2}\Omega_n(t-r)}\left[F_n(r) + (\alpha_n(r) + \varepsilon_n\Omega_n)Y_n(r) + \mathcal{K}_n(Y_n)(r)\right]dr.$$

Define the nonnegative comparison function

$$R_n(t) = e^{2\sqrt{2}\Omega_n t}\max_{0\le r\le t} e^{-2\sqrt{2}\Omega_n r}Y_n(r).$$

Then $Y_n \le R_n$ and $R_n(r) \le e^{-2\sqrt{2}\Omega_n(t-r)}R_n(t)$ for $r \le t$. In particular,

$$\mathcal{K}_n(Y_n)(r) \le C_G\Xi^2\int_0^r e^{\beta_n(r-u)}R_n(u)\,du \le \frac{C\Xi^2}{\Omega_n}R_n(r).$$

Multiply the preceding inequality for Y_n by $e^{-2\sqrt{2}\Omega_n t}$. Its right side is nondecreasing, so taking the maximum over earlier times gives

$$e^{-2\sqrt{2}\Omega_n t}R_n(t) \le C\int_0^t e^{-2\sqrt{2}\Omega_n r}F_n(r)\,dr + C\int_0^t\left[\alpha_n(r) + \varepsilon_n\Omega_n + \frac{\Xi^2}{\Omega_n}\right]e^{-2\sqrt{2}\Omega_n r}R_n(r)\,dr.$$

Gronwall costs only $C\int_0^T\alpha_n + C\varepsilon_n\Omega_n T + C\Xi^2 T/\Omega_n$, already bounded above. Step 2 therefore gives

$$\begin{aligned} Y_n(t) \le R_n(t), \qquad R_n(r) \le e^{-2\sqrt{2}\Omega_n(t-r)}R_n(t) \quad (0 \le r \le t),\\ e^{-2\sqrt{2}\Omega_n(t-\tau_{n+1})}R_n(t) \le C\big(M_0 + C_{\mathrm{sec}}M_{\mathrm{hist}}\zeta_{\Lambda,B}\big)\kappa_n. \end{aligned} \tag{7.12}$$

This estimate uses absolute values. The signed coefficient $\mathcal{A}_n$ is used only to determine the departure time.

Apply the same argument with $T = t_0 = \tau_{n+1}$. The nearest source contributes only its motion before τ_{n+1}, whose weighted input is bounded by the first inequality in (7.6). Its response through slower quadrupoles has the additional small factor $C\Xi/(\Omega_n d_{n+1})$. Equations (7.7)–(7.8) bound the other sources. The coefficient integral in Gronwall uses only (7.10) and the reference, patch, and return bounds on $[0, t_0]$. Hence

$$\sup_{0\le t\le t_0} e^{2\sqrt{2}\Omega_n(t_0-t)}Y_n(t) \le CM_{\mathrm{hist}}\kappa_n B^{-2} + C_{\mathrm{sec}}(1 + M_{\mathrm{hist}})\kappa_n e^{-c\Omega_{n+2}^{\alpha}}.$$

Increasing Λ absorbs the last term into the first. This proves the bound used in Section 5.3 and Figure 2, without using the target's later motion.

Step 4. Slower quadrupoles and the crossing $Q_n = q_*$. By (7.12) and the deterministic upper time, $R_n(t) \le C_{\mathrm{sec}} q_*$. We prove, for every current stopped time,

$$Y_i(t) \le C_{\mathrm{sec}} \frac{\Gamma_n \ell_n^2}{\Omega_n |d_i - d_n|^4} \left(1 + \frac{d_i}{d_n} + \frac{\Xi}{\Omega_n d_n}\right) R_n(t) + \mathcal{R}_{i,n}(t), \qquad i < n. \tag{7.13}$$

Here $\mathcal{R}_{i,n}$ is the nonnegative comparison contribution from completed indices greater than n.

Fix the actual coefficients and iterate the slower-quadrupole comparison inequalities from time zero. Write the resulting nonnegative bounds as $Y_i \le Y_i^{\mathrm{target}} + \mathcal{R}_{i,n}$, where Y_i^{target} contains the inputs from n and $\mathcal{R}_{i,n}$ contains those from completed indices. Both comparison terms have zero initial value. The multipole estimates and $Y_n \le C_{\mathrm{sec}} R_n$ give coefficients

$$D_{in} = C \frac{\Gamma_n \ell_n^2}{|d_i - d_n|^4} \left(1 + \frac{d_i}{d_n}\right), \qquad \max_{i<n} \left(\frac{d_i}{d_n}\right)^4 D_{in} \le C \frac{\Gamma_n \ell_n^2}{d_n^4} (1 + d_n^{-1}).$$

By $R_n(r) \le R_n(t) e^{-2\sqrt{2}\Omega_n (t-r)}$ and Lemma 7.1,

$$\max_{i<n} \left(\frac{d_i}{d_n}\right)^4 Y_i^{\mathrm{target}}(t) \le \frac{C_G}{2\sqrt{2}\Omega_n - \beta_n} \max_{j<n} \left(\frac{d_j}{d_n}\right)^4 D_{jn}\, R_n(t).$$

Apply (7.3) again to index i. Its input from scale n is $D_{in} R_n$, and (7.2) bounds the remaining input by Ξ times the preceding weighted norm. Integration gives

$$\begin{aligned} Y_i^{\mathrm{target}}(t) \le{}& \frac{C_G D_{in}}{2\sqrt{2}\Omega_n - C_f \Omega_i} R_n(t) \\ &+ \left(\frac{d_n}{d_i}\right)^4 \frac{C_G^2 \Xi}{(2\sqrt{2}\Omega_n - C_f\Omega_i)(2\sqrt{2}\Omega_n - \beta_n)} \max_{j<n} \left(\frac{d_j}{d_n}\right)^4 D_{jn}\, R_n(t). \end{aligned}$$

Both denominators are comparable to Ω_n, since $i < n$, and $|d_i - d_n| \asymp d_i$. In particular,

$$\int_0^t e^{C_f \Omega_i (t-r)} R_n(r)\, dr \le \frac{R_n(t)}{2\sqrt{2}\Omega_n - C_f \Omega_i}.$$

Substitution of the bounds for D_{in} gives

$$Y_i^{\mathrm{target}}(t) \le C_{\mathrm{sec}} \frac{\Gamma_n \ell_n^2}{\Omega_n |d_i - d_n|^4} \left(1 + \frac{d_i}{d_n} + \frac{\Xi}{\Omega_n d_n}\right) R_n(t).$$

Adding $\mathcal{R}_{i,n}$ proves (7.13). The same calculation holds on the compact outgoing segment with a fixed larger multipole constant, provided its continuation satisfies $R_n(r) \le e^{-2\sqrt{2}\Omega_n (t-r)} R_n(t)$.

For $n \ge 2$, the subsystem $i < n$ has linear evolution bounded by $C e^{\beta_n (t-r)}$, where $\beta_n = C_f \Omega_{n-1} + C_G \Xi \asymp \Omega_{n-1}$. The contribution of $k > n$ before τ_k costs $C\Gamma_k^2/\Omega_k^2$. After factoring out $\Gamma_k^2 e^{\beta_n (t-\tau_k)_+}$, integrating the linear, constant, and quadratic terms in $t - \tau_k$ gives $C\beta_n^{-2}$, $C(\beta_n \Omega_k)^{-1}$, and $C\mathsf{T}\beta_n^{-3}$, respectively. Since $\beta_n \ge 1$, $\mathsf{T} \le 1$, and $\Omega_k \ge \beta_n$,

$$\mathcal{R}_{i,n}(t) \le \frac{C_{\mathrm{sec}}(1 + M_{\mathrm{hist}})}{\beta_n^2 d_i^4} \sum_{k>n} (1 + d_k^{-1}) \Gamma_k^2 e^{\beta_n (t-\tau_k)_+}, \qquad i < n.$$

The local time bound, including continuation up to τ_n, gives

$$t - \tau_{n+1} \le C_T \log(1/\kappa_n)/\Omega_n.$$

Together with the completed delays, $\beta_n \le C\Omega_n/B$, and $B^{1-\alpha} \ge 2$, this yields

$$\beta_n (t - \tau_k)_+ \le C_2 B^{-1} \Omega_{n+1}^{\alpha}, \qquad k > n,$$

with C_2 fixed before B. Hence

$$\log\frac{\Gamma_k^2}{\Gamma_n^2}+\beta_n(t-\tau_k)_+\le-\left(4-\frac{4}{B^\alpha}-\frac{C_2}{B}\right)\Omega_k^\alpha+2(k-n)\log B.$$

Choose B so that the parenthesis is at least three, then increase Λ to absorb $\log(1+d_k^{-1})$ and the index terms. The sum is at most $C\Gamma_n^2e^{-c\Omega_{n+1}^\alpha}$. Since $\beta_n\asymp\Omega_{n-1}$ and $|d_{n-1}-d_n|=d_n$,

$$\mathcal{R}_{n-1,n}(t)\le C_{\mathrm{sec}}(1+M_{\mathrm{hist}})\kappa_{n-1}e^{-c\Omega_{n+1}^\alpha}.$$

For $n=1$, there are no slower quadrupoles.

For $n\ge2$, use $\Gamma_n\ell_n^2/\Omega_n=2\pi\ell_n^4$ and $d_i\ge2d_n$ in (7.13) to obtain

$$\sup_{i<n}Y_i(t)\le C_{\mathrm{sec}}(1+M_{\mathrm{hist}})\left[\frac{\ell_n^4}{d_n^5}\left(1+\frac{\Xi}{\Omega_n}\right)+\frac{\Gamma_n^2}{\beta_n^2d_n^4}e^{-c\Omega_{n+1}^\alpha}\right]=o_{\Lambda\to\infty}(1).$$

The convergence is uniform in n for fixed α,B. Choose Λ so that this is less than half the radius of the slower-quadrupole chart. The norm Y_i includes every shape, impulse, phase, first-moment, translation, and integral component, so no such exit occurs. The geometric estimates improve patch confinement and separation. The estimates of Section 6.2, with Step 2, exclude $Q_n=-q_*$, the remaining target chart boundaries, and the deterministic upper time. Thus $Q_n=q_*$ is reached at

$$T_n=\tau_{n+1}+\frac{1}{2\sqrt{2}\Omega_n}\log\frac{q_*}{\kappa_n\mathcal{A}_n}+\frac{O_{\mathrm{sec}}(\eta_n\log(1/\kappa_n)+\kappa_n^{3/4})}{\Omega_n}.$$

Step 5. Reach the prescribed dipole separation. Continue along the fixed compact outgoing segment, stopping at a slower-quadrupole exit or the boundary of its noncollision neighborhood. Use the physical centroid norm of Section 7.2 and retain $W_n(T_n)$ as prescribed after Theorem 3.10. In normalized time, the centroid derivatives and the coefficient of centroid input to W_n are bounded. The return from W_n has coefficient $O(\varepsilon_n)$, and the first-moment and translation coefficients have the bounds above. The linear evolution on this interval is therefore bounded independently of n and κ_n. Multiply R_n on $[0,T_n]$ by a fixed norm-equivalence factor and keep the notation R_n. This preserves both inequalities in (7.12), with a larger fixed constant. In the new norm $Y_n(T_n)\le R_n(T_n)$. For $t>T_n$, extend R_n continuously by

$$\dot R_n=K_{\mathrm{sec}}\Omega_nR_n+C_{\mathrm{sec}}F_n+C_{\mathrm{sec}}\mathcal{K}_n(R_n),\qquad K_{\mathrm{sec}}\Omega_n\ge2\sqrt{2}\Omega_n.$$

In these coordinates,

$$\limsup_{h\downarrow0}\frac{Y_n(t+h)-Y_n(t)}{h}\le C_{\mathrm{sec}}\Omega_nY_n(t)+C_{\mathrm{sec}}F_n(t)+C_{\mathrm{sec}}\mathcal{K}_n(Y_n)(t).$$

Choose $K_{\mathrm{sec}}\ge\max\{C_{\mathrm{sec}},2\sqrt{2}\}$ and enlarge the return coefficients by the same comparison constants. Positive comparison gives $Y_n\le R_n$ and $\dot R_n\ge2\sqrt{2}\Omega_nR_n$. Combining this with (7.12) gives, also across T_n,

$$R_n(r)\le e^{-2\sqrt{2}\Omega_n(T_n-r)}R_n(T_n)\le e^{-2\sqrt{2}\Omega_n(t-r)}R_n(t),\qquad r\le T_n\le t.$$

In normalized time $s=\Omega_n(t-\tau_{n+1})$,

$$s=\frac{\log(1/\kappa_n)}{2\sqrt{2}}+O_{\mathrm{sec}}(1),\qquad\frac{F_n(t)}{\Omega_n}\le C_{\mathrm{sec}}\kappa_n(1+s)^3e^{\sigma s/2}\le C_{\mathrm{sec}}\kappa_n^{3/4}.$$

The bound for the linear evolution on the outgoing segment and the small return coefficient imply

$$R_n(t) \le C_{\mathrm{sec}}\big(R_n(T_n) + \kappa_n^{3/4}\big) \le C_{\mathrm{sec}}, \qquad 0 \le \Omega_n(t - T_n) \le C_{\mathrm{sec}}.$$

The finite-time comparison in Section 6.2 improves the compact noncollision bounds. At every current time, (7.13) follows again from the physical multipole bounds and $R_n(r) \le R_n(t)e^{-2\sqrt{2}\Omega_n(t-r)}$. The displayed bound on R_n excludes a slower-quadrupole exit. Hence the pair-center distance reaches $r_{\mathrm{out}}\ell_n$ at τ_n, within the deterministic duration used in Step 1. All fixed compact-passage factors are included in C_{out}.

Step 6. Bounds for the next stage. The signed delay formula and (7.12) give

$$\kappa_n e^{2\sqrt{2}\Omega_n(T_n - \tau_{n+1})} \le Cq_*/A_*,$$
$$R_n(T_n) \le C_{\mathrm{sec}} q_* A_*^{-1}(M_0 + C_{\mathrm{sec}} M_{\mathrm{hist}}\zeta_{\Lambda,B}).$$

For $t \le T_n$, the comparison gives $R_n(t) \le R_n(T_n)e^{-2\sqrt{2}\Omega_n(T_n - t)}$. Since $\Omega_n(\tau_n - T_n) \le C_{\mathrm{sec}}$,

$$e^{-2\sqrt{2}\Omega_n(T_n - t)} \le e^{C_{\mathrm{sec}}} e^{-c\Omega_n(\tau_n - t)}, \qquad c < 2\sqrt{2}.$$

On $[T_n, \tau_n]$, the same exponential weight is bounded below by a fixed positive constant. Including these and the compact-passage factors in C_{out}, the constant in (7.5) for n is at most

$$C_{\mathrm{out}} A_*^{-1}(M_0 + C_{\mathrm{sec}} M_{\mathrm{hist}}\zeta_{\Lambda,B}) \le \tfrac{3}{4} M_{\mathrm{hist}}.$$

This proves (7.5), including the first moment, translation, and W_n. The time and angle estimates give (7.9) with the stated strict margin.

The estimate (7.13) also includes W_i. Indeed, the direct centroid response to $D_{in}R_n$ costs Ω_n^{-1}. The external input to the equation for W_i costs the same factor, while its centroid input contributes $\Omega_i/\Omega_n \le 1$. This is also contained in (7.3). Retain the resulting value of W_i at the next starting time.

For $n \ge 2$, set $i = n - 1$ in (7.13). The spatial ratio is bounded, and (7.4) controls the last term. At τ_n,

$$Y_{n-1}(\tau_n) \le CM_{\mathrm{hist}}\kappa_{n-1}B^{-2} + C_{\mathrm{sec}}(1 + M_{\mathrm{hist}})\kappa_{n-1}e^{-c\Omega_{n+1}^{\alpha}}.$$

Here

$$\frac{\Gamma_n \ell_n^2}{\Omega_n |d_{n-1} - d_n|^4} = \frac{\Gamma_n^2}{2\pi\Omega_n^2 |d_{n-1} - d_n|^4} \asymp \kappa_{n-1}\left(\frac{\Omega_{n-1}}{\Omega_n}\right)^2 = \kappa_{n-1}B^{-2}.$$

For $i < n - 1$, retain the factor $1 + d_i/d_n$ in (7.13).

Descending from $N - 1$ to 1, the new constant in (7.5) is at most $3M_{\mathrm{hist}}/4$, the timing error is at most $3C_h\varepsilon_*/4$, and every slower quadrupole stays within half its chart radius. The next recipient has the bound just proved. The estimates of Section 6.3 keep the completed dipoles separating, while the geometric and patch boundary estimates continue. Thus the induction closes with constants independent of N.

The deterministic-duration sum gives $\tau_1 < 1/2$, and (7.9) gives $|\tau_n - \tau_{n,N}| \le C_h\varepsilon_*/\Omega_n$. The separation and geometric estimates keep the dipoles in every quadrupole separating through time 1.

Proposition 7.2. *With the choices above, for every $N \ge 2$ there are two finite patch solutions on $[0, 1]$, a prepared reference and a second solution, whose initial data agree in every quadrupole $n < N$. The reference remains in its rhombus charts. The second solution reaches pair-center distance $r_{\mathrm{out}}\ell_n$ at each scale n, in descending order, with $\tau_1 < 1/2$, and satisfies the geometric and patch bounds uniformly in N. Its times τ_n obey* (7.9)*, with $|h_n| \le C_h\varepsilon_*$, and its dipole angles satisfy $\theta_{d,n} - \vartheta_n = -h_n + O(\varepsilon_*)$. Every completed quadrupole satisfies* (7.5)*, and the slower quadrupoles satisfy* (7.13) *before their intended stages.*

Together with the reference construction and prescribed initial replacement, Proposition 7.2 proves Proposition 5.1.

7.6 Separation in a fixed annulus at time 1

Since $\tau_1 < 1/2$, the estimates of Section 6.3 apply for at least half a unit of time. The separation bound gives $|U_{\mathrm{ext},1}(d_1(t))| \le C d_1^{-1} \sum_{j\ge 2} \Gamma_j$. Integrating the center residual equation, for each solution separately, gives

$$\sup_{0\le t\le 1} |d_1(t) - d_1| \le C d_1^{-1} \sum_{j\ge 2} \Gamma_j + C_{\mathrm{sec},A}\big(\mathsf{T}\Omega_1^2\ell_1^2 + \ell_1\Omega_1^{-4}\big) = o(\ell_1).$$

At time 1, the pair centers are separated by a distance comparable to $\Omega_1\ell_1$, the dipole lengths and patch radii are $O(\ell_1)$, and their arithmetic center is $d_1 + o(\ell_1)$.

Each pair center is at distance $R(1)/2$ from the arithmetic center, and each patch is within $C\ell_1$ of its pair center. Hence

$$c\Omega_1\ell_1 - C\ell_1 - o(\ell_1) \le |x - d_1| \le C\Omega_1\ell_1 + C\ell_1 + o(\ell_1)$$

for every point of the four outer patches of the second solution. The four outer patches of the reference lie within $C_{\mathrm{sec}}\ell_1 + o(\ell_1)$ of d_1.

For large Λ, these patches lie between radii $c\Omega_1\ell_1/2$ and $2C\Omega_1\ell_1$ for the second solution and within radius $(C_{\mathrm{sec}}+1)\ell_1$ for the reference. Choose radii, independent of N, such that

$$2(C_{\mathrm{sec}}+1)\ell_1 < r_- < \frac{c}{4}\Omega_1\ell_1, \qquad 3C\Omega_1\ell_1 < r_+ < \frac{d_1}{16}.$$

All four outer patches of the second solution at time 1 lie in $\{r_- < |x-d_1| < r_+\}$, and those of the reference lie in $\{|x-d_1| < r_-/2\}$. The annulus contains no other quadrupole, and its boundary has positive distance from both indicated supports, uniformly in N. It contains total absolute vorticity $4\Gamma_1$ for the second solution and zero for the reference, as required in Section 5.4.

8 Limit of solution sequences and nonuniqueness

We keep α, A, B, Λ fixed and extract the two solution limits. The limits have the same initial datum. Renormalization and conservation of norms give the strong convergence needed to pass (5.4) to the limit.

8.1 Common initial data and vorticity norms

By Proposition 4.1, the initial disk centers of the first family lie in compact sets at each fixed scale. Choose a diagonal subsequence along which all these centers converge, again indexed by N. The radii and signed amplitudes are fixed, and the limiting disks remain separated. Thus each finite collection of patches converges in every finite L^p. Let ω_0 be the signed sum of the limiting disks. Equation (1.5) bounds both tails, so

$$\limsup_{N\to\infty} \|\omega_N^{(1)}(0) - \omega_0\|_{L^p} \le 2\left(8\pi A^{p-1} \sum_{n>m} \Omega_n^{4p-3} e^{-2\Omega_n^\alpha}\right)^{1/p} \longrightarrow 0 \quad (m\to\infty).$$

Equation (1.4) then gives $\omega_N^{(k)}(0) \to \omega_0$ in every finite L^p for $k = 1, 2$. The choices for different N need not be compatible. The common datum is compactly supported, has integral zero, and satisfies

$$\|\omega_0\|_{L^p}^p = 8\pi A^{p-1} \sum_{n\ge 1} \Omega_n^{4p-3} e^{-2\Omega_n^\alpha} < \infty.$$

The estimate in Section 1.4 gives $cp^{4/\alpha} \le \|\omega_0\|_{L^p} \le Cp^{4/\alpha}$ for $p \ge 2$.

8.2 Compactness and strong convergence

Lemma 8.1. *Let $0 < T < \infty$ and suppose*

$$\partial_t \omega_j + \operatorname{div}(u_j \omega_j) = 0, \qquad u_j = K * \omega_j \quad \text{on } [0,T].$$

Assume that $\omega_j : [0,T] \to L^2$ is weakly continuous, has zero integral and support in a ball independent of j, t, and satisfies

$$\|\omega_j(t)\|_{L^p} = \|\omega_j(0)\|_{L^p}, \qquad 0 \le t \le T, \quad 1 \le p < \infty.$$

Suppose that

$$\omega_j(0) \longrightarrow \omega_0 \quad \text{in } L^p, \qquad 1 \le p < \infty.$$

Then a subsequence satisfies $u_j \to u$ in $C([0,T]; L^2)$ and $\omega_j \to \omega$ in $C([0,T]; L^p)$ for every finite p. The limit satisfies $u = K * \omega$, has initial datum ω_0, and obeys renormalized vorticity transport, conservation of every finite L^p norm, and the weak momentum equation.

Proof. Let $B(0,R)$ contain all vorticity supports. The Biot–Savart law and $\partial_t u_j = -K * \operatorname{div}(u_j \omega_j)$ give

$$\sup_j \Big(\|u_j\|_{L^\infty_t (H^1_x \cap L^\infty_x)} + \|\partial_t u_j\|_{L^\infty_t L^2_x} \Big) \le C.$$

Zero circulation also gives $|u_j(t,x)| \le C|x|^{-2}$ for $|x| > 2R$. Local compactness, time equicontinuity, and this tail bound yield $u_j \to u$ in $C([0,T]; L^2)$ along a subsequence. Since $\omega_j = \operatorname{curl} u_j$ is uniformly bounded in $L^\infty_t L^2_x$, a subsequence satisfies

$$\sup_{0 \le t \le T} |\langle \omega_j(t) - \omega(t), \phi \rangle| \longrightarrow 0 \qquad (\phi \in L^2).$$

The support, circulation, and finite L^p bounds pass to ω, with $\omega(0) = \omega_0$ and $u = K * \omega$. Strong velocity convergence permits passage to the vorticity equation.

Since $u \in L^\infty_t (H^1_x \cap L^\infty_x)$ and $\operatorname{div} u = 0$, the DiPerna–Lions renormalization theorem [31] applies and gives $\|\omega(t)\|_{L^p} = \|\omega_0\|_{L^p}$ for every $t \in [0,T]$ and $1 \le p < \infty$. Weak continuity and conservation of the L^2 norm give strong L^2 continuity of ω and each ω_j.

The set $\{\omega(t) : 0 \le t \le T\}$ is compact in L^2, so the uniform weak convergence above also holds with the test $\phi = \omega(t)$. Consequently,

$$\|\omega_j(t) - \omega(t)\|_{L^2}^2 = \|\omega_j(0)\|_{L^2}^2 - \|\omega_0\|_{L^2}^2 - 2\langle \omega_j(t) - \omega(t), \omega(t) \rangle \longrightarrow 0$$

uniformly in t. The common support gives convergence in $C([0,T]; L^p)$ for $1 \le p < 2$, and interpolation with the uniform L^{2p} bound gives it for $p > 2$.

Finally, $u \in H^1 \cap L^\infty$ implies $\operatorname{curl} \operatorname{div}(u \otimes u) = \operatorname{div}(u\omega)$ in distributions. Testing the vorticity equation with compactly supported stream functions gives the weak momentum equation with initial velocity $u_0 = K * \omega_0$. □

Extend each $\omega_N^{(k)}$ globally by Yudovich theory [68]. These solutions agree with the constructed solutions on $[0,1]$, are L^2-continuous, and conserve circulation and every finite L^p norm. By (1.5), $\|u_N^{(k)}(t)\|_{L^\infty} \le C$ and $\operatorname{supp} \omega_N^{(k)}(t) \subset B(0, R + Ct)$, with C, R independent of N, k, t.

Section 8.1 gives the common initial limit $\omega_N^{(k)}(0) \to \omega_0$. Applying Lemma 8.1 to both families and taking a common diagonal subsequence gives, for $k = 1, 2$, every finite T, and $1 \le p < \infty$,

$$\omega_N^{(k)} \longrightarrow \omega^{(k)} \quad \text{in } C([0,T]; L^p), \qquad \omega^{(1)}(0) = \omega^{(2)}(0) = \omega_0.$$

The lemma shows that $\omega^{(k)}$ solve renormalized vorticity transport and the weak momentum equation, with $u^{(k)} = K * \omega^{(k)}$. Strong L^1 convergence at time 1 preserves the two values 0 and $4\Gamma_1$ in (5.4). Since $0 \le \chi \le 1$,

$$\|\omega^{(2)}(1) - \omega^{(1)}(1)\|_{L^1} \ge \int \chi(|\omega^{(2)}(1)| - |\omega^{(1)}(1)|)\, dx = 4\Gamma_1 > 0.$$

This proves Theorem 1.1.

References

[1] D. Albritton, E. Bruè and M. Colombo, *Non-uniqueness of Leray solutions of the forced Navier–Stokes equations*, Ann. of Math. (2) **196** (2022), 415–455. doi:10.4007/annals.2022.196.1.3.

[2] D. Albritton, E. Bruè, M. Colombo, C. De Lellis, V. Giri, M. Janisch and H. Kwon, *Instability and Non-uniqueness for the 2D Euler Equations, after M. Vishik*, Annals of Mathematics Studies **219**, Princeton University Press, 2024. doi:10.1515/9780691257846.

[3] H. Aref, *Point vortex dynamics: A classical mathematics playground*, J. Math. Phys. **48** (2007), 065401. doi:10.1063/1.2425103.

[4] A. L. Bertozzi and P. Constantin, *Global regularity for vortex patches*, Comm. Math. Phys. **152** (1993), 19–28. doi:10.1007/BF02097055.

[5] T. Binz and M. P. Coiculescu, *Stability of the inviscid power-law vortex*, preprint (2024), revised 2026. arXiv:2411.13397v4.

[6] A. Bressan and W. Shen, *A posteriori error estimates for self-similar solutions to the Euler equations*, Discrete Contin. Dyn. Syst. **41** (2021), 113–130. doi:10.3934/dcds.2020168.

[7] E. Bruè and M. Colombo, *Nonuniqueness of solutions to the Euler equations with vorticity in a Lorentz space*, Comm. Math. Phys. **403** (2023), 1171–1192. doi:10.1007/s00220-023-04816-4.

[8] E. Bruè, M. Colombo and A. Kumar, *Flexibility of two-dimensional Euler flows with integrable vorticity*, Duke Math. J. **175** (2026), no. 9, 1593–1647. doi:10.1215/00127094-2025-0056.

[9] T. Buckmaster, C. De Lellis, L. Székelyhidi Jr., and V. Vicol, Onsager's conjecture for admissible weak solutions, *Communications on Pure and Applied Mathematics* **72** (2019), 229–274.

[10] P. Buttà and C. Marchioro, *Long time evolution of concentrated Euler flows with planar symmetry*, SIAM J. Math. Anal. **50** (2018), 735–760. doi:10.1137/16M1103725.

[11] J.-Y. Chemin, *Persistance de structures géométriques dans les fluides incompressibles bidimensionnels*, Ann. Sci. École Norm. Sup. (4) **26** (1993), 517–542. doi:10.24033/asens.1679.

[12] A. Cheskidov, M. Dai and S. Friedlander, *Dyadic models for fluid equations: A survey*, J. Math. Fluid Mech. **25** (2023), article 62. doi:10.1007/s00021-023-00799-3.

[13] A. Cheskidov, M. Dai and S. Palasek, *Instantaneous Type I blow-up and non-uniqueness of smooth solutions of the Navier–Stokes equations*, preprint (2025), revised 2026. arXiv:2511.09556v2.

[14] H. Choi, *Asymmetric self-similar spiral solutions of 2-D incompressible Euler equations*, Ann. PDE **12** (2026), article 28. doi:10.1007/s40818-026-00254-2.

[15] H. Choi and M. P. Coiculescu, *Multi-sink solutions to the self-similar Euler equations*, preprint (2026). arXiv:2602.15152.

[16] H. Choi, *Rigidity of monotone radial vortices with unbounded vorticity*, in preparation.

[17] H. Choi, *Self-Similar Solutions of the Two-Dimensional Incompressible Euler Equation from Large Initial Data*, preprint (2026). arXiv:2607.19700v3.

[18] K. Choi and I.-J. Jeong, *Stability and instability of Kelvin waves*, Calc. Var. Partial Differential Equations **61** (2022), article 221. doi:10.1007/s00526-022-02334-0.

[19] M. P. Coiculescu, *Ill-posedness of the Euler equations linearized around homogeneous steady states*, preprint (2026). arXiv:2609.06313.

[20] M. P. Coiculescu and S. Palasek, *Non-uniqueness of smooth solutions of the Navier–Stokes equations from critical data*, Invent. Math. **244** (2026), 165–219, published online 2025. doi:10.1007/s00222-025-01396-z.

[21] M. P. Coiculescu, *Non-uniqueness of weak solutions to the unforced two-dimensional Euler equations with vorticity in $L^1 \cap L^p$, Part I: A compactness criterion and the linear analysis*, preprint, 22 October 2026. arXiv:2610.30655v1. Companion Part II in preparation, with a working draft linked from the arXiv record.

[22] P. Constantin, *Far-field perturbations of vortex patches*, Philos. Trans. Roy. Soc. A **373** (2015), 20140277. doi:10.1098/rsta.2014.0277.

[23] P. Constantin and E. S. Titi, *On the evolution of nearly circular vortex patches*, Comm. Math. Phys. **119** (1988), 177–198. doi:10.1007/BF01217737.

[24] D. Córdoba, L. Martínez-Zoroa and W. S. Ożański, *Instantaneous gap loss of Sobolev regularity for the 2D incompressible Euler equations*, Duke Math. J. **173** (2024), 1931–1971. doi:10.1215/00127094-2023-0052.

[25] D. Córdoba, L. Martínez-Zoroa and F. Zheng, *Finite time singularities to the 3D incompressible Euler equations for solutions in $C^\infty(\mathbb{R}^3 \setminus \{0\}) \cap C^{1,\alpha} \cap L^2$*, Ann. PDE **11** (2025), article 19. doi:10.1007/s40818-025-00214-2.

[26] J. Dávila, M. del Pino, M. Musso and S. Parmeshwar, *Global-in-time vortex configurations for the 2D Euler equations*, J. Eur. Math. Soc. (2026), published online first. doi:10.4171/JEMS/1776.

[27] J. Dávila, M. del Pino, M. Musso and J. Wei, *Gluing methods for vortex dynamics in Euler flows*, Arch. Ration. Mech. Anal. **235** (2020), 1467–1530. doi:10.1007/s00205-019-01448-8.

[28] C. De Lellis and L. Székelyhidi Jr., *The Euler equations as a differential inclusion*, Ann. of Math. (2) **170** (2009), 1417–1436. doi:10.4007/annals.2009.170.1417.

[29] J.-M. Delort, *Existence de nappes de tourbillon en dimension deux*, J. Amer. Math. Soc. **4** (1991), 553–586. doi:10.1090/S0894-0347-1991-1102579-6.

[30] R. J. DiPerna and A. J. Majda, *Concentrations in regularizations for 2-D incompressible flow*, Comm. Pure Appl. Math. **40** (1987), 301–345. doi:10.1002/cpa.3160400304.

[31] R. J. DiPerna and P.-L. Lions, *Ordinary differential equations, transport theory and Sobolev spaces*, Invent. Math. **98** (1989), 511–547. doi:10.1007/BF01393835.

[32] T. D. Drivas and T. M. Elgindi, *Singularity formation in the incompressible Euler equation in finite and infinite time*, EMS Surv. Math. Sci. **10** (2023), no. 1, 1–100. doi:10.4171/EMSS/66.

[33] B. Eckhardt and H. Aref, *Integrable and chaotic motions of four vortices. II. Collision dynamics of vortex pairs*, Philos. Trans. Roy. Soc. London Ser. A **326** (1988), 655–696. doi:10.1098/rsta.1988.0117.

[34] V. Elling, *Algebraic spiral solutions of 2d incompressible Euler*, J. Differential Equations **255** (2013), 3749–3787. doi:10.1016/j.jde.2013.07.021.

[35] V. Elling, *Self-similar 2d Euler solutions with mixed-sign vorticity*, Comm. Math. Phys. **348** (2016), 27–68. doi:10.1007/s00220-016-2755-z.

[36] N. Filonov and P. A. Khodunov, *Nonuniqueness of Leray–Hopf solutions for a dyadic model*, St. Petersburg Math. J. **32** (2021), 371–387; Russian original in Algebra i Analiz **32** (2020), no. 2, 229–253. doi:10.1090/spmj/1651.

[37] V. Giri and R.-O. Radu, The Onsager conjecture in 2D: a Newton-Nash iteration, *Inventiones Mathematicae* **238** (2024), 691–768.

[38] F. Grotto and U. Pappalettera, *Burst of point vortices and non-uniqueness of 2D Euler equations*, Arch. Ration. Mech. Anal. **245** (2022), 89–125. doi:10.1007/s00205-022-01784-2.

[39] J. Guillod and V. Šverák, *Numerical investigations of non-uniqueness for the Navier–Stokes initial value problem in borderline spaces*, J. Math. Fluid Mech. **25** (2023), article 46. doi:10.1007/s00021-023-00789-5.

[40] M. Hampton, G. E. Roberts and M. Santoprete, *Relative equilibria in the four-vortex problem with two pairs of equal vorticities*, J. Nonlinear Sci. **24** (2014), 39–92. doi:10.1007/s00332-013-9184-3.

[41] T. Y. Hou, Y. Wang and C. Yang, *Nonuniqueness of Leray–Hopf solutions to the unforced incompressible 3D Navier–Stokes equation*, preprint (2025), revised 2026. arXiv:2509.25116v2.

[42] T. Y. Hou, X. Qin, P. Song and W. Zhang, *Self-Similar Solutions of the 2D Incompressible Euler Equations via a Lagrangian Construction*, preprint (2026). arXiv:2610.25783.

[43] T. Y. Hou, X. Qin, P. Song and W. Zhang, *Nonuniqueness of the 2D Euler Evolutions with $L^1 \cap L^p$ Vorticity*, preprint (2026). arXiv:2610.40553.

[44] A. D. Ionescu, H. Jia and S. Palasek, *On the non-uniqueness of solutions of the axi-symmetric swirl-free Navier–Stokes equations, I*, preprint (2026). arXiv:2606.07501.

[45] P. Isett, A proof of Onsager's conjecture, *Annals of Mathematics* **188** (2018), 871–963.

[46] H. Jia and V. Šverák, *Local-in-space estimates near initial time for weak solutions of the Navier–Stokes equations and forward self-similar solutions*, Invent. Math. **196** (2014), 233–265. doi:10.1007/s00222-013-0468-x.

[47] H. Jia and V. Šverák, *Are the incompressible 3d Navier–Stokes equations locally ill-posed in the natural energy space?*, J. Funct. Anal. **268** (2015), 3734–3766. doi:10.1016/j.jfa.2015.04.006.

[48] T. Kato, *On classical solutions of the two-dimensional non-stationary Euler equation*, Arch. Ration. Mech. Anal. **25** (1967), 188–200. doi:10.1007/BF00251588.

[49] N. H. Katz and N. Pavlović, *Finite time blow-up for a dyadic model of the Euler equations*, Trans. Amer. Math. Soc. **357** (2005), 695–708. doi:10.1090/S0002-9947-04-03532-9.

[50] S. Kida, *Motion of an elliptic vortex in a uniform shear flow*, J. Phys. Soc. Japan **50** (1981), 3517–3520. doi:10.1143/JPSJ.50.3517.

[51] K. Lydon, S. V. Nazarenko and J. Laurie, *Dipole dynamics in the point vortex model*, J. Phys. A: Math. Theor. **55** (2022), 385702. doi:10.1088/1751-8121/ac89bc.

[52] Y. Long, Y. Wang and C. Zeng, *Concentrated steady vorticities of the Euler equation on 2-d domains and their linear stability*, J. Differential Equations **266** (2019), 6661–6701. doi:10.1016/j.jde.2018.11.011.

[53] C. Marchioro and M. Pulvirenti, *Euler evolution for singular initial data and vortex theory*, Comm. Math. Phys. **91** (1983), 563–572. doi:10.1007/BF01206023.

[54] C. Marchioro and M. Pulvirenti, *Vortices and localization in Euler flows*, Comm. Math. Phys. **154** (1993), 49–61. doi:10.1007/BF02096831.

[55] F. Mengual, *Non-uniqueness of admissible solutions for the 2D Euler equation with L^p vortex data*, Comm. Math. Phys. **405** (2024), article 207. doi:10.1007/s00220-024-05065-9.

[56] D. Meyer, *Long time confinement of multiple concentrated vortices*, preprint (2025), revised 2026. arXiv:2506.01477v3.

[57] S. Palasek, *Finite-time blow-up in an elementary model of the 3D Navier–Stokes equations*, preprint (2026). arXiv:2605.13827.

[58] S. Palasek, *Non-uniqueness in the Leray–Hopf class for a dyadic Navier–Stokes model*, Int. Math. Res. Not. **2025** (2025), no. 22, rnaf344. doi:10.1093/imrn/rnaf344.

[59] S. Palasek, *Arbitrary norm growth in the 3D Navier–Stokes equations*, preprint (2025). arXiv:2509.18595.

[60] U. Pappalettera and M. Sorella, *Non-unique vanishing-viscosity solutions of 2D Euler with vorticity in L^p*, Hexagon preprint, version 1, 17 October 2026, hexagon:2610.00314v1.

[61] C. Shao, D. Wei and Z. Zhang, *Self-similar algebraic spiral solution of 2-D incompressible Euler equations*, Ann. PDE **11** (2025), article 13. doi:10.1007/s40818-025-00203-5.

[62] T. C. Sideris and L. Vega, *Stability in L^1 of circular vortex patches*, Proc. Amer. Math. Soc. **137** (2009), 4199–4202. doi:10.1090/S0002-9939-09-10048-5.

[63] T. Tao, *Finite time blowup for an averaged three-dimensional Navier–Stokes equation*, J. Amer. Math. Soc. **29** (2016), 601–674. doi:10.1090/jams/838.

[64] B. Turkington, *On the evolution of a concentrated vortex in an ideal fluid*, Arch. Ration. Mech. Anal. **97** (1987), 75–87. doi:10.1007/BF00279847.

[65] M. Vishik, *Instability and non-uniqueness in the Cauchy problem for the Euler equations of an ideal incompressible fluid*, Parts I and II, preprints (2018). arXiv:1805.09426 and arXiv:1805.09440.

[66] Y. H. Wan and M. Pulvirenti, *Nonlinear stability of circular vortex patches*, Comm. Math. Phys. **99** (1985), 435–450. doi:10.1007/BF01240356.

[67] W. Wolibner, *Un théorème sur l'existence du mouvement plan d'un fluide parfait, homogène, incompressible, pendant un temps infiniment long*, Math. Z. **37** (1933), 698–726. doi:10.1007/BF01474610.

[68] V. I. Yudovich, *Non-stationary flow of an ideal incompressible liquid*, USSR Comput. Math. Math. Phys. **3** (1963), 1407–1456. doi:10.1016/0041-5553(63)90247-7.

[69] V. I. Yudovich, *Uniqueness theorem for the basic nonstationary problem in the dynamics of an ideal incompressible fluid*, Math. Res. Lett. **2** (1995), 27–38. doi:10.4310/MRL.1995.v2.n1.a4.

[70] S. Zbarsky, *From point vortices to vortex patches in self-similar expanding configurations*, Comm. Math. Phys. **388** (2021), 707–733. doi:10.1007/s00220-021-04227-3.

Hyungjun Choi
Department of Mathematics, Princeton University
hyungjun.choi@princeton.edu, web.math.princeton.edu/~hc9325/